2. SITE 597[1]

Shipboard Scientific Party[2]

HOLE 597

Date occupied: 2 March 1983

Date departed: 3 March 1983

Time on hole: 1 day, 7 hr., 15 min.

Position: 18°48.38′S; 129°46.23′W

Water depth (sea level; corrected m, echo-sounding): 4166.5

Water depth (rig floor; corrected m, echo-sounding): 4176.5

Bottom felt (m, drill pipe): 4157.1

Penetration (m): 54.7

Number of cores: 8

Total length of cored section (m): 54.7

Total core recovered (m): 42.1

Core recovery (%): 77

Oldest sediment cored:
Depth sub-bottom (m): 52.7
Nature: Clayey nannofossil ooze
Age: late Oligocene

Basement:
Depth sub-bottom (m): 52.7
Nature: Basalt rubble

HOLE 597A

Date occupied: 3 March 1983

Date departed: 4 March 1983

Time on hole: 1 day, 2 hr., 10 min.

Position: 18°48.43′S; 129°46.22′W

Water depth (sea level; corrected m, echo-sounding): 4162.6

Water depth (rig floor; corrected m, echo-sounding): 4172.6

Bottom felt (m, drill pipe): 4160.1

Penetration (m): 48.6

Number of cores: 7

Total length of cored section (m): 48.16

Total core recovered (m): 48.64

Core recovery (%): 100.1

Oldest sediment cored:
Depth sub-bottom (m): 47.6
Nature: Clayey nannofossil ooze
Age: late Oligocene
Measured velocity (km/s): 1.52

Basement:
Depth sub-bottom (m): 47.6
Nature: Basalt rubble with basalt glass breccia

HOLE 597B

Date occupied: 4 March 1983

Date departed: 7 March 1983

Time on hole: 2 days, 4 hr., 30 min.

Position: 18°48.43′S; 129°46.22′W

Water depth (sea level; corrected m, echo-sounding): 4162.6

Water depth (rig floor; corrected m, echo-sounding): 4172.6

Bottom felt (m, drill pipe): 4160.0

Penetration (m): 72.6

Number of cores: 3

Total length of cored section (m): 24.6

Total core recovered (m): 5.43

Core recovery (%): 22.1

Oldest sediment cored: None recovered

Basement:
Depth sub-bottom (m): 48.0
Nature: Altered, massive vesicular basalt

HOLE 597C

Date occupied: 7 March 1983

Date departed: 15 March 1983

Time on hole: 8 days, 7 hr., 45 min.

Position: 18°48.43′S; 129°46.22′W

Water depth (sea level; corrected m, echo-sounding): 4164.0

Water depth (rig floor; corrected m, echo-sounding): 4174.0

Bottom felt (m, drill pipe): 4160.0

Penetration (m): 143.5

Number of cores: 12

Total length of cored section (m): 100.0

Total core recovered (m): 55.21

Core recovery (%): 55.2

Oldest sediment cored:
Depth sub-bottom (m): 52.5
Nature: Clayey nannofossil ooze
Age: late Oligocene

[1] Leinen, M., Rea, D. K., et al., *Init. Repts. DSDP*, 92: Washington (U.S. Govt. Printing Office).

[2] Margaret Leinen (Co-Chief Scientist), The University of Rhode Island, Narragansett, Rhode Island; David K. Rea (Co-Chief Scientist), The University of Michigan, Ann Arbor, Michigan; Keir Becker, Scripps Institution of Oceanography, La Jolla, California (present address: University of Miami, Miami, Florida); Jacques J. Boulègue, University of Paris, Paris, France; Jörg Erzinger, Justus-Liebig University, Giessen, Federal Republic of Germany; Joris M. Gieskes, Scripps Institution of Oceanography, La Jolla, California; Michael A. Hobart, Lamont-Doherty Geological Observatory, Palisades, New York; Miriam Kastner, Scripps Institution of Oceanography, La Jolla, California; Stephen Knüttel, Florida State University, Tallahassee, Florida; Mitchell W. Lyle, Oregon State University, Corvallis, Oregon; Daniel Moos, Lamont-Doherty Geological Observatory, Palisades, New York; Robin L. Newmark, Lamont-Doherty Geological Observatory, Palisades, New York (present address: Lawrence Livermore National Laboratory, Livermore, California); Tadashi Nishitani, Akita University, Akita, Japan; Robert M. Owen, The University of Michigan, Ann Arbor, Michigan; Julian A. Pearce, The Open University, Milton Keynes, United Kingdom (present address: The University, Newcastle-upon-Tyne, United Kingdom); Karen Romine, The University of Rhode Island, Kingston, Rhode Island (present address: Exxon Production Research Company, Houston, Texas).

Basement:
Depth sub-bottom (m): 52.5
Nature: Basalt
Velocity range (km/s): 5.1 to 6.6 km/s (average 5.86 ± 0.39 km/s)

Principal results: Site 597, the first transponder-navigated DSDP site, is the westernmost site in the east-west hydrogeology transect of the southeast Pacific along 19°S. It is located on crust generated at 5.5 cm/yr. half-rate from the Mendoza Rise, and it is in a region of moderate heat flow. At Holes 597 and 597A the hydraulic piston corer (HPC) penetrated 52.7 and 48.6 m, respectively, of pelagic and hydrothermal sediment. The underlying basalt was recovered with the extension core barrel (XCB). Sedimentary Unit I is 1.4 m of Pleistocene to middle Miocene dark brown clay. Unit IIA is middle Miocene to late Oligocene brown clay-bearing nannofossil ooze. Making up the lowest 10 m in each site is late Oligocene brown clayey nannofossil ooze that contains up to 50% of a fine-grained component that appears to be hydrothermal in origin. Interstitial water samples from the *in situ* sampler and from squeezed sediments show no evidence of fluid advection. Heat flow is 89 mW/m^2, in agreement with the site survey data. Hole 597B, the pilot hole for the re-entry site, penetrated 24.6 m into basalt with 22% recovery.

Hole 597C, the re-entry hole, recovered 9.0 m of Unit IIB basal sediments and penetrated 91.0 m of basalt, recovering 48.5 m (53.3%) and debunking the theory that basalt generated at fast-spreading rises cannot be drilled. The basalts show the normal range of compositions for mid-ocean ridge tholeiites. They are massive flows; only one small piece has a glassy rim. The upper 47 m, Unit I, are vesicular; the lower 44 m, Units II and III, are not. Three stages of alteration have been identified. The first is a late magmatic, possibly deuteric, alteration in which saponite replaced olivine and groundmass and filled vesicles. The second is an episode characterized by dark green smectite, chlorite, pyrite, chalcopyrite, and native copper. This alteration is clearly associated with veins. Celadonite is also associated with veins but may be a transitional stage. A third, late-stage oxidative alteration is characterized by calcite, aragonite, zeolite, iron oxides, and brown smectite. This alteration is pervasive in basalt Unit I and is vein related in Units II and III. Paleomagnetic analyses indicate that the entire section, with the exception of two samples, is reversely magnetized, placing Hole 597C in the reversed interval between Anomalies 8 and 9. Magnetic inclinations in samples subjected to alternating-field demagnetization average 45°.

The successful downhole experiments conducted at Hole 597C included two televiewer logs and a caliper log, which appear to show variations in formation fracturing that can be associated with both the recovery and petrology of basalts. Attempts at Holes 597B and 597C to acquire a 12-channel sonic log were unsuccessful. A packer experiment failed when the packer deflate plug sheared, prematurely deflating the packer. A wireline re-entry test was not successful, but the problems were due to a defective cable head, and it appears that this operation could become routine, given the proper equipment.

BACKGROUND AND OBJECTIVES

Site 597 is located 2100 km east southeast of Tahiti on crust of late Oligocene age. It is situated 150 km northwest of the Austral Fracture Zone and is therefore on crust generated by the Mendoza Rise system, which now lies east of the East Pacific Rise (EPR) in the middle of the northern Nazca Plate. The crust at Site 597 was thought to have been generated at a (half) spreading rate of about 6.5 cm/yr. (Handschumacher, 1976), a rate similar to the present west flank accretion rate of about 7.0 cm/yr. along the EPR between the Garrett Fracture Zone at 13°S and the Easter miniplate at 23°S (Rea, 1981). Seafloor depth is about 4160 m, unusually shallow for crust nearly 30 m.y. old. Such shallow depths are typical of the southeast Pacific between about 10°S and 35°S and from the EPR axis west at least to the Tuamotu and Austral islands.

Low-relief abyssal hills characterize the area surveyed for Site 597. The hills trend about 350° and are buried by sediment except for a few peaks that appear from the reflection records to be igneous outcrops. A transparent sediment layer with a thickness of about 0.07 s (50 to 55 m) overlies a strong, smooth reflector that was interpreted as chert. Abyssal hills to the east and west of the area lack the transparent sediment layer. Heat flow values measured in the site survey area ranged from 49 to 118 mW/m^2.

The drilling at Site 597 was undertaken to obtain a long-term record of hydrothermal sedimentation in the south central Pacific and to obtain basalts from a fast-spreading rise crest. As an additional criterion in site selection, the site was to be old enough to have been sealed to ridge-flank hydrothermal circulation, perhaps 25 to 30 m.y. old. Although heat flow in the site survey area is similar to theoretical values for Oligocene crust, the measurements did not show conclusively that the crust was sealed. Finally, all the Leg 92 sites were chosen to lie south of the equatorial high-productivity zone so that the nonbiogenic sedimentation history would not be masked by changes in biological productivity or altered by suboxic diagenesis. Site 597 is not a true element of the Leg 92 hydrogeology transect because it was generated at the fossil ridge system now in the center of the Nazca Plate. Nevertheless, it was generated at about the same rate as the EPR west flank, and there is no EPR crust in the region older than about 20 or 25 Ma, the approximate age of the Mendoza Rise–EPR ridge jump (Handschumacher, 1976; Mammerickx et al., 1980).

Our specific objectives were to recover a continuous geological section that would include the unfossiliferous clays presently accumulating at the site, the underlying Neogene and upper Paleogene biogenic sediments and chert, and the basaltic basement beneath. We intended to compare the nature of the basalt alteration, sediment pore-water chemistry, and hydrothermal phases in the sedimentary column to formulate an improved description of the various geochemical processes that alter basalts and result in the formation of hydrothermal sediments. Further, we planned to test the hypothesis that the flux of hydrothermal phases to the sediments covaries with longer-term fluctuations in spreading rates and volcanism in the Pacific region.

Additional objectives for Site 597 included the recovery of upper Oligocene through Miocene or Pliocene sediments suitable for the description of the subtropical and transitional microfossil assemblages and the interpretation of the paleoceanographic and paleoclimatic history of the Southern Hemisphere subtropical gyre. We were particularly interested in completing geophysical logging experiments using a 12-channel sonic logging tool and a borehole televiewer, and in determining the permeability of the crust with a packer experiment.

To meet these objectives we planned to use the hydraulic piston corer (HPC) to recover paired cores of the sediment and to use the extended core barrel (XCB) to recover chert and any softer sediments beneath. After the piston coring we planned a rotary-drilled pilot hole into basalt to determine the feasibility of a re-entry hole. If re-entry seemed feasible we planned to drill the basement as deep as possible and then to complete the various downhole experiments.

OPERATIONS

Site Survey

The general area of Site 597 was chosen as a target for more detailed surveys and as a potential drilling location on the basis of three criteria: 25- to 30-Ma crustal age, generally smooth basement character with few large escarpments or seamounts, and continuous sediment cover. The proposed site itself (HY-1) was selected from the detailed Ariadne II survey of the area between 129°44′W and 129°47′W, 18°46′S and 18°50′S (Fig. 1). This is a sediment-covered area roughly 25 km across in which the relief averages 20 to 40 m. The area lies between two abyssal hill ridges oriented 350°. Seabeam data were collected during the survey but were insufficient to generate a bathymetric map.

A rather uniform blanket of sediment 0.07 s (about 55 m) thick covers the area. It is acoustically transparent in the Ariadne II air gun profiles (Fig. 2), although the water gun records from the *Glomar Challenger* profile show several internal reflectors (Figs. 3A and B). According to the air gun profiles, total sediment thickness is 0.63 s at the beacon drop point, which represents 47 m at an acoustic velocity of 1.5 km/s or 50 m at 1.6 km/s. The basement reflector in the Ariadne II profiles is unusually smooth and strong and has an accompanying bubble pulse. Basement was interpreted as sedimentary, perhaps chert. The water gun records from *Glomar Challenger* showed a less smooth basement reflector.

The exact location of HY-1 was chosen to coincide with station HF 4/1, the location of the highest heat flow measured in the area (118 mW/m^2) during the site survey. Station HF 4/1 lies approximately 1000 m northeast of one of two acoustic transponders left in the area to permit the *Glomar Challenger* to return to precisely the same survey locations (Fig. 1).

Navigation

Since one of the major objectives of Leg 92 was to evaluate the effect of localized ridge-flank hydrothermal systems on the sediments and basement rocks, it was critical that our sites be positioned precisely with respect to the previously surveyed areas. To make this possible, two acoustic transponders were left in the area of Site 597 during the Ariadne II site survey. The X-Y location of each transponder was determined during the site survey by finding the best fit of the distance between them on all crossings of the line between them. A third transponder used in the triangulation net was retrieved at the end of the site survey. The latitude and longitude of each transponder were determined by finding the best fit of the X-Y triangulation grid to satellite fixes collected while the ship was in the survey area. The site survey stations, located accurately in the X-Y reference frame, were subsequently assigned latitudes and longitudes that were based on the positions determined for the transponders.

We decided to drop the *Glomar Challenger* site beacon at the latitude and longitude of the heat flow target while steaming onto station in case neither of the transponders was still working. We planned to use the ship's dynamic positioning system guided by transponder navigation to maneuver ourselves onto the target. The beacon for Site 597 was dropped at 0918 hr. on 2 March 1983 in 4167 m of water. The transponders were interrogated by using a portable Benthos deck interrogator unit through a transducer that was deployed over the port side of the ship, hung from the port crane, and kept at a depth of about 12 m. One transponder left in the area (the so-called green transponder) received on 10.0 kHz and one (red transponder) on 10.5 kHz; both transmitted at 12 kHz. The interrogator was programmed to output a digital slant range value after each interrogation, but it was also coupled to the ship's 12-kHz recorder, which keyed on the outgoing pulse and gave an analog record of the return. Upon interrogating the transponders we found that only the 10.5-kHz (red) transponder responded. Although the signal from it was received reliably by the 12-kHz recorder through its hull-mounted transducer, the deck unit interrogator received a signal only once.

In the absence of two transponders for navigation, we used a set of offsets from the *Challenger* beacon monitored with the red transponder to navigate precisely to the chosen target. The site was then defined by the resulting offset from the site beacon, 1710 ft. (521.2 m) north and 1200 ft. (365.8 m) west. The satellite fixes obtained while on Site 597 indicate a position of 18°48.38′S, 129°46.23′W (Hole 597), which is offset from the position of 18°48.68′S, 120°45.97′W indicated by the site survey. Since the X–Y positions are more accurate than the satellite fixes, we assumed that the site was accurately located with respect to the heat flow target and that the difference in position represents error in satellite fixes from one of the cruises, probably in those from the site survey, which did not occupy a single location for a long time.

Drilling Program

We began running drill pipe into the hole at 2100 hr. on Wednesday, 2 March. The drill pipe was strapped (its length was measured) and drifted (its inside diameter was verified) on this first trip into the hole to ensure the compatibility of all coring and logging equipment to be used, and to acquire an accurate drill pipe measurement of the mud line. The average length of a drill stand (three joints) was 28.73 m.

The first core recovered with the variable-length hydraulic piston corer (VLHPC) was full. In order to make sure we had not overpenetrated the mud line, a second mud line core was attempted 9.6 m higher and came up empty. Mud line was established on the third try at 4157.1 m. Hole 597 was continuously cored using the VLHPC to 52.7 m below seafloor (BSF) and deepened to 54.7 m in rubbly basalt using the XCB (Table 1). Two

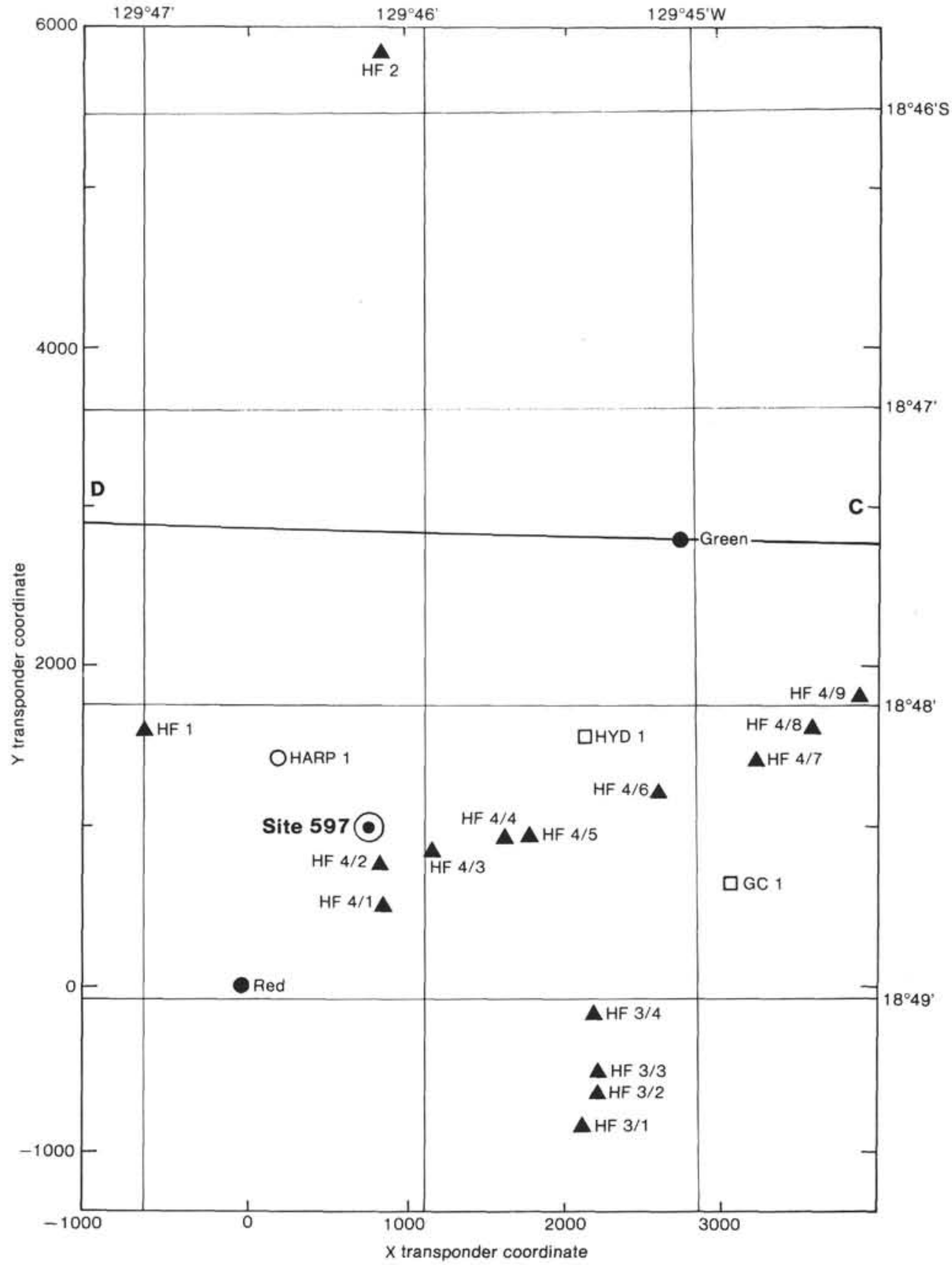

Figure 1. Map showing location of Site 597 in site survey transponder grid. Locations of site survey stations are included. Stations labeled HF are multipenetration heat flow stations. Numbers following the HF designation are the number of the heat flow run and the penetration number. HARP, *in situ* pore water harpoon sample; GC, gravity core; HYD, hydrocast.

VLHPC Von Herzen heat flow probe measurements were made. Both were unsuccessful as a result of damage to wiring. Hole 597 terminated at 4211.8 m (54.7 m BSF), and operations ceased at 1633 hr. on 3 March, when the bit cleared the mud line.

Hole 597A was spudded at 1735 hr. on 3 March, with an offset 100 ft. (30.5 m) to the south of Site 597. The hole was cored continuously with the VLHPC to 47.6 m and deepened to 48.6 m in rubbly basalt with the XCB. Two VLHPC Von Herzen heat flow probe measurements were made, one of which was successful. The Barnes/Uyeda/Kinoshita water sampler/heat flow tool was deployed twice; one deployment was successful. The hole was terminated at 4208.7 m (48.6 m BSF); operations at the hole ceased at 1945 hr. on 4 March with the bit on deck.

For Hole 597B, the bottom-hole assembly (BHA) was changed to that used for rotary coring and the pipe was run to bottom. A special abbreviated version of the BHA was used for this hole; it was shorter and lighter in weight than the standard assembly to minimize the risk to the equipment of spudding and drilling the basalt in this area, which provided the assembly only limited support from the thin sediment layer. Hole 597B was an explor-

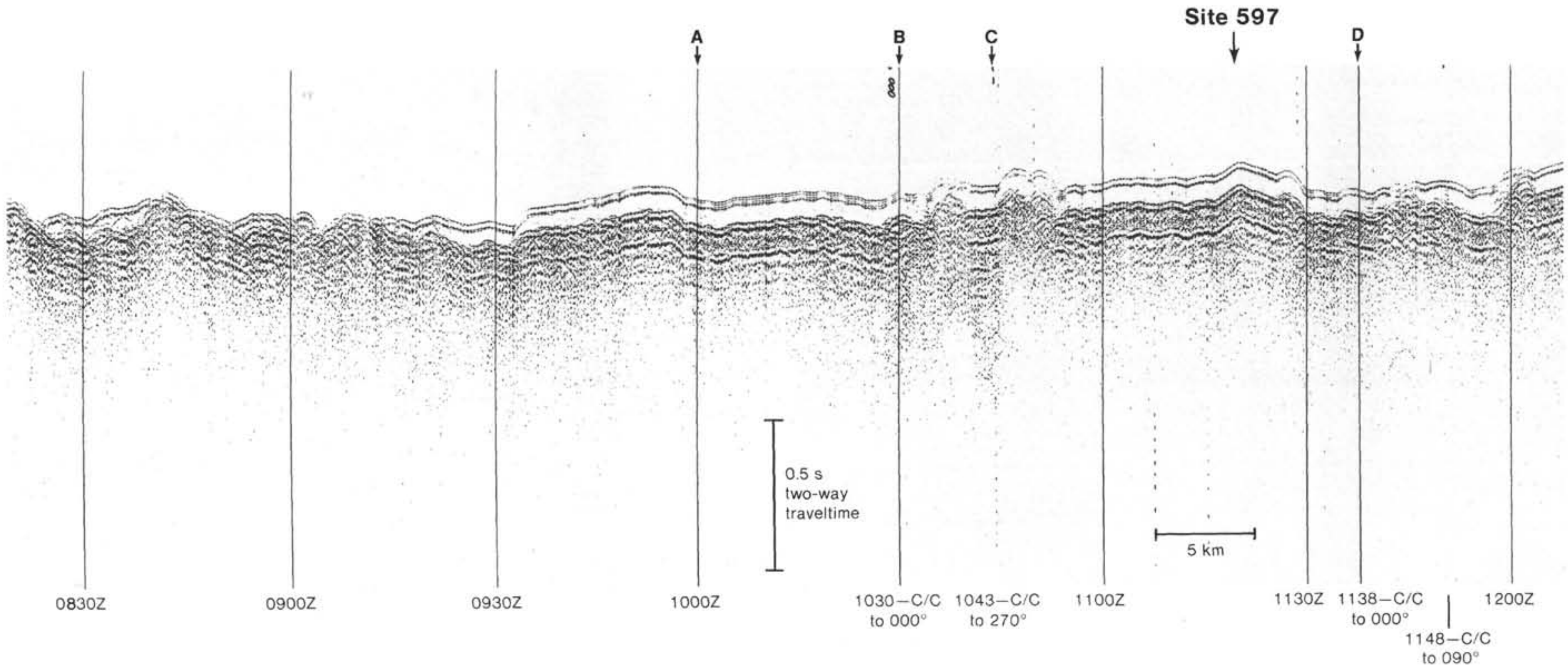

Figure 2. Seismic reflection profile across Site 597 area from single-channel 40-in^3 air gun system. Position of Line C–D is shown in Figure 1 and in Lonsdale (this volume). Positions of other lettered points are shown in Lonsdale (this volume). C/C, course change.

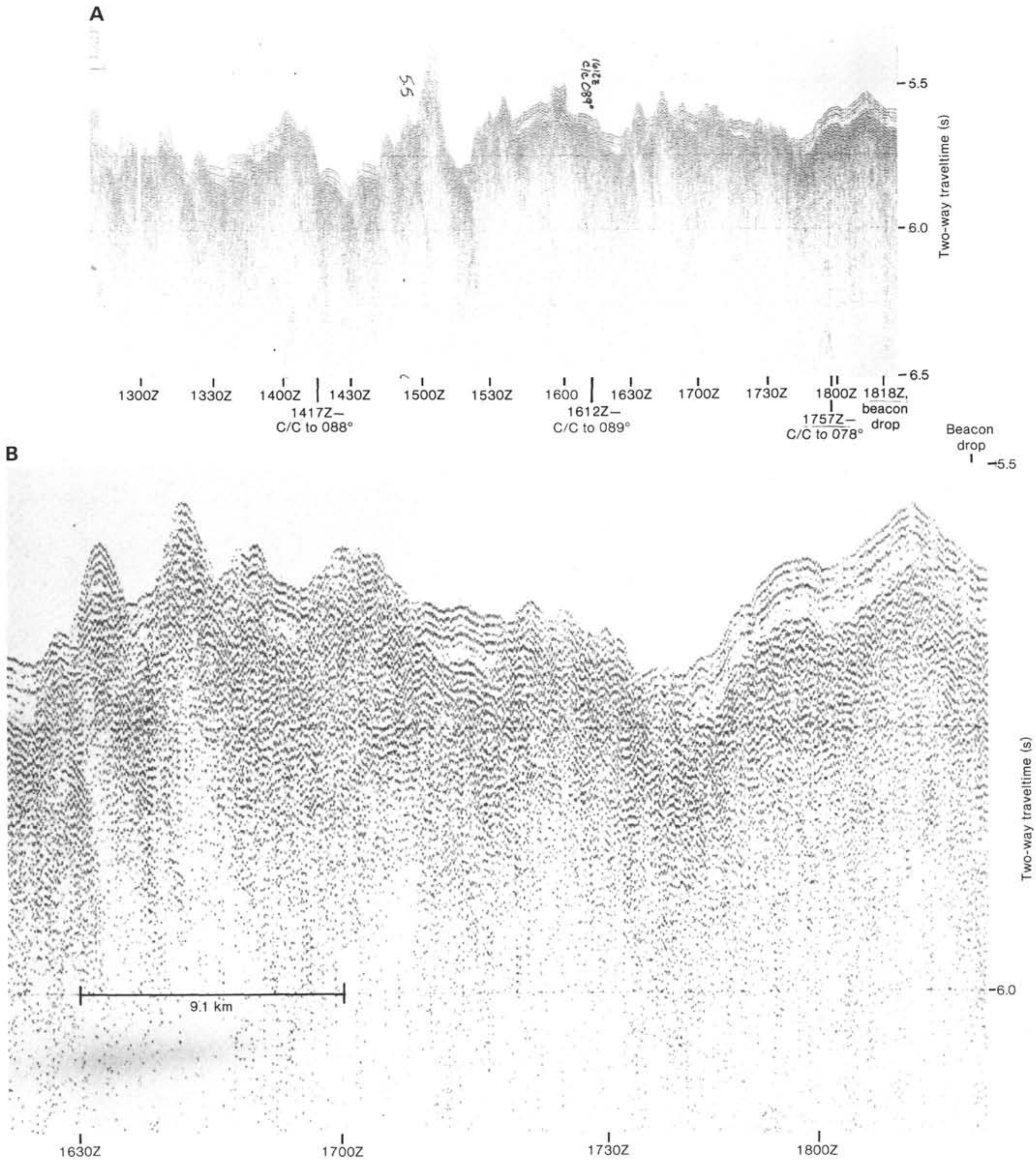

Figure 3. *Glomar Challenger* water gun profiles of the approach to Site 597. A. 5-s sweep. B. 2.5-s sweep.

atory pilot hole; it was drilled to determine whether drilling conditions were good enough to justify the deployment of a re-entry cone and a major basement drilling effort. Operations were delayed briefly when a pipe dope brush handle broke off and fell into the open pipe from the rig floor. After we recovered it with a core barrel, operations resumed. The pipe was washed down to basement at 4208.0 m. The first core was cut with considerable torquing and sticking. A particularly bad zone of rubble approximately 9 m thick at the top of the basalt seemed to be responsible for most of the drilling problems. After the rubble was cleared out conditions improved significantly. Penetration rate was approximately 1.5 m/hr. The pilot hole was terminated at 4232.6 m

Table 1. Coring summary, Site 597.

Core	Date (Mar. 1983)	Time (hr.)	Depth from drill floor (m)	Depth below seafloor (m)	Length cored (m)	Length recovered (m)	Recovery (%)
Hole 597							
1	3	0240	4157.1–4161.7	0–4.6	4.6	4.64	100
2	3	0400	4161.7–4171.3	4.6–14.2	9.6	9.19	96
3	3	0600	4171.3–4180.3	14.2–23.8	9.6	8.90	93
4	3	0705	4180.3–4190.5	23.8–33.4	9.6	8.84	92
5	3	0840	4190.5–4200.1	33.4–43.0	9.6	0	0
6	3	1015	4200.1–4209.7	43.0–52.6	9.6	8.44	89
7	3	1130	4209.7–4209.8	52.6–52.7	0.1	0.02	20
8	3	1613	4209.8–4211.8	52.7–54.7	2.0	2.07	105
Total					54.70	42.10	77.0
Hole 597A							
1	3	1720	4160.1–4165.7	0–4.6	4.6	4.64	100
2	3	2001	4164.7–4174.3	4.6–14.2	9.6	9.68	100
W1	3	2230	4174.3–4175.3	14.2–15.2			
3	4	0015	4174.3–4183.9	14.2–23.8	9.6	8.96	93
4	4	0200	4183.9–4193.5	23.8–33.4	9.6	8.84	93
5	4	0330	4193.5–4203.1	33.4–43.0	9.6	8.75	92
W2	4	0540	4203.1–4204.6	43.0–44.5			
6	4	0715	4198.1–4207.7	43.0–47.6[a]	4.6	7.56	164
7	4	1130	4207.7–4208.7	47.6–48.6	1.0	0.21	21
Total					48.60	48.64	100.1
Hole 597B							
Wash	5		4160.0–4208.0	0–48.0			
1	5	1215	4208.0–4214.4	48.0–54.4	6.4	0	0
2	5	2040	4214.4–4223.5	54.4–63.5	9.1	3.65	40
3	6	0730	4223.5–4232.6	63.5–72.6	9.1	1.78	20
Total					24.6	5.43	22.1
Hole 597C							
1	7	2210	4203.5–4212.5	43.5–52.5	9.0	6.73	75
2	8	0100	4212.5–4215.5	52.5–55.5	3.0	0	0
3	8	0750	4215.5–4224.5	55.5–64.5	9.0	3.29	37
4	8	1445	4224.5–4233.5	64.5–73.5	9.0	7.59	84
5	8	2140	4233.5–4242.5	73.5–82.5	9.0	1.65	18
6	9	0510	4242.5–4251.5	82.5–91.5	9.0	5.17	57
7	9	1115	4251.5–4260.5	91.5–100.5	9.0	4.87	54
8	9	1915	4260.5–4269.5	100.5–109.5	9.0	8.48	94
9	11	0545	4269.5–4279.5	109.5–118.5	9.0	4.45	49
10	11	1145	4279.5–4287.5	118.5–127.5	9.0	8.31	92
11	11	1635	4287.5–4296.5	127.5–136.5	9.0	4.52	51
12	11	2235	4296.5–4303.5	136.5–141.5	7.0	0.15	2
Total					100.0	55.21	55.2

[a] Cored 4.6 m (i.e., 9.6 m less a 5-m recored interval); recovered 7.6 m.

(72.6 m BSF), 24.6 m into basement. The bit was dropped in the hole using the mechanical bit release.

A logging run with the 12-channel sonic logging tool was attempted in the pilot hole. The signal from the tool was good, but the test was unsuccessful because we were unable to lower the tool out of the pipe and into the open hole (see Downhole Logging). It is possible that the end of the drill pipe was in the rubble zone and that the tool could not enter the narrower borehole beneath. There were several kinks in the cable connecting the source unit with the receiver assembly when the tool was retrieved. The tool was modified for future deployment by eliminating the flexible cable link. The drill pipe was pulled, and operations at the hole terminated with the bit release on deck at 0015 hr. on 7 March.

A re-entry cone with 39.81 m of 16-in. casing was made up and deployed for Hole 597C. The cone and casing were washed in and released from the drill pipe without incident. The cone was set at mud line (4160.0 m); the top of the cone is at 4157.0 m and the casing shoe is at 4201 m (7 m above basement). The abbreviated BHA used for Hole 597B was also used in this hole. Hole 597C was spudded at 1918 hr. on 7 March. Drilling conditions were similar to those in the pilot hole, with some torquing and sticking in the upper part of the hole; penetration rate was about 1.5 m/hr.

We stopped coring at 1915 hr. on 9 March with 32.7 hr. on the bit. Although the bit was drilling well, we decided not to risk its failing in the hole, because the site was drilling smoothly. In addition, we thought we could increase penetration rate by using a new bit and a heavier BHA. When the BHA was recovered, the flow-through latch sleeve was not on the running tool; it had hung up on the drill bit. Apparently both tools had become worn by the rotation of the drill collars and the drill pipe, and the latch sleeve had rotated enough to align the flats in both assemblies.

Re-entry of Hole 597C was a routine 4.75 hr. from the start of scanning to verification of re-entry. No fill was evident in the hole. Recovery percentages with the new bit were very good, and penetration rate improved to 2.1 to 2.6 m/hr. Drilling was terminated at 4303.5 m (143.5 m BSF), 91.0 m into basement, at 2215 hr. on 11 March to allow enough time to log the hole and to conduct a packer experiment.

Re-entry for logging and the packer experiment was delayed by a squall, which blew the *Challenger* 280 ft. (85.3 m) off station just as the scanning operations with the re-entry tool were about to begin. Re-entry took about 7.1 hr. including this delay; re-entry was verified at 0345 hr. on 13 March. After the re-entry tool was retrieved, the drill pipe was run to the bottom of the hole to determine whether there was any fill. There appeared to be none. The drill bit was lifted to 4232 m, the logging sheaves were picked up, and the caliper tool was run into the hole. Four caliper runs were made in basement, two at 4800 ft./hr. (1463 m/hr.) and two at 2400 ft./hr. (732 m/hr.). The slower speed resulted in better data. After the caliper runs, two borehole televiewer runs were made in basement, one with a 1.2-MHz transducer and one with a 500-kHz transducer. The logging rate was 300 ft./hr. (91 m/hr.) for both runs, and all data were good. A 12-channel sonic log was scheduled after the televiewer runs. The sonic tool did not appear to be functioning correctly while it was being run into the hole, and the malfunction was confirmed when the tool emerged into the open hole. Because the sonic logging experiment had high priority, we retrieved the tool and attempted to repair it before going on to the packer experiment. However, the hydrophone wiring in the receiver section of the sonic tool was severely damaged, and we could not repair it because spare parts were not available.

We then tried to run the pipe to the bottom of the hole for the packer experiment, but the drill bit stopped 6 m above the total depth of the hole. Three attempts to move it deeper failed. Several of the logging tools had stopped at the same depth, so we assumed that the hole had partially filled from above. The packer safety go-devil was run into the hole, and we continued to try to get to the bottom of the hole. The safety go-devil was seated, and we applied 1400 lb/in^2 of pressure by using the Byron Jackson (BJ) cementing unit. This should have set the packer. All pressure was bled off, and the flow test manifold was rigged. The driller was advised to watch for a weight loss on his indicator, which would indicate that the packer was being forced up the hole and that the water pressure should be vented. The drill string was pressured up to 2200 lb/in^2 to shear the circulation plug in the safety go-devil and allow circulation below the packer. The pin appeared to shear and the pressure fell to zero, but the bumper subs were pounding (i.e., were fully extended) and the drill string weight began to increase. The pressure had vented off at the rig floor standpipe. We believed that the bit had hung on and then broken through a bridge or ledge 6 m off the bottom; this would have caused the bumper subs to scope out and the drill string weight to increase. The drill string was picked up to the nearest connection, which required a 50,000-lb pull. The circulating head was broken out, and one joint of knobby drill pipe was added to put the bumper subs in neutral. When pumping began for a flow test, no pressure could be built up. A pull test was made, but there was no noticeable pull on the drill string to indicate a packer seat. We assumed that the packer element had torn when the drill string broke through the bridge and the bumper subs scoped out. The drill string was pulled, with the bit arriving on deck at 1330 hr. on 14 March. We found that the deflate plug in the packer had sheared at some point, causing the packer to deflate. The packer element was not damaged.

Although no operations had been planned to follow the packer experiment, we received word after the drill string had been pulled that the rendezvous ship *Papenoo*, which was to exchange personnel, would be delayed. Since there was insufficient time before the arrival of the *Papenoo* to complete another re-entry, we decided to deploy the wireline re-entry system. The attempt to reenter Hole 597C with this system failed because the Edo sonic tool did not receive return signals from the cone. This was not clear until we attempted to lower the reentry tool all the way to the mud line to pick up a signal. With 247 m of extra cable out no mud line signal was received. We retrieved the tool and found sediment jammed into the end of it and into crevices at least 0.5 m up the frame of the tool. Later examination of the tool indicated that a cable head was faulty.

The exchange of personnel was completed at 0800 hr. on 15 March. We then attempted to recall the two acoustic navigation transponders. The red (10.0-kHz) transponder was recalled and recovered intact. We sent recall signals to the green (10.5-kHz) transponder for about 2 hr., but it did not signal that it had received the recall instruction. At 1438 hr. on 15 March, we abandoned the effort to recall the transponder, and the vessel got under way for Site 598 (HY-1A).

SEDIMENT LITHOLOGY

At this site, Holes 597 and 597A were hydraulic piston cored, with sediment recovery of 78 and 92.1%, respectively. A third hole (597C) was rotary drilled. A summary of the sediment sections recovered is shown in Figure 4. A thin layer of dark brown zeolitic clay, Unit I, is underlain by nannofossil ooze and clay-bearing nannofossil ooze, Unit IIA, and clayey nannofossil ooze, Unit IIB. The ooze is composed mainly of coccoliths and discoasters, with some foraminifers (less than 2%). No radiolarians or diatoms were observed. Yellow to red brown, translucent to semiopaque oxyhydroxides are present throughout Unit II and increase in abundance with depth (Fig. 5). They are generally isotropic but occasionally have low birefringence and are generally between 5 and 40 μm in diameter (some are up to 100 μm). This yellow to red brown material was designated by Leg 34 scientists as RSO (red brown to yellow brown semiopaque oxides; see Quilty et al., 1976; Bass, 1976a). Oxides appear to stain and/or impregnate the other sediment components, in particular the clay-sized fraction and minerals. Some palagonite is also present throughout Unit II; these particles closely resemble some of the RSO, but they are generally larger. In smear slides in which RSO and palagonite had the same grain size range, it would be difficult or impossible to distinguish between the two.

Fish debris and micronodules are surprisingly rare. Basaltic detritus is more common in the lowermost 2 to 5 m of the sediment section than higher up, but it is present in minor to trace amounts at most depths. A very high concentration of coarse silt to fine sand-sized (up to 150 μm) basaltic debris composes a siltstone that occurs 2.5 m above basement; most of the grains and the coarsest grains in this rock are composed of plagioclase.

A silicic to intermediate ash layer occurs at 48.4 m in Hole 597 (Sample 597-6-4, 92–95 cm); at 41.3 m in Hole 597A (Sample 597A-5-6, 35–38 cm); and at 49.7 m in Hole 597C (Sample 597C-1-5, 15–18 cm). The glass shards in the ash layer are colorless, transparent, anhedral, equant irregular grains up to 120 μm in diameter; however, most are less than 80 μm. The index of refraction is lower than 1.54. Occasional devitrification is present. Other terrigenous components are rare to absent. The grain size of trace quartz and feldspars is less than 10 μm, with occasional grains up to 40 μm, the typical size range of the eolian dust component in oceanic sediments (Arrhenius, 1963; Windom, 1969).

The zeolite in Unit I is phillipsite, which is known to be derived from volcanic matter under both submarine and subaerial conditions. It occurs as euhedral to subhedral prisms up to 100 μm long; most are isotropic, although some are zoned and/or twinned. The crystals contain numerous inclusions, and the prism planes seem to be etched. Minor to trace amounts of phillipsite are present in many other sediment intervals.

The X-ray diffraction patterns of the brown zeolitic clay layer and of the HCl-insoluble residues from the basal sediments (lowermost 4 m, Hole 597C) fail to indicate the presence of any unequivocally terrigenous clay minerals like illite or kaolinite. Hence, with the exception of the one silicic to intermediate ash layer, 96 to 98% of the sediment is composed of mixtures of three end-member components: (1) calcareous ooze, (2) very poorly crystalline smectite and amorphous material present as yellow brown to dull yellow extremely fine-grained particles to silty aggregates, and (3) RSO. Thus, the lithologic units were defined on the basis of these components (Figs. 5 and 6).

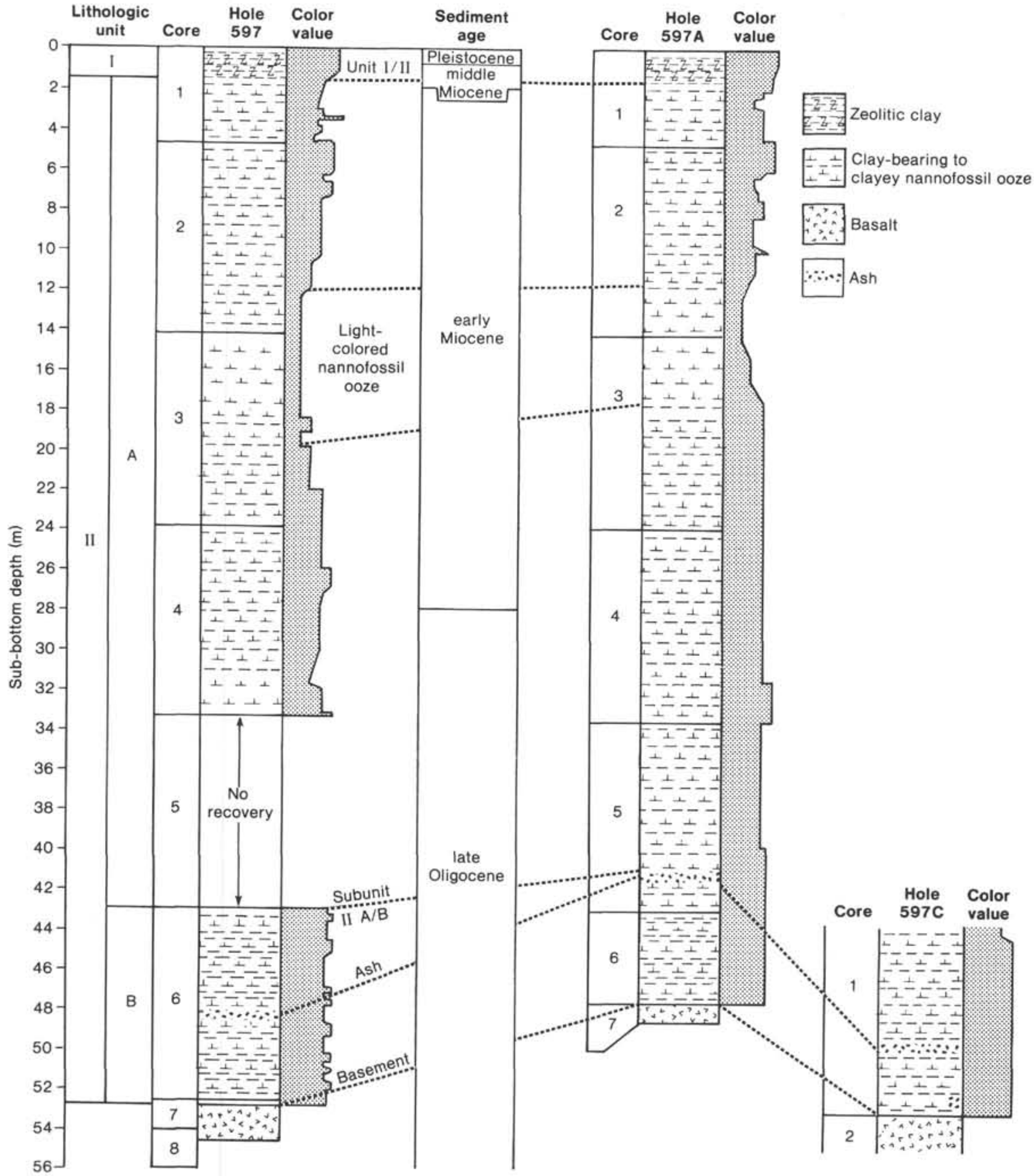

Figure 4. Lithologic sections and correlations, Holes 597, 597A, and 597C. Color value is a measure of "lightness" (lighter to the left) used in Munsell soil color charts and all core descriptions.

Unit I, which is present only in the uppermost 1.4 m of the sediment, is almost carbonate free and seems similar to the clay section of Site 75 (Tracey, Sutton, et al., 1971). It is also similar to, although much thinner than, the clay section of Site 319 in the Bauer Deep (Quilty et al., 1976). Unit II comprises the rest of the section. It is divided into two subunits. Unit IIA commonly contains 75 to 90% calcareous nannofossils. In Unit IIB (the basal 10 m), the abundance of clay plus RSO increases rapidly with depth and constitutes up to 50% of the sediment (Figs. 4 and 6). This material is dominantly silt sized.

$CaCO_3$ Dissolution

The sedimentation rates at Site 597 (Fig. 7) are very low, ranging from about 0.1 to 7.7 mm/10^3 yr. These calculated values represent minimum rates, however, because much evidence of $CaCO_3$ dissolution can be observed in the smear slides and inferred from the dissolved Ca^{2+} profiles. $CaCO_3$ dissolution is most extensive in the uppermost 10 m, and it is significant between about 10 and 25 m. Below 25 m, even though dissolution features are present, $CaCO_3$ overgrowth is observed as well. During the second half of the early Miocene, sedimen-

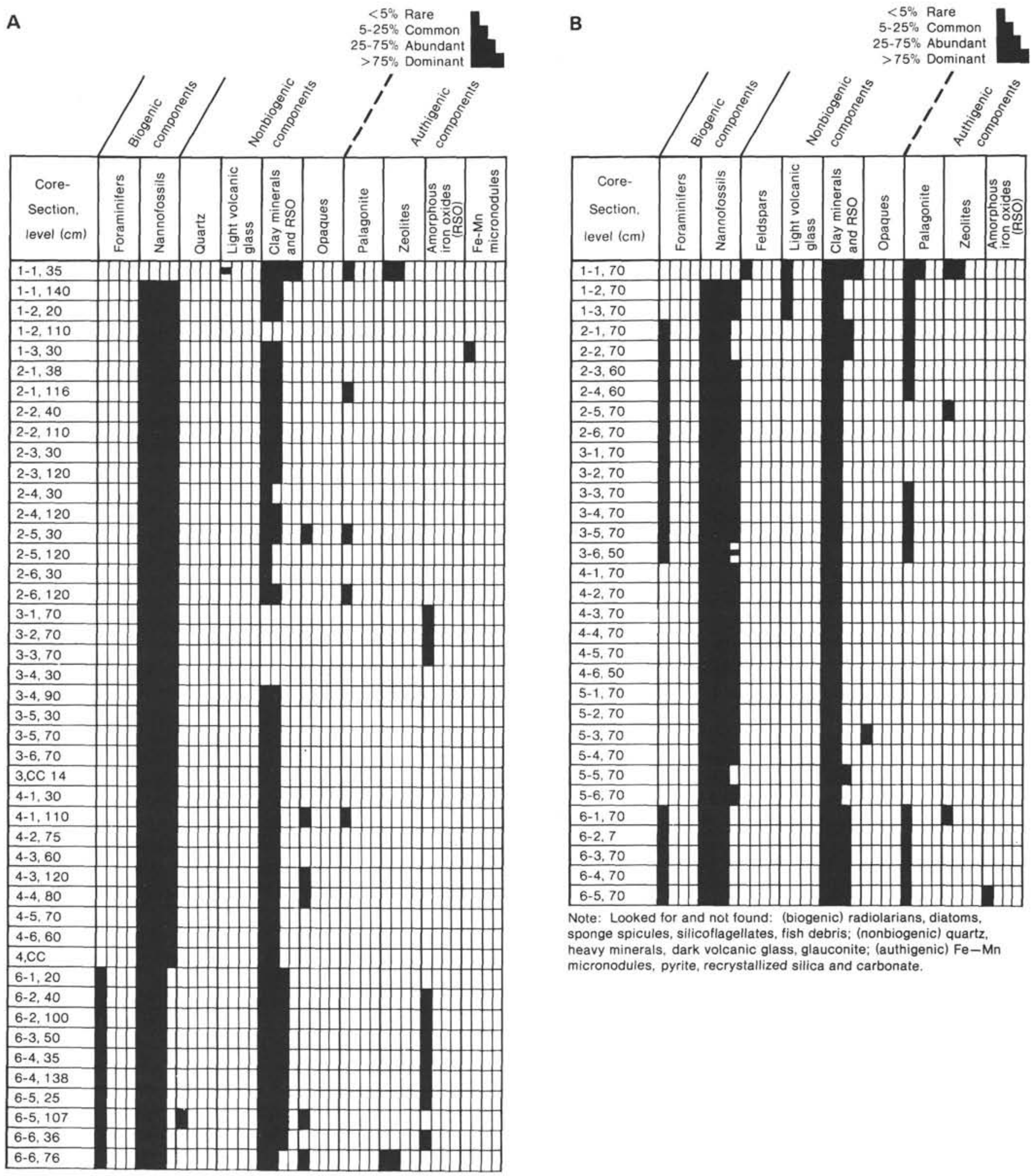

Note: Looked for and not found: (biogenic) radiolarians, diatoms, sponge spicules, silicoflagellates, fish debris; (nonbiogenic) feldspars, heavy minerals, dark volcanic glass, glauconite; (authigenic) pyrite, recrystallized silica and carbonate.

Note: Looked for and not found: (biogenic) radiolarians, diatoms, sponge spicules, silicoflagellates, fish debris; (nonbiogenic) quartz, heavy minerals, dark volcanic glass, glauconite; (authigenic) Fe—Mn micronodules, pyrite, recrystallized silica and carbonate.

Figure 5. Smear slide summary, Site 597. A. Hole 597. B. Hole 597A.

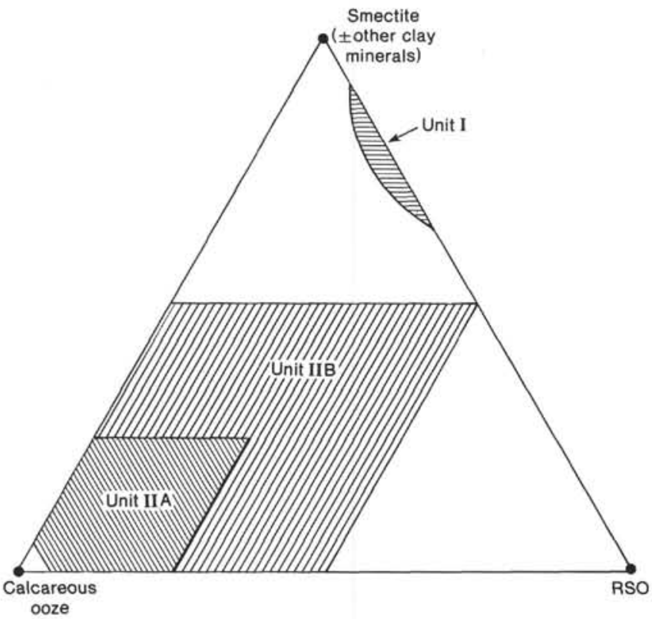

Figure 6. Ternary diagram of the three major sediment components, Site 597.

tation rates decreased significantly. At about this time the carbonate compensation depth (CCD) started a general shallowing trend, which culminated during the middle Miocene (10 to 15 Ma) (see Berger and Winterer, 1974; van Andel et al., 1975). In the middle early Miocene, the site moved below the CCD, and it has probably remained there since (Rea and Leinen, this volume). At present, the CCD lies at about 3950 to 4050 m, and it is sharply defined (Broecker and Broecker, 1974). The water depth at Site 597 is 4160 m; a sedimentation history of about 14 m.y. is condensed in the top 1.5 m of the sediment column.

Sedimentation History

Sedimentation in this area is controlled primarily by variations in productivity, the dissolution of $CaCO_3$, erosion, and redeposition. Because of the very slow sedimentation rates, stratigraphic resolution is poor. Consequently, no detailed information about erosion, redeposition, or hiatuses can be inferred for the middle early Miocene to present.

In the vicinity of ridge crests, especially fast-spreading ridges, particles rich in metal, especially Fe and Mn, accumulate in the sediment as a result of ridge crest hydrothermal activity. The rate at which such particles accumulate and/or other particles become coated with Fe-Mn oxyhydroxides should decrease rapidly away from the ridge crest. Thus, at any given location the Fe- and Mn-rich particles become a less important diluent with time (although there may be short periods during which the flux increases). We assumed that at least some and possibly much of the RSO was derived from ridgecrest hydrothermal activity; and, indeed, the concentration of RSO is greatest in the late Oligocene basal sediments (Unit IIB).

Sedimentation began above the CCD; the accumulation of calcareous sediment continued for about 14 m.y. Subsequent sedimentation took place below the CCD. Despite the CCD variations that occurred during the Tertiary (Berger and Winterer, 1974; van Andel et al., 1975), the late Oligocene and early Miocene sediments are similar, except for the basal sediments (Fig. 4). The intervals contain about the same average percent $CaCO_3$ and have about the same total sediment thickness. The late Oligocene section, however, represents a maximum of about 4.4 m.y., and the early Miocene section represents about 10.2 m.y. If we assume the absence of hiatuses, erosion, or redeposition, at least some of similarity in $CaCO_3$ content can be explained by the dilution of the late Oligocene carbonate by a significant amount of RSO and the enhanced preservation of $CaCO_3$; the average flux of RSO was considerably lower, and $CaCO_3$ dissolution was greater, in the early Miocene.

From the early Miocene through the Pleistocene, the sediment thickness of Holes 597 and 597A is similar (Fig. 4). The early Oligocene sections are dissimilar, probably because of the effects of local gentle basement topography. Hole 597A is upslope of Hole 597.

The glass shards in the ash layer are assumed to have been transported by wind, so their coarse grain size requires proximity to their explosive source. The low index of refraction of the glass, and thus its silicic nature, suggests an Andean source. Extrapolating from the nearest biostratigraphic datum suggests that the age of the ash layer should be about 26 Ma. If so, it may record an unusually explosive volcanic event in the Andes, presumably one caused by the reorientation of oceanic plate boundaries that occurred at this time (Handschumacher, 1976). Site 597 was much closer to the Andes then. It is also noteworthy that there are no other distinct ash layers, although there are some disseminated fine-grained silicic to intermediate glass shards. Sediment studies at Site 321 (e.g., Donnelly, 1976) suggested the inception of intense volcanism in the Andes in the late Miocene, but no evidence of this was observed at Site 597, which by then was much farther downwind.

The nonuniformity of the grain size of the basaltic detritus suggests a mixture from local sources, such as exposed basement (seen in air gun records) and, possibly, volcanic highs. Similarly, the rather large variations in the grain size, color, and shape of the RSO, which appear even within a single sample, suggest that these particles were not subjected to long-distance hydraulic transport. Some of the observed variations, especially those in color and grain size, however, may reflect diagenetic processes. X-ray diffraction analysis of this material shows that it is primarily amorphous.

The nature and origin of the diagenetic poorly crystalline to X-ray amorphous smectites of Unit I are still obscure. Any of the co-existing components, especially the basaltic glass, palagonite, and RSO, could be, and most probably are, precursors of the diagenetic smectites.

BIOSTRATIGRAPHY

Planktonic foraminifers and calcareous nannofossils were present in all the cores from Holes 597 and 597A. No siliceous microfossils were found. A condensed middle and late Neogene interval was recovered in Core 1 in both Holes 597 and 597A; zonable lower Miocene and

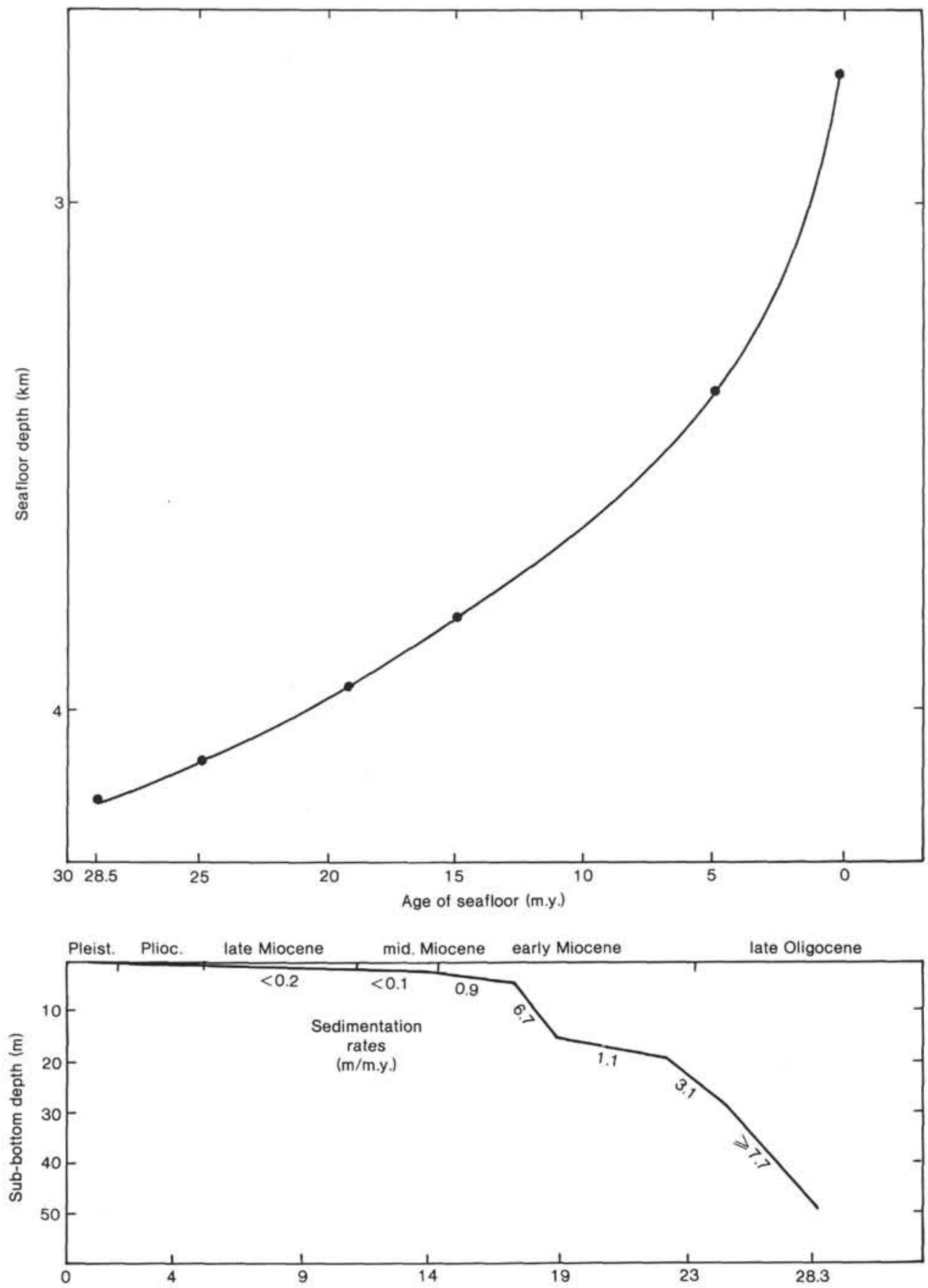

Figure 7. Age/depth plot and sedimentation rates, Hole 597.

uppermost Oligocene sediments make up the remainder of the section to basement. The calcareous nannofossils also indicated that uppermost Oligocene sediments immediately overlie basement (Sample 597C-1,CC).

The top 30 cm or so of Hole 597 (0.3 m BSF) contain Pleistocene nannofossils. Immediately underneath lies a barren interval that extends to about 1.4 m sub-bottom. The interval below the barren zone and above approximately 28 m in both Holes 597 and 597A is early Miocene in age. The remainder of the sediment (below 28 m) is uppermost Oligocene. The preservation of planktonic foraminifers was poor in both Samples 597A-1,CC and 597-1,CC, and the lower/middle Miocene boundary could not be identified by using the *Orbulina* datum. However, the planktonic foraminifers indicated that the Oligocene/Miocene boundary occurred within Cores 597-4 and 597A-4. More precise determination by calcareous nannofossils places the boundary in Core 597-4 at approximately 28.3 m (between -4-3, 5–6 cm and -4-4, 56–57 cm) and in Core 597A-4 at approximately 26.8 m (between -4-2, 75–76 cm and -4-3, 90–91 cm).

According to the paleomagnetic age assigned by Haq (1984) to the nannofossil zonation scheme of Okada and Bukry (1980), the age of the sediment in contact with basement (28.3 Ma) agrees with the magnetic anomaly age for the site of 28.6 Ma (using the Harland et al., 1982, time scale), within the precision associated with the determination of faunal zone boundaries.

Planktonic Foraminifers

The tropical zonation scheme proposed by Blow (1969) was adopted for use at the Leg 92 sites. The modifications of this zonation scheme proposed by Srinivasan and Kennett (1981) have been incorporated; that is, the Oligocene/Miocene boundary is defined by the first appearance of *Globoquadrina dehiscens*, which splits Blow's Zone N4 into two parts, 4A and 4B. The base of the upper Oligocene (Zone N4A) is defined by first appearance of *Globigerinoides* spp., and the base of the lower Miocene (Zone N4B) is defined by the first appearance of *Globoquadrina dehiscens*.

The sediment overlying basement at Site 597 yielded planktonic foraminifers of latest Oligocene to early Miocene age (note that only core catchers were examined). Preservation was generally moderate to poor, and abundances in most core catchers were dependent on the state of sample preservation (see Table 2).

The sediment near the surface (Samples 597-1,CC and 597A-1,CC) had very few foraminifers, and those present were poorly preserved. The foraminifers in Sample 597-1,CC (4.6 m) indicate a latest early Miocene age (Zone N7/N8; Fig. 8). The lack of any specimens of *Orbulina* also suggests an early Miocene age, but the poor preservation of the sample and the paucity of species other than the dissolution-resistant *Sphaeroidinellopsis disjuncta* and *S. seminulina seminulina* make it impossible to rule out an earliest middle Miocene age. Samples 597-2,CC and -3,CC span the lower Miocene Zones N5/N6 through N4B (4.6 to 23.8 m). The Oligocene/Miocene boundary occurs within Core 597-4, as indicated by the first appearance of *G. dehiscens*, which occurs between -3,CC and -4,CC (23.8 to 33.4 m). An uppermost Oligocene fauna indicative of Zone N4A occurs in

Table 2. Abundance and preservation of planktonic foraminifers, Site 597.

Sample (interval in cm)	Abundance	Preservation
Hole 597		
1,CC	Few	Poor
2,CC	Abundant (small forms)	Moderate
3,CC	Abundant (small forms)	Moderate
4,CC	Abundant (small forms)	Moderate
6,CC[a]	Rare	Poor
7,CC	Rare to few	Poor
8,CC	Rare to few	Poor
Hole 597A		
1,CC	Rare	Poor
2,CC	Few	Poor to moderate
3-6 (148–150)	Few	Poor to moderate
4,CC	Common	Poor to moderate
5,CC	Few	Poor to moderate
6,CC	Common	Moderate

[a] There was no recovery in Core 5.

Samples 597-4,CC, -6,CC, -7,CC, and -8,CC (no sediment was recovered from Core 597-5): *Globorotalia kugleri, Globigerina angulisuturalis*, and *Globorotalia nana*. The poor preservation, lower diversity, and low abundances of foraminifers in Samples 597-6,CC through -8,CC are probably responsible for the lack of *Globigerinoides* spp., which would normally occur in association with the species listed and the first appearance of which defines the base of Zone N4A.

Sample 597A-1,CC has a poorly preserved and impoverished association of early lower Miocene foraminifers that could not be adequately zoned. Sample 597A-2,CC (14.2 m) contains lowermost Miocene species, with abundant *Globorotalia* cf. *kugleri* co-occurring with *Neogloboquadrina continuosa* and *Globigerinoides primordius*. The presence of some younger fossils suggests that this sample is younger than Zone N4B. Sample 597A-3,CC (23.8 m) appears to be within Zone N4B, inasmuch as there are no strictly Oligocene species to indicate otherwise. The Oligocene/Miocene boundary lies within Core 597A-4, as indicated by the presence in Sample 597A-4,CC (33.4 m) of *Globorotalia kugleri* in association with *Globigerina angulisuturalis*; the last appearance of the latter is latest Oligocene (near the top of Zone N4A; Kennett and Srinivasan, 1981). The remaining samples (597A-5,CC and -6,CC) are within Zone N4A, with a species association consisting of common *G. angulisuturalis* and rare (-5,CC) to abundant (-6,CC) *Globigerinoides primordius*; the first appearance of *G. primordius* occurs at the base of this zone.

Nannofossils

Sediments recovered at Site 597 were zoned by using the low-latitude nannofossil biostratigraphic zonation of Okada and Bukry (1980). Only Zones CN1 to CN5 and CP19B were found at this site except for a very thin Pleistocene section (CN14 to 15) above the barren interval between 0.3 and 1.4 m. The absence of *Discoaster druggii* suggests that the CN2 Zone (*Sphenolithus belemnos* Zone) may be present above Sample 597-1-3, 56–57 cm; however, no specimens of *S. belemnos* could be positively identified. The CN1A and CN1B subzones were grouped together because the termination of the *Cyclicargolithus abisectus* acme that separates them was not clear.

Pleistocene

The upper, approximately 0.2 to 0.3 m, of both holes (Samples 597-1-1, 5–6 cm and 597A-1-1, 10–11 cm) contain calcareous nannofossils of Pleistocene age. Specimens are few to common in abundance and of poor to moderate preservation. These samples are tentatively placed within the *Gephyrocapsa oceanica* Zone, CN14; however, the presence of *Emiliania huxleyi* was not confirmed because of its small size. *Ceratolithus cristatus* and *Gephyrocapsa* spp. are the most common forms found, with *Cyclococcolithina leptopora, C. macintyrei, Helicopontosphaera kamptneri*, and *Coccolithus pelagicus* forming most of the remaining assemblage. *Pseudoemiliania lacunosa* may also be present. Various dis-

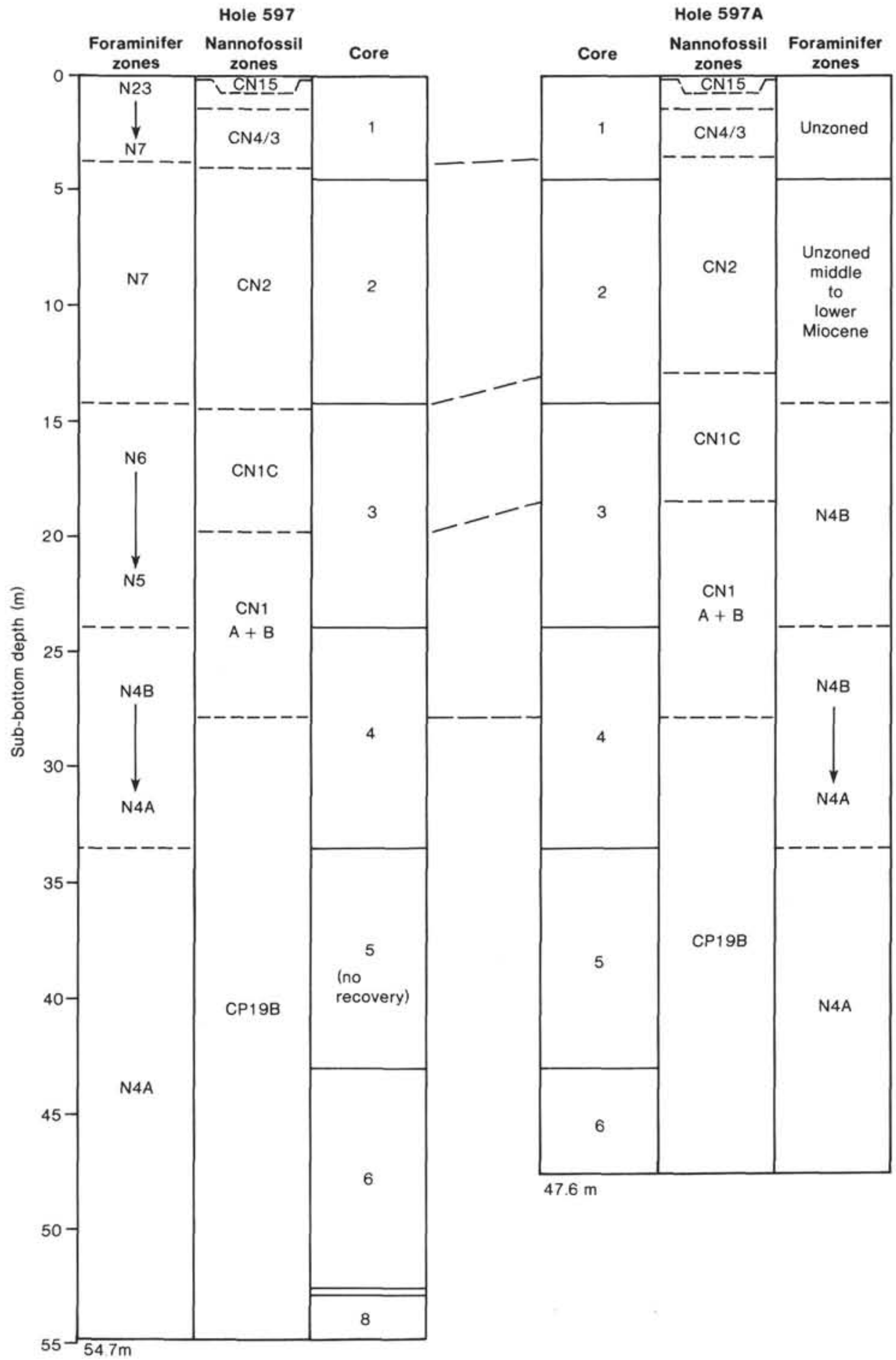

Figure 8. Comparison of biostratigraphic zonations, Site 597.

coaster and sphenolithus species are reworked into the interval; *Cyclicargolithus floridanus* and *Triquetrorhabdulus carinatus* are also reworked.

Below this interval, from approximately 0.3 to 1.4 m sub-bottom depth, the sediment is barren of calcareous nannofossils. The interval represents the period of time from the late early Miocene to the Pleistocene.

Early Miocene

Sediments from Samples 597-1-2, 56–57 cm through -4-3, 56–57 cm (approximately 2.1 to 27.3 m) and 597A-1-3, 133–134 cm through -4-2, 75–76 cm (approximately 4.3 to 26.0 m) are of early Miocene age. Calcareous nannofossils are abundant and preservation is moderate. Most discoasters are overgrown, and placoliths show effects of dissolution (isolated placolith rims are common). Dissolution effects are more pronounced above Sample 597-2-3, 56–57 cm. The interval is dominated throughout by *Discoaster deflandrei* and *Cyclicargolithus floridanus*.

The late early Miocene *Sphenolithus belemnos* Zone (CN2) may occur above Samples 597-1-3, 56–57 cm and 597A-1-3, 56–57 cm, because *D. druggii* is absent. However, the occurrence of *S. belemnos* could not be verified because of the poor preservation of the samples.

Samples 597-2-1, 56–57 cm through -3-4, 56–57 cm (approximately 5.1 to 19.2 m) and 597A-1-3, 133–134 cm through -3-3, 56–57 cm (approximately 4.3 to 17.7 m) are within the *Triquetrorhabdulus carinatus* Zone, *D. druggii* Subzone (CN1C). *D. druggii* is present in the upper and lower portion of the zone, but it is absent in the middle portion (597-2-3, 56–57 cm through -3-2, 56–57 cm and 597A-2-3, 100–101 cm through -3-1, 56–57 cm). *C. abisectus* was first noted in this subzone and become more numerous downhole. It is, however, still rare to few in abundance. Only one individual of *Orthorhabdus serratus* was observed within this subzone (Sample 597A-1,CC). Preservation is moderate, with most forms showing overgrowths. *Discoaster* sp., *S. moriformis, T. carinatus*, and *T. milowii* are also present.

The lower two subzones (*D. deflandrei*, CN1B; and *C. abisectus*, CN1A) of the *T. carinatus* Zone were not separated within these sites because the end of the *C. abisectus* acme was unclear. The reduction in numbers of *C. abisectus* is gradual, and the end of its acme may be partially obscured by reworking. Samples from 597-3-5, 56–57 cm through -4-3, 56–57 cm (approximately 20.7 to 27.3 m) and 597A-3-4, 56–57 cm through -4-2, 75–76 cm (approximately 18.2 to 26.0 m) fall within these two subzones. *T. carinatus* and *C. abisectus* become few to common in abundance. The remaining assemblage consists primarily of *Coccolithus pelagicus, C. miopelagicus, Coronocyclus* sp., *S. moriformis, S. dissimilis*, and *T. milowii*.

Upper Oligocene

Calcareous nannofossils found in the lower half of the sediment column, Samples 597-4-4, 56–57 cm to basement (approximately 28.7 to 54.7 m) and 597A-4-3, 90–91 cm to basement (approximately 27.7 to 48.6 m) were placed within the uppermost Oligocene *Sphenolithus ciperoensis* Zone, *Dictyococcites bisectus* Subzone (CP19B). Basal sediments from Hole 597C (597C-1,CC) indicate a similar age. Nannofossils are abundant throughout most of the section, but a decrease in numbers was noted in the lower portion of Core 597-6. Preservation is moderate, with poor preservation associated with the lower abundance in Core 597-6. Overgrowths increase downhole and preservation becomes poorer (Samples 597-7,CC and -8,CC). Most discoasters, which are presumably *Discoaster deflandrei*, show rays that are almost totally fused together; placoliths are heavily overgrown by secondary calcite.

Specimens of *S. ciperoensis* are few to common in most samples, and *S. distentus* was not observed. *D. deflandrei* is the most dominant discoaster. *Cyclicargolithus floridanus* is also abundant, with *C. abisectus* beginning to dominate the placoliths downsection. *Dictyococcites bisectus* makes its first appearance within this zone; it is rare in abundance, increasing in numbers towards the bottom. *S. moriformis* and *S. dissimilis* are generally more common. *Triquetrorhabdulus carinatus* are few to common throughout.

SEDIMENTATION AND ACCUMULATION RATES

Sedimentation rates were calculated for both Holes 597 and 597A by using nannofossil zone boundaries (Table 3; Figs. 8 and 9). Sedimentation rates have been very low at both holes during the past 17.0 m.y. Below the early/middle Miocene boundary the rates increase, and they are higher throughout the rest of the section. The interval between 0.3 m sub-bottom depth in Core 597-1 (Pleistocene in age) and 1.4 m (early to middle Miocene in age) in both holes lacks calcium carbonate.

Mass accumulation rates were calculated for Holes 597 and 597A (Table 3) by using the sedimentation rates determined by nannofossil biostratigraphy and dry bulk densities calculated from averaged porosity and grain densities (see Physical Properties). The equation for mass accumulation rate is $R = S[(1 - P)\rho]$, where S is sedimentation rate, P is porosity in percent, and ρ is grain density. Mass accumulation rates decreased by two orders of magnitude, from 0.69 to less than 0.005 g/(cm^2 $\times$ 10^3 yr.), in sediments younger than 14.2 Ma. The timing of the change in rates coincides with a shallowing in the CCD in the Pacific that began near the early/middle Miocene boundary and is responsible for the poorer preservation and/or the absence of carbonate microfossils in sediment younger than about 16 to 17 Ma (van Andel et al., 1975). In addition, Moore et al. (1978) showed that hiatuses began to increase in abundance in the southeastern tropical Pacific at 15 Ma, a phenomenon that became most widespread at about 12 Ma. A combination of dissolution and erosion is probably responsible for the extremely low sedimentation and mass accumulation rates in the section younger than the early/middle Miocene boundary (Table 3). The deepening of basement as the crust on which Site 597 is located spread away from the Mendoza Rise and cooled probably amplified the effect of the shallowing CCD.

PHYSICAL PROPERTIES

Sediment Measurements

The sediment physical properties measured at Site 597 included wet bulk density, porosity, compressional sonic velocity, thermal conductivity, and electrical resistivity. Since the first HPC hole, Hole 597, was to be very heavily sampled, it was decided to make detailed measurements only on cores from the second HPC hole, Hole 597A. Each parameter listed above was measured once per section in Hole 597A, and all parameters were measured within the same 5- to 10-cm interval in the section. In addition, each section of each hole was run through the GRAPE (gamma ray attentuation porosity evaluator), generating a set of measurements (Boyce, 1976)

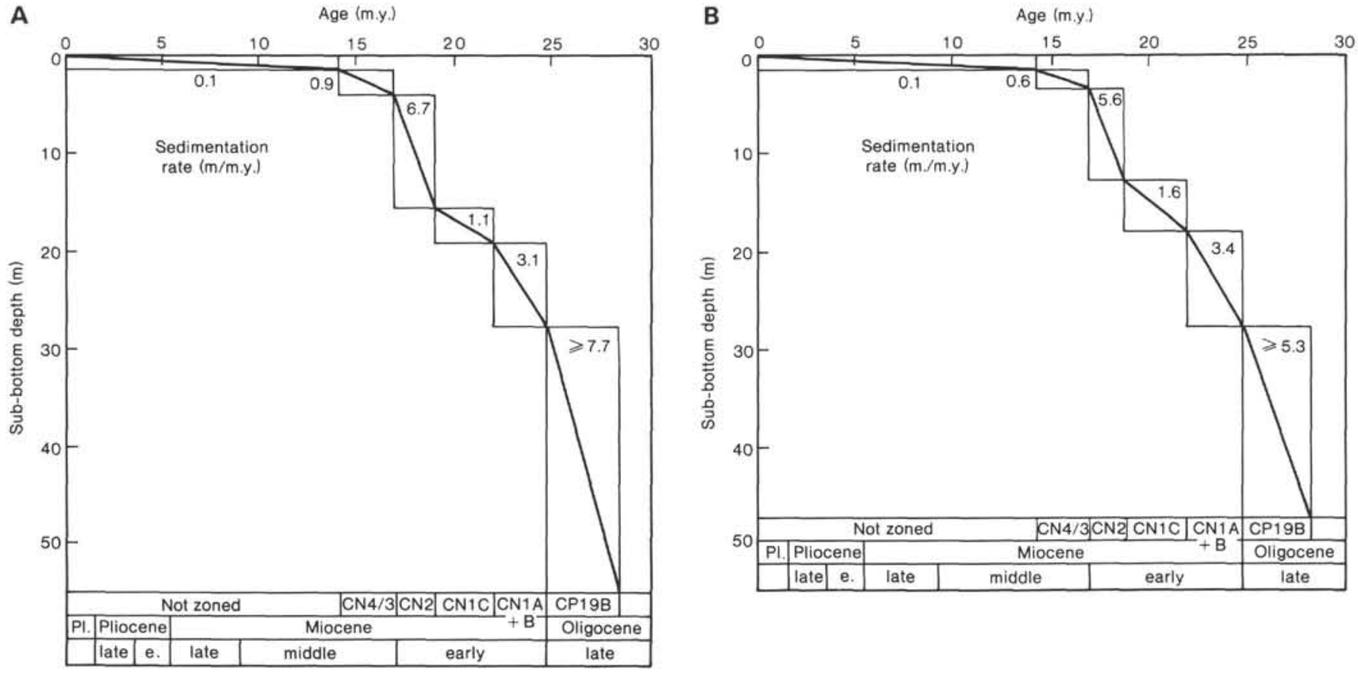

Figure 9. Sedimentation rates. A. Hole 597. B. Hole 597A.

Table 3. Sedimentation and accumulation rates, Holes 597 and 597A.

Depth interval (m)	Age (Ma)	Sedimentation rate (m/m.y.)	Dry bulk density (g/cm^3)	Mass accumulation rate (mg/[cm^2 × 10^3 yr.])
Hole 597				
0–1.5	0–14.2	0.1	0.511	5
1.5–4.1	14.2–17.0	0.9	0.774	72
4.1–15.5	17.0–18.7	5.8	1.026	688
15.5–19.2	18.7–22.0	1.6	1.113	125
19.2–27.8	22.0–24.8	3.1	1.052	323
27.8–54.7	24.8–28.3	≥7.1	0.975	≥750
Hole 597A				
0–1.5	0–14.2	0.1	0.66	7
1.5–3.4	14.2–17.0	0.6	0.92	55
3.4–12.9	17.0–18.7	5.6	0.92	515
12.9–18.2	18.7–22.0	1.6	0.92	147
18.2–27.8	22.0–24.8	3.4	0.95	323
27.8–46.5	24.8–28.3	≥5.3	0.91	≥482

that when processed on shore provided continuous plots of density and porosity versus depth. All measurements were made at atmospheric pressure and an ambient temperature of 25 to 26°C.

The sonic velocity measurements were made with a Hamilton frame velocimeter, across a split core in liner; that is, parallel to any natural horizontal stratification. The wet bulk density and porosity measurements resulted from the gravimetric analysis of samples in stainless steel cylinders. These techniques for making velocity and density–porosity measurements are standard for DSDP and are described by Boyce (1976).

Electrical resistivity was measured with a simple, four-electrode apparatus that was similar to that described by Manheim and Waterman (1974), but the accuracy of the apparatus was uncertain. Measurements were made by inserting the electrodes into the split core in its liner. Readings were taken both across and along the split core liner. A significant cell factor due to the liner was apparent: values taken along the split core averaged about 10% higher than those taken across the core. Because of this cell factor and the undetermined accuracy of the apparatus, results are presented as apparent "formation factors," normalized to the readings obtained with surface seawater at 25 to 26°C. Formation factor is defined as the ratio of the resistivity of the porous matrix (R_m) to that of the pore fluid (R_f), and it generally bears an inverse square relationship to porosity (Archie, 1942): $F = R_m/R_f \cong \phi^{-2}$. The resistivity of surface seawater was used to approximate that of the pore fluids, which is reasonable as long as the salinity of the pore fluids does not vary significantly. The conversion to formation factor removed the cell effect due to the liner. The values presented here are averages of the formation factors calculated for the two electrode/sample geometries. Although the values themselves are of uncertain accuracy (probably no better than ±10 to 20%), the relative variation downhole is realistic.

The thermal conductivity measurements were made with a digital needle-probe apparatus (Von Herzen and Maxwell, 1959), which has an inherent accuracy of about ±5%. The paper tapes produced by this apparatus could not be read on board, so the data were reduced after the leg.

Sediment Measurement Results

The physical properties data, and sample means and standard deviations, are listed and plotted in Table 4 and Figure 10, respectively. The mean porosity values of 60 to 65% for the clay-bearing carbonate oozes cored at Site 597 are fairly typical. With the exception of the uppermost 10 m, the mean values fit the data well; that is, the physical properties show no evidence of lithification processes in the 42 m sampled. The significant down-

Table 4. Sediment physical properties, Hole 597A.

Core	Section	Sub-bottom depth (m)	Wet bulk density (g/cm^3)	Uncorrected for salt: Porosity (%)	Uncorrected for salt: Grain density (g/cm^3)	Corrected for salt: Porosity (%)	Corrected for salt: Grain density (g/cm^3)	Sonic velocity (km/s)	Acoustic impedance (Gg/m^2·s)	Formation factor
1	1	0.75	1.27	79.8	2.34	80.7	2.29	1.52	1.93	1.86
	2	2.27	1.46	69.7	2.51	70.5	2.49	1.50	2.19	2.00
	3	3.68	1.47	70.3	2.57	71.1	2.56	1.49	2.19	2.19
2	2	6.86	1.55	64.2	2.52	64.9	2.51	1.52	2.36	2.17
	3	8.35	1.56	58.0	2.33	58.7	2.32	1.52	2.37	2.19
	4	9.87	1.54	65.4	2.56	66.1	2.55	1.51	2.33	2.10
	5	11.37	1.61	59.2	2.50	59.9	2.48	1.52	2.45	2.35
	6	12.77	1.66	56.3	2.51	56.9	2.50	1.54	2.56	2.44
3	2	16.59	1.63	56.1	2.43	56.7	2.42	1.55	2.52	2.49
	3	18.10	1.62	58.6	2.49	59.3	2.48	1.53	2.48	2.36
	4	19.72	1.63	58.1	2.51	58.8	2.50	1.54	2.51	2.64
	5	21.18	1.57	61.2	2.47	61.9	2.46	1.53	2.39	2.22
	6	22.35	1.56	58.8	2.37	59.5	2.36	1.54	2.40	2.61
4	1	24.73	1.52	58.4	2.25	59.1	2.24	1.51	2.30	2.74
	2	26.16	1.56	60.2	2.41	60.9	2.39	1.52	2.36	2.54
	3	27.75	1.58	61.1	2.50	61.8	2.48	1.52	2.40	2.53
	4	29.20	1.57	61.0	2.45	61.7	2.44	1.51	2.37	2.30
	5	30.74	1.58	61.0	2.49	61.7	2.48	1.52	2.40	2.54
	6	32.17	1.58	63.5	2.58	64.3	2.57	1.53	2.41	2.48
5	1	34.35	1.54	60.1	2.37	60.8	2.35	1.53	2.36	2.38
	2	35.85	1.56	62.1	2.47	62.8	2.46	1.53	2.39	2.39
	3	37.44	1.54	63.1	2.45	63.8	2.44	1.52	2.34	2.26
	4	38.83	1.54	63.2	2.46	63.9	2.45	1.52	2.35	2.57
	5	40.45	1.51	65.0	2.45	65.7	2.44	1.52	2.29	2.25
	6	41.52	1.55	63.1	2.50	63.9	2.49	1.52	2.35	2.27
			1.55	62.3	2.46	63.0	2.45	1.52	2.36	2.36
			0.07	5.1	0.08	±5.2	±0.08	0.01	0.12	0.21

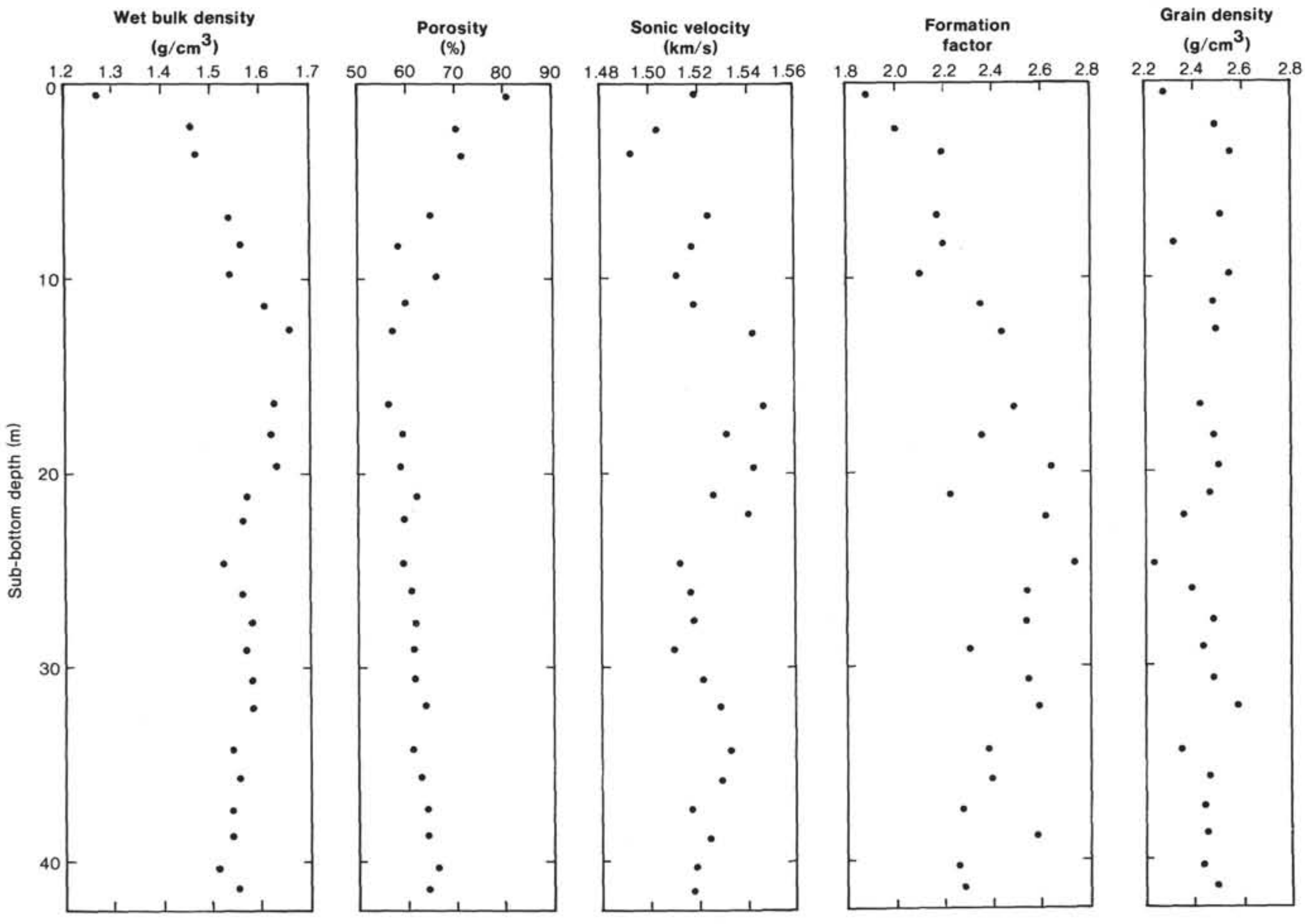

Figure 10. Sediment physical properties, Hole 597A.

hole gradients in the uppermost 10 m (decreasing porosity and increasing density, sonic velocity, and formation factor) are probably related to the amount of calcium carbonate, which decreased as a result of dissolution as the aging, cooling crust passed through the CCD. This pattern does not seem to correlate directly to sedimentation rate, however (Figs. 7, 9).

The downhole trends in density, sonic velocity, and formation factor tend to mirror the trend in porosity. This pattern holds true both overall—in that there are gradients in the upper 10 m and relatively constant values deeper—and, to a lesser degree, in the finer-scale variations. The finer-scale variations are also correlated to changes in the percentage of carbonate in the sediments. Since water content is a function of carbonate content, it is unclear whether the variation in physical properties is due to variations in water content only or to some combination of variations in water content and the properties of the solid component.

The shipboard values of porosity and formation factor are fairly consistent with the simplest form of Archie's law, $F = \phi^{-m}$. A least-squares analysis gave a value for the exponent, m, of 1.9.

Basalt Measurements and Results

Thermal conductivity, sonic velocity, and wet bulk density were measured on 1 to 4 samples of homogeneous basalts from each section of both Holes 597B and 597C (all together, about 30 samples). The samples were kept saturated with seawater at atmospheric pressure, and the measurements were made at laboratory temperatures of 25 to 26°C. The thermal conductivity measurements were made with a half-space adaptation (Carvalho et al., 1980) of the needle-probe technique (Von Herzen and Maxwell, 1959). The sonic velocity and wet bulk density measurements were made by using standard DSDP techniques (Boyce, 1976). Afterward, eight samples from Hole 597C were dried to provide gravimetric estimates of porosities and evaluated for grain density.

The results are given in Table 5 and plotted in Figure 11. The mean values (1.83 W/m-K thermal conductivity, 5.86 km/s sonic velocity, and 2.92 g/cm^3 wet bulk density) are fairly typical of oceanic basalts. The downhole variation of the physical properties corroborates the petrologic division into three major lithologic units. Specifically, the thermal conductivities increase by about 10% at the boundary between Units I and II (100.5 m BSF or 48 m into basement), where the proportion of magnetite in the basalts increases; and sonic velocities increase by about 10% at the boundary between basalt Units II and III (118.5 m BSF or 66 m into basement).

IGNEOUS PETROLOGY

Igneous Basement Recovery

Igneous basement was reached at all four holes, with the recovery of small fragments from Holes 597 and 597A, a short section from Hole 597B, and 48.48 m (of the 91 m of basement drilled) from Hole 597C.

Table 5. Basalt physical properties, Site 597.

Core-Section, interval (cm)	Piece	Wet bulk density (g/cm^3)	Porosity (%)	Grain density (g/cm^3)	Sonic velocity (km/s)	Thermal conductivity (W/m·K)
Hole 597B						
2-1, 12-15	1A	2.83			5.40	1.68
2-2, 106-109	7B	2.93			5.67	1.74
2-3	6					1.73
3-1, 11-14	1	2.89			5.54	1.83
3-2, 47-50	8	2.95			5.96	1.72
3-3	2					1.85
Hole 597C						
3-1, 119-122	6	2.71			5.15	1.62
3-2, 119-122	4	3.00	2.3	3.05	5.89	1.68
3-3, 29-32	2	2.84			5.49	1.72
4-1, 114-117	1G	2.88	6.9	3.02	5.46	1.77
4-2, 136-139	5E	2.97			5.75	1.75
4-3, 82-85	3A	2.94	4.0	3.02	5.74	1.84
4-6, 45-48	4B	2.91			5.77	1.81
5-2, 57-60	7	2.91			5.81	1.74
6-1, 114-117	12A	2.93			5.89	1.73
6-4, 122-125	10	2.86			5.32	1.82
7-1, 50-53	2C	2.97			6.13	1.77
7-2, 47-50	1C	2.95	3.0	3.02	6.11	1.79
7-2, 51-54	1C	2.92			5.95	
7-4	8B					1.76
7-5	7					1.84
8-1, 128-131	2B	2.96	5.5	3.07	5.50	1.96
8-1, 134-137	2B	2.92			5.55	
8-2	1C					1.87
8-3	9A					1.97
8-5, 35-38	1C	2.92			5.60	1.93
9-1, 99-102	4D	2.92			5.58	1.97
9-3, 49-52	1C	2.91			5.50	1.93
10-2, 130-133	1I	3.00	1.9	3.03	6.41	2.01
10-2, 135-138	1I	2.97			6.48	
10-5, 66-69	1D	2.96	1.7	2.99	6.58	1.92
10-7, 71-74	1G	2.93			6.08	1.95
11-1, 104-107	2F	2.93			6.11	1.92
11-3, 31-34	1B	2.95	2.3	3.00	6.30	1.87
11-3, 35-38	1B	2.94			6.40	

Hole 597

Two meters of rock fragments were recovered in Core 597-8; the largest fragment is about 5 cm long. All the fragments studied are vesicular fine-grained basalts that exhibit spherulitic texture and oxidative weathering. They are very similar to the rocks recovered from the uppermost basement in Holes 597B and 597C.

Hole 597A

About 25 cm of rock fragments were recovered in Sample 597A-7,CC. The rock is a basalt glass breccia. It contains angular clasts, up to 2 cm across, of fresh basaltic glass covered by 2-mm rinds of palagonite. The matrix is pink to white in color and comprises fine-grained phillipsite, calcite, and minor iron oxyhydroxide, and it contains drusy cavities partially filled by well crystallized calcite.

Hole 597B

At this hole, 24.6 m of igneous basement were penetrated and 5.4 m were recovered (in Cores 597B-2 and -3), a recovery of 22%. The rock is a fine- to medium-grained basalt, which probably makes up one or more massive flows; no pillow textures were recognized. Two fine-grained zones, possibly chilled contacts, can be seen (one in Section 597B-3-1 and one in Section 597B-3-2), although they are of minor lithologic significance. The

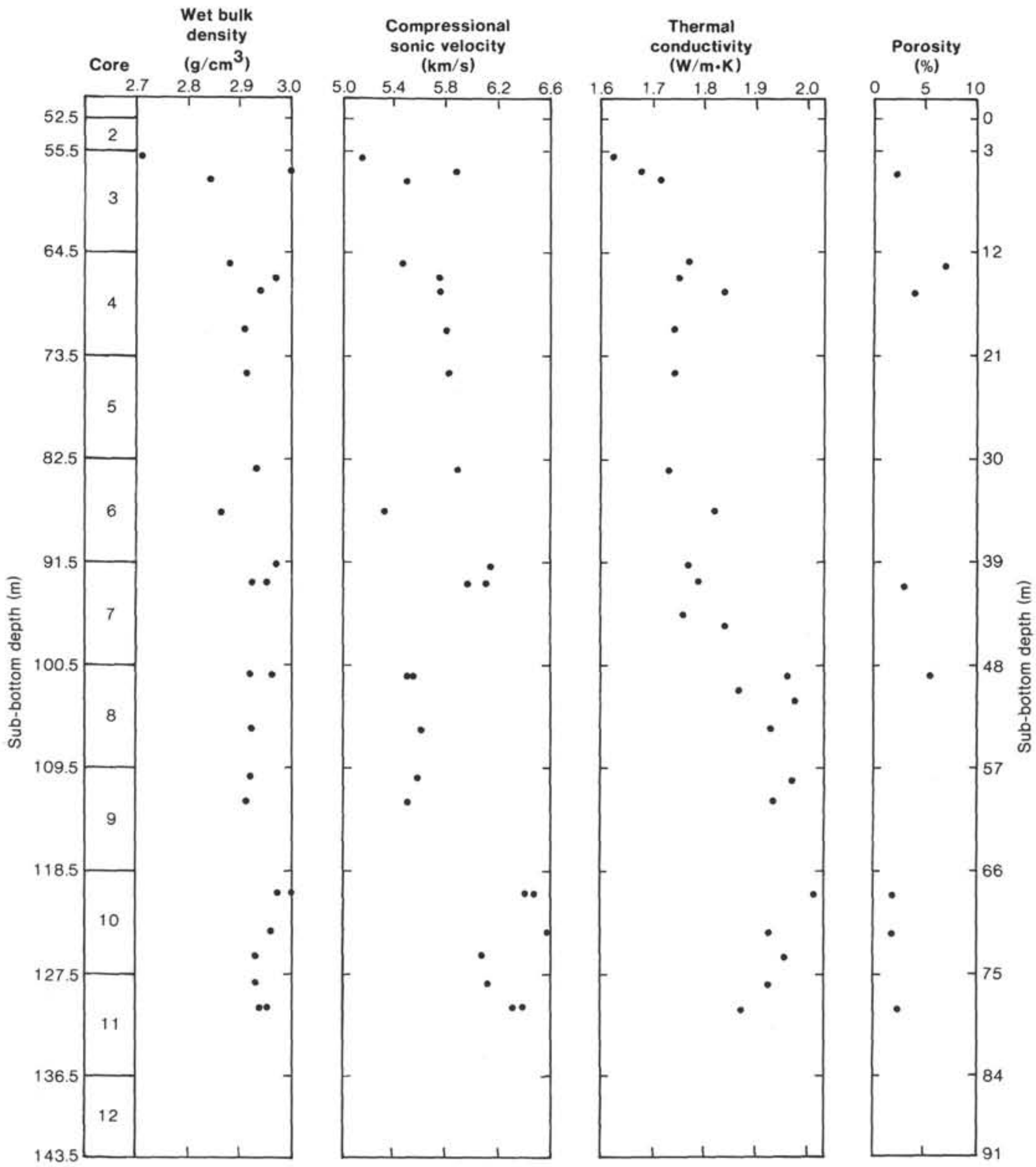

Figure 11. Basalt physical properties, Hole 597C.

rocks are typically aphyric to sparsely plagioclase microphyric and contain a small proportion of plagioclase-rich crystal aggregates (glomerocrysts). The mineralogy is, in average order of abundance, plagioclase, clinopyroxene, magnetite, glass, and olivine. Textures vary from spherulitic through intersertal to intergranular. Olivine and glass are completely altered to palagonite, iddingsite, and various smectites. The rocks are all moderately vesicular (5 to 15% by volume) and fractured. Oxidative alteration has affected over two-thirds of the rocks recovered and is characterized by calcite, aragonite, phillipsite, iron oxyhydroxides, and brown smectite in veins, vesicles, and the basalt. The products of earlier alteration events (e.g., green smectite, celadonite, and palagonite) can also be identified occasionally. The rocks therefore resemble those in basalt Unit I in Hole 597C (see below).

Hole 597C

Because of the depth to which igneous basement was cored at this hole (91 m) and the high rate of recovery (53.2%), more core was recovered from Hole 597C (48.48 m) than has been recovered from any other hole drilled in fast-spreading crust. Rock was recovered in Cores 597C-3 through -12, with a maximum recovery of 94% (in Core 597C-8). The discussion below summarizes the findings of the examination of hand specimens of the core and the preliminary findings of microscopic and X-ray diffraction (XRD) studies.

Lithologies

The predominant lithology is a fine- to medium-grained gray basalt that has undergone incipient to moderate alteration. The uppermost core (597C-3) is moderately vesicular (greater than 5% vesicles by volume), the next three cores are slightly vesicular, and the remainder are virtually nonvesicular. The first 5-cm piece of core contains a curved glassy margin 3 mm thick (the only fresh glass in the core) and may represent a pillow fragment. However, the remainder of the core contains no pillow lava characteristics and is assumed to represent massive flows. In the upper part of the section, where recovery was low (notably in Cores 597C-3 and -5), the drilling may have penetrated, but failed to recover, pillowed units; but in the lower part of the section (Cores 597C-7 to -12), recovery was high, and that in addition to the general continuity of the petrology provides convincing evidence that pillowed units were absent in the lower part of the section.

There are no contacts that can be used to define cooling units unequivocally. Most promising are fine-grained, dark gray zones, normally 10 to 20 cm thick, which may represent chilled margins. None of these show any evidence of surficial submarine weathering and are therefore assumed to represent minor boundaries, such as sheet flow margins in a composite massive flow. There is, however, petrographic evidence for the presence of three distinct lithologic units, which we have termed Units I, II, and III. The boundary between Units I and II is defined as the change from olivine-bearing to olivine-free basalts; the contact is not visible in recovered core and is inferred to lie between Sections 597C-7-5 and -8-1. The boundary between Units II and III is defined as the point of reappearance of olivine and is marked by a fine-grained zone in Section 597C-10-2.

Primary Mineralogy

All the rocks exhibit basaltic mineralogy, containing, in average order of abundance, plagioclase, clinopyroxene, magnetite (probably titanomagnetite), olivine, glass, and minor phases such as primary sulfides and spinel. The texture varies from holohyaline (in the uppermost piece only) through spherulitic, intersertal, and intergranular to poikilophitic.

Unit I (52.5 to 100.5 m BSF)

This unit exhibits mainly subspherulitic and intersertal textures in its upper part and subophitic textures toward its base. The rocks classify as aphyric, rarely plagioclase microphyric, if they are described on the basis of the content of isolated crystals of relatively large grain size. It is common, however, to find glomerocrysts of plagioclase or plagioclase and olivine, which can occupy up to 5% of the total volume of the rock. Grain sizes within the unit typically range from less than 0.1 to 2 mm for plagioclase, olivine, and clinopyroxene and less than 0.15 mm for magnetite. The typical mineral composition is 40 to 60% of plagioclase, 30 to 50% of clinopyroxene, 2 to 5% of magnetite and titanomagnetite, 0 to 10% of glass (or cryptocrystalline groundmass), and 0 to 5% of olivine.

Unit II (100.5 to 121.3 m BSF)

This unit is dominated by intergranular and poikilophitic textures. Where the latter texture is best developed (in Core 597C-8), pale brown augite crystals up to 1 cm or more in size enclose numerous plagioclase laths and subhedral crystals of titanomagnetite. The latter can reach 1 mm in size and can be seen in reflected light to contain exsolution lamellae of ilmenite and to carry inclusions of primary sulfide. Olivine is absent in this unit.

Unit III (121.3 to 143.5 m BSF)

Unit III is also dominated by intergranular and poikilophitic textures. It differs from Unit II, however, in the ubiquitous presence of olivine and in the much lower abundance of inclusions within the titanomagnetite. The olivine is typically euhedral and ranges in grain size from 0.1 to 2 mm.

Each of the three units described above contains a number of fine-grained zones: 11 in Unit I, two in Unit II, and four in Unit III. However, because these fine-grained zones cannot be unequivocally described as chilled margins, lithologic subunits have not been defined.

Secondary Mineralogy

A preliminary investigation of the sequence of alteration in the basalts and the frequency of vesicle and vein filling suggests that water–rock reactions may have taken place in three stages.

The first stage is characterized by the formation of a pale blue trioctahedral smectite (saponite; XRD identification), which is deposited in vesicles and which replaces the cryptocrystalline or glassy groundmass and olivine crystals in rocks that are otherwise unaffected by alteration. It is encountered very rarely in veins.

The second stage is characterized by the presence of dark green (sometimes blue green or black) smectite (XRD identification). Accompanying minerals (preliminary XRD identifications) may include paler green celadonite, talc, and chlorite (in deeper levels only). Mica and a black manganese oxide may also be present. Sulfide minerals (pyrite and chalcopyrite) and native copper have also been identified in many parts of the core in association with this alteration assemblage. This alteration type is most commonly found in veins and in vein alteration halos. In the veins themselves, a complex mineralogy may be present. In the alteration halos, it is most common to find glass and olivine totally replaced by a dark green smectite, although it is not certain whether it is primary glass and olivine or the secondary saponite that has actually been replaced by the smectite. Dark green smectite may also replace saponite in vesicles or fill vesicles. Such vesicles sometimes contain sulfides, and secondary sulfides (and occasionally native copper) have even been found in the groundmass of very altered rocks.

The third stage is characterized by the assemblage calcite, aragonite, zeolite, iron oxyhydroxide, and brown smectite (preliminary XRD identification). The zeolite is phillipsite in the upper part of the core and phillipsite with possible chabazite (preliminary XRD identification) at lower levels. This alteration type is quite pervasive in some intervals of the uppermost part of the section, but at deeper levels it commonly occurs only as alteration halos around veins. Where present it sometimes replaces the products of earlier stages of alteration in the rock and in vesicles. In larger veins, zeolites and calcite can occupy central, drusy cavities.

By analogy with more detailed work on the products of alteration in the oceanic crust (e.g., Bass, 1976b) it is possible that the first stage of alteration represents deuteric alteration, that the second stage represents nonoxidative diagenesis, and that the third stage represents oxidative diagenesis. It will be noted that there are some differences between the sequence described above and that described by Bass (1976b) for the basalts of Leg 34. The differences may be real or may simply reflect the cursory nature of our shipboard observations.

In general, the intensity of alteration decreases with depth, probably partly as a result of a decrease in vesicularity and fracture spacing. The intensity of first stage (deuteric) and third stage (oxidative) alteration is significantly greater in the upper part of the section. However, the products of the second stage of alteration can best be seen in the lower part of the section, where, although less abundant originally, they are less often replaced by the products of oxidative alteration.

Veins and Vesicles

Both veins and vesicles become less abundant with increasing depth. Vein spacing decreases from about 5 cm in the uppermost part of the section to about 15 cm in the lowermost part. Veins normally vary from very thin to about 1 mm in thickness, although there are two prominent irregular veins (in Section 597C-4-7) that reach a thickness of 1 cm. A preliminary study suggests that the veins have two main orientations: about 30° to the vertical and close to horizontal. As mentioned earlier, the proportion of vesicles decreases rapidly with depth, and the lower half of the core is almost nonvesicular. The vesicles are usually subspherical and have diameters ranging from 0.5 to 1 mm. The mineral filling of both veins and vesicles reflects the sequence of alteration. The vesicle zonations are complex where several pulses of fluid have been involved. Where oxidative alteration has taken place, calcite commonly occupies the centers of vesicles and veins.

Summary

The basalts recovered from Hole 597C can be tentatively divided into three major lithologic units. Each unit is made up almost entirely of massive flows, some thick enough to have cooled slowly and to have produced poikilophitic texture. The basalts appear to be typical ocean-ridge tholeiites; they are olivine-bearing in Units I and III and olivine-free in Unit II. The rocks have undergone at least three stages of alteration, the last of which is oxidative alteration. The sequence of vesicle and vein filling corresponds to this alteration history. The results are broadly consistent with observations made during DSDP Legs 34 and 54, which also acquired samples from fast-spreading oceanic crust, although the ratio of massive flows to pillows at Site 597 appears to be the greatest so far encountered.

INTERSTITIAL WATER STUDIES

At this site, nine interstitial water samples were obtained on board ship by squeezing pore water from cores from Hole 597, two such samples were obtained from Hole 597A, and one was obtained from Hole 597C. In addition, one successful *in situ* sample was taken in Hole 597A at 14.5 m BSF. Unfortunately, an attempt to acquire another *in situ* sample from this hole (at 47 m BSF) obtained pipe water (a mixture of surface water, mud, and pore water).

All the laboratory samples were obtained from the cores by squeezing 10-cm core sections at room temperature (about 25°C), with the exception of Sample 597C-1-4, 140–150 cm, which was squeezed at 12.9°C. A shipboard comparison of the data from these two temperatures and the data from the *in situ* sample allowed us to work out an optimum program for the sites to be drilled subsequently.

Methods

We analyzed the constituents of the water by various means and methods, which are stated below along with the precision of measurement:

Salinity: Goldberg refractometer, ±0.3%.

Chloride: Potentiometric and Mohr titrations, ±0.5%.

Calcium: EGTA titration, ±1%.

Magnesium: EDTA titration, corrected for Ca, ±1%.

Potassium, lithium and sulfate: Wescan ion analyzer: K, ±0.5 mM; Li, not precise at seawater concentrations; SO_4, ±1 mM (occasionally erratic). The Wescan process is very laborious; 13 pore water samples and interspersed standards take well over 10 hr. of analysis time.

Alkalinity: Potentiometric Gran titration, ±2%.

Nitrate: Cu-Cd reduction to nitrite, colorimetric diazo compound method, ±5%. The nitrate values were erratic, especially those from the large volume squeezers. The Scripps all-plastic squeezer, however, yielded results in close agreement with the *in situ* sample and the results of Bender et al. (1985) from the site survey cruise. Experimentation with large filter papers established that these papers may contain as much as 1 μM of nitrate, which is probably left after Whatman's filter cleaning process (HNO_3?). Washing the filters proved effective in removing this contaminant, and all further work was carried out with washed filters. We decided to accept the plastic squeezer data uncorrected on the basis of the good agreement with the *in situ* sample.

Ammonia: Colorimetry–Solorzano method, ±10% or lower at concentrations less than 4 μM.

Silica: Molybdenum blue, colorimetry, ±2%. Silica content was determined in samples contained in glass vials that were used for further sample storage. This affected the silica data, but by using a kinetic dissolution curve obtained both on board ship and in the shore laboratory, we were able to correct these data to ±10 μM.

Results

The data gathered from this site indicate that the site is essentially dead with respect to sediment–pore water interaction, with the possible exception of carbonate dissolution. Sedimentation during the last 10 to 15 m.y. has been very slow, and any organic diagenetic signals like those at younger sites in the Pacific have died away, either because current diagenesis is insignificant or because diffusive processes, which tend to annihilate any signals caused by diagenetic reactions, dominate. Because of the conservative nature of some of the major constituents, particularly K and Mg, this site does provide an excellent opportunity to study sampling artifacts (the effects of sampling interstitial waters at other than *in situ* temperature and pressure). A large amount of work has been done on the so-called temperature-of-squeezing artifact; see for instance Gieskes (1973) and Sayles et al. (1973). Table 6 (after Sayles et al., 1973, and Gieskes, 1973) summarizes the effects of the temperature of squeezing (4° and 23°C) established during Leg 15.

The sediments obtained from Site 597 are clayey nannofossil oozes. An interesting problem occurs with calcium. Although the temperature-of-squeezing effect is negative (Table 6), the dissolved calcium in both the *in situ* sample and the squeezed water samples from Site 597 measured at room temperature and pressure is greater than that of the sample measured at 12.9°C. This increase occurs because the pressure effect more or less cancels the temperature effect; that is, the calcium depletion caused by squeezing at about room temperature is more than made up for by an increase caused by the difference between the pressure on the system during squeezing (about 1 atmosphere) and the *in situ* pressure. The two effects largely cancel because both ion exchange and solubility effects are present. The same applies to alkalinities.

Table 6. Effects of sampling temperature (4° to 23°C) on constituents of squeezed interstitial water.

	Clays and marls	Calcareous sediment	Siliceous sediment
Change in K			
meq	+1.6 (±2)	+1.2	+0.6
%	+20 (±2)	+16	+12
Change in Ca			
meq	−0.8	−1.3	−1.1
%	−5 (±2)	−3.1	−1
Change in Mg			
meq	−5.5	−2.5	−0.7
%	−7	−3	−1.4
Change in Si (μM)	+50 (±20)	+60 (±20)	+100 (±20)
Change in alkalinity (meq dm^{-3})	—	+0.2	+0.2

Note: + denotes enrichment, and − depletion, with increasing temperature. Values for K, Ca, and Mg are based on Sayles et al. (1973); values for Si and alkalinity are from Gieskes, 1973. Dash indicates no data.

Below we briefly comment on the interstitial water data, which are presented in Table 7 and Figure 12.

Calcium: The effects discussed above show up quite clearly. The samples at 50 m BSF indicate a reduction in Ca due to temperature (12.9 versus 25°C). When corrected for this effect, the *in situ* sample shows reasonable agreement with the 25°C squeezed data. We conclude that the slight downcore increases in dissolved calcium in the upper 10 m are real and probably reflect the dissolution of calcium carbonate. This in turn suggests the migration of Ca and possibly the continuing dissolution of carbonates in the upper 10 m of this site.

Magnesium: The observed downhole decreases in Mg are due almost entirely to temperature-of-squeezing artifacts. If the difference between the *in situ* value at 47 m and the bottom water value is real, a very small gradient (2 mM/50 m) might exist, but this is pure speculation.

Potassium: The temperature-of-squeezing effect is particularly pronounced in potassium at this site. Enrichment due to this effect is greatest in the more clayey sections of the upper few meters and in the basal sediments. The *in situ* value is slightly less than the bottom-water value, but the difference is not significant.

Silica: Silica values from the squeezed samples, as expected, are higher than the *in situ* value. Bender et al. (1985) report concentrations of about 180 μM at $\approx$1.5 m; our *in situ* sample suggests a value of about 208 μM at 15 m. The main value of all this information is that it confirms the constant contribution to dissolved silica of the noncarbonate fraction. A small increase in silica in the lowermost part of Hole 597 may represent a slight increase in clay content.

Nitrate: In spite of the previously mentioned measurement difficulties, we believe that Figure 12, which is based on uncontaminated data only, presents a realistic profile. The bottom water value is from Bender et al. (1985). This profile would be a reasonable continuation of the Bender et al. (1985) profiles and would suggest that nitrification occurs in approximately the upper 15 m, roughly the same zone in which the dissolution of carbonate is apparent.

Alkalinity: Not much change occurs downhole, as expected.

Ammonia: Low, but nonzero concentrations of <6 μM occur throughout.

Sulfate: A small decrease appears to occur with increasing depth. However, we are not sure whether the decrease (of about 2.3 mM) is significant.

Chloride and salinity: As expected, no significant downhole variations in these constituents were observed.

Conclusions

1. With the exception of calcium and nitrate, the major constituents of interstitial water at this site show essentially conservative distributions. The production of calcium in the upper 10 m is presumably associated with carbonate dissolution, and the production of nitrate (maximum about 45 μM) is the result of nitrification occurring in the upper 10 to 15 m of the sediment column.

Table 7. Interstitial water chemistry, Site 597.

Sample (interval in cm)	Sub-bottom depth (m)	pH	Alkalinity (meq dm^{-3})	Ca (mM)	Mg (mM)	K (mM)	Cl (mM)	SO_4 (mM)	NO_3[a] (μM)	NH_4 (μM)	SiO_2 (μM)	S (‰)
Hole 597												
1-2, 140-150	3.0	7.57	2.68	10.89	49.6/49.8	11.2	554	27.0	59	4 ± 1	276	35.2
2-2, 140-150	7.6	7.77	2.69	11.09	49.7	10.6	552	27.4	70	5.5 ± 1	278	35.2
2-4, 140-150	10.6			11.09	49.5	10.9	547	27.4	46	2 ± 1.5	298	35.2
3-2, 140-150	17.2	7.70	2.77	10.97	50.5	11.2	555	27.8	68	5.5 ± 1	300	35.2
3-4, 140-150	20.2	7.64	2.62	10.92	50.6	11.7	557	27.8	63	6 ± 1	307	35.2
4-2, 140-150	26.8	7.73	2.64	11.15	50.0	11.6	560	28.4	70	3 ± 1.5	302	35.5
4-4, 140-150	29.8			11.09	50.0	11.8	558	28.0/27.4	66	3 ± 1.5	302	35.5
6-2, 140-150	46.0	7.83	2.98	10.93	47.5	13.1/12.9	563	26.2	85	5 ± 1	297	34.9
6-4, 140-150	49.0	7.75	2.79	11.29/11.17	47.0	12.9	559	26.2	72	4.5 ± 1	339	34.6
Hole 597A												
1-1, 140-150	1.5	7.71	2.69	10.79	48.9	12.4	554	26.2	55	3 ± 1.5	274	34.9
1-2, 140-150	3.0			10.75	49.6	11.2	565	26.2	53	6.5 ± 1	267	35.5
In situ 1	14.5			11.31	53.3	10.0	566	27.0	46	5.5 ± 1	208	35.5
In situ 2[b]	43.0			10.79	55.3		604	28.0	18	4 ± 1	0	36.6
Hole 597C												
1-4, 140-150	49.5	7.55	2.32	10.65	51.0	11.7	558		45.65			35.0

Note: All Li concentrations were <27 μM (i.e., surface water). Values with slash indicate replicate determinations on same sample.
[a] Data above 45 μM are suspected of resulting from pollution during squeezing.
[b] Data are suspect; *in situ* water sampler triggered in hole as a result of delay in triggering; hence, water sampled is a mixture of surface water and formation water.

2. Temperature-of-squeezing artifacts are particularly evident in the data for Mg, K, and silica.

PALEOMAGNETISM

Eleven samples from Hole 597B and 58 samples from Hole 597C were measured for paleomagnetism. One or two oriented samples (2.54 cm in diameter) were taken from every section of each core. Natural remanent magnetization (NRM) was measured by using the onboard Digico spinner magnetometer. The noise level of the magnetometer was less than 1×10^{-7} emu/cm^3. All measurements were made by using 128 rotations to increase the signal-to-noise ratio. At first, the values read from the magnetometer fluctuated because the rock holder did not fit the shaft. This problem was not severe, but it took a long time to ascertain the reason for it. Alternating field demagnetization was not carried out. Low field susceptibility (χ) was measured with a susceptibility meter. Koenigsberger ratio (Q), the ratio of the intensity of NRM to that induced by the Earth's field at the sampling site (0.36 Oe), was also calculated.

Koenigsberger ratio is used as a measure of stability. In general, a rock with Q of ≥ 1.0 is suitable for paleomagnetic study. Koenigsberger ratios and measurements of NRM intensity, susceptibility, inclination, and declination are presented in Table 8. The values of declination are shown for reference, although they are not very meaningful because the cores are not oriented.

Figure 13 shows the results for Hole 597B. NRM intensities and inclinations, susceptibilities, and Q ratios for Hole 597C are shown in Figure 14.

The average NRM intensity and susceptibility in Hole 597B are $1.6 \pm 1.0 \times 10^{-3}$ emu/cm^3 and $1.5 \pm 1.2 \times 10^{-3}$ emu/cm^3 Oe, respectively.

The average NRM intensity in Hole 597C is $3.4 \pm 2.0 \times 10^{-3}$ emu/cm^3. There is a sudden increase in intensity in Section 597C-4-1; thereafter intensity decreases slowly to the bottom of the hole, except for prominent peaks in Sections 597C-7-2 and -7-4. The Q ratios also tend to decrease downhole.

Inclinations were calculated with respect to the horizontal plane, positive down. It was assumed that each core was drilled vertically. A positive inclination indicates reversed polarity at this latitude (18°48′S). All samples except two (Samples 597C-7-4, 137-140 cm and -7-5, 70-73 cm) showed reversed polarity. These two normal values are not measurement artifacts, because the values of susceptibility and Q ratio in the same samples are not abnormal. Some relationship may exist between the two normal values and the peaks in NRM intensity that lie slightly upsection.

The mean inclinations for Holes 597B and 597C are 60 ± 9° and 57 ± 12°, respectively. These values are much greater than the 34° value calculated for this site (a dipole field is assumed). High inclination angles were also reported for Sites 319 and 320 (Ade-Hall and Johnson, 1976). The mechanisms proposed to explain this discrepancy (Ade-Hall and Johnson, 1976) include secular variation, geomagnetic excursions, tectonic rotation, or a change in NRM, none of which is particularly satisfying.

HEAT FLOW

In Holes 597 and 597A, attempts were made to measure heat flow both with the Barnes/Uyeda/Kinoshita pore water/heat flow sampler and with the Von Herzen VLHPC heat flow tool. Two attempts were made to measure temperature in Hole 597, both with the VLHPC tool, but both were unsuccessful for mechanical rea-

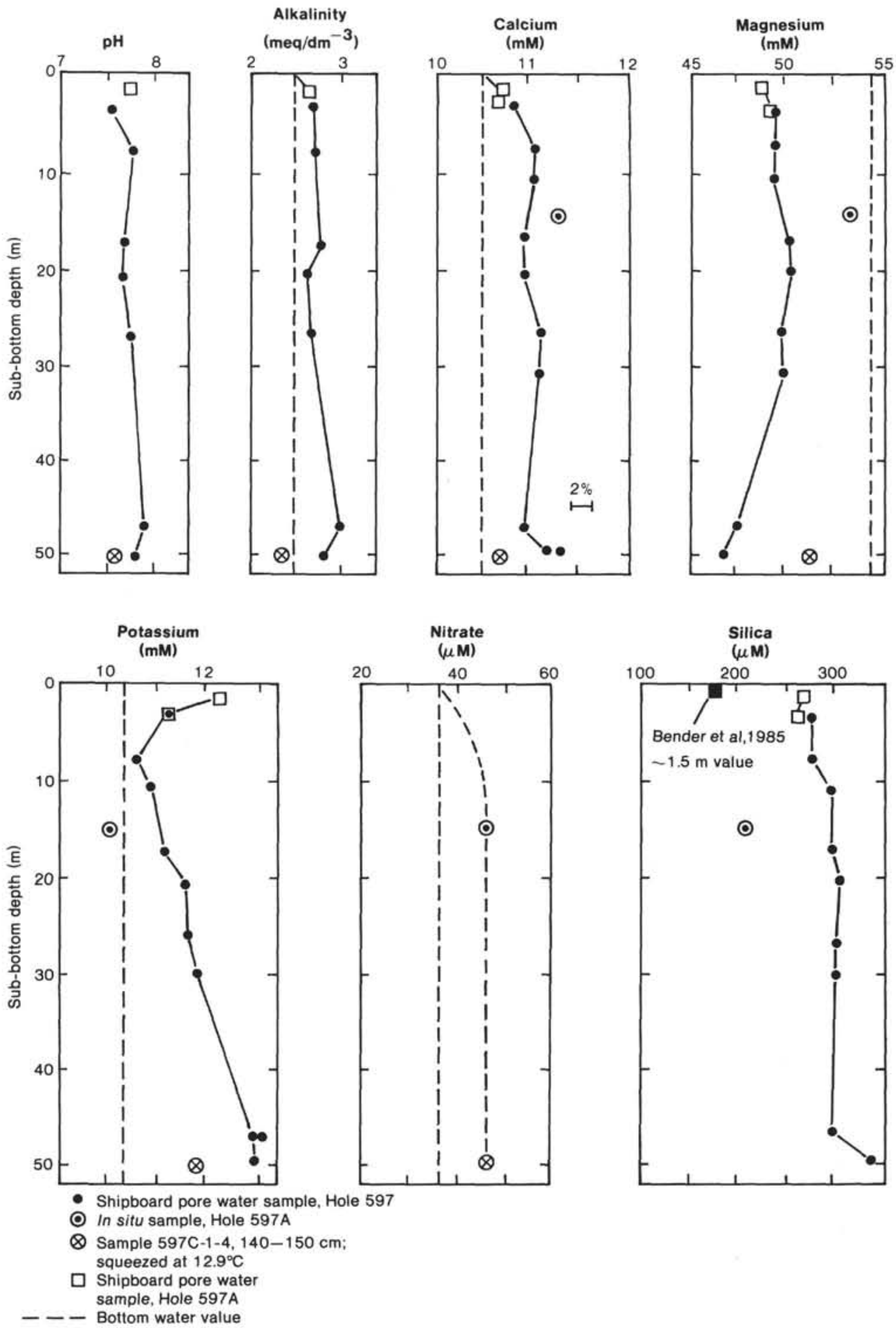

Figure 12. Interstitial water chemistry, Site 597.

sons. Six attempts were made to measure temperature in Hole 597A using the VLHPC and the pore water/heat flow sampler. Two temperatures were measured successfully with the VLHPC tool. The temperature gradient is 115 m/km, and the heat flow is 89 mW/m^2.

The cutting shoe of the VLHPC is designed to hole the heat flow tool and its battery pack (Fig. 15). The shoe is made of high strength maraging iron 250, so the thermistor can be within 5 mm of the outer surface of the shoe and still be protected against pressure. The heat flow instrument fits into a cavity in the shoe wall (Fig. 15). The battery pack fits onto a similar, adjacent cavity, with a connecting cable running through a slot between them. One disadvantage of the design is that the tolerances around the heat flow instrument and the battery pack are very small. The connecting cable comes out of the side of the battery pack and can be fitted into the slot with relatively few problems. The connection to the

Table 8. Paleomagnetic results, Holes 597B and 597C.

Core-Section (interval in cm)	Piece	NRM intensity (G × 10^3)	χ (G/Oe × 10^3)	Q	NRM inclination (°)	Polarity[a]	NRM declination (°)
Hole 597B							
2-1, 17-20	1A	1.34	1.03	3.64	66.5	R	121.8
2-1, 83-85	5B	0.82	0.76	3.02	65.2	R	322.9
2-2, 45-48	2	0.26	1.25	0.57	56.7	R	276.0
2-2, 110-113	7B	1.99	0.51	10.93	65.4	R	321.9
2-2, 131-134	9	0.88	1.86	1.32	47.5	R	129.9
2-3, 29-32	3A	0.94	0.55	4.68	63.3	R	85.1
2-3, 114-117	12	2.20	0.55	11.16	73.4	R	9.7
3-1, 3-6	1	2.29	3.28	1.94	62.9	R	58.7
3-1, 132-135	8	1.33	0.39	9.56	41.5	R	61.1
3-2, 23-26	1B	1.50	2.05	2.03	53.0	R	305.8
3-2, 40-43	2	4.02	3.80	2.94	61.7	R	311.5
Hole 597C							
3-1, 21-24	2	1.55	0.62	6.90	53.8	R	172.4
3-1, 131-134	7	1.75	2.43	2.00	68.9	R	137.1
3-2, 40-43	2B	4.14	4.56	2.52	55.2	R	326.8
3-2, 143-146	5B	0.53	0.39	3.76	31.3	R	18.8
3-3, 5-8	1	0.89	0.43	5.72	72.2	R	126.5
3-3, 52-55	3	0.69	0.41	4.71	56.9	R	285.3
4-1, 60-63	1D	3.75	0.77	13.44	51.3	R	342.7
4-1, 120-123	1G	6.70	3.25	5.73	58.9	R	342.3
4-2, 21-24	2A	7.12	4.75	4.17	59.7	R	16.9
4-2, 111-114	5B	3.77	2.71	3.87	84.4	R	281.3
4-3, 27-30	1B	5.99	4.11	4.05	81.4	R	75.3
4-3, 91-94	3B	5.27	4.59	3.19	73.2	R	39.4
4-4, 23-26	1B	5.15	4.65	3.08	67.6	R	332.8
4-4, 76-79	2C	3.18	1.60	5.51	54.6	R	331.7
4-5, 26-29	3	4.72	3.80	3.45	58.1	R	16.1
4-5, 71-74	5A	3.10	5.70	1.51	56.7	R	6.8
4-6, 21-24	2	4.05	5.19	2.16	82.7	R	12.3
4-6, 73-76	5	1.14	0.39	8.02	46.2	R	0.0
5-1, 129-132	18	0.97	0.38	7.00	51.0	R	311.4
5-2, 63-66	7	3.93	0.52	20.87	49.9	R	24.7
6-1, 109-112	12A	4.25	0.89	13.21	50.5	R	343.2
6-2, 49-52	4	1.47	2.07	1.97	47.7	R	29.6
6-3, 62-65	3	3.51	3.32	2.93	71.2	R	45.9
6-4, 74-77	1L	3.38	2.43	3.87	71.3	R	273.5
6-5, 58-61	4E	2.66	0.74	10.01	37.8	R	3.6
7-1, 115-118	3D	5.86	3.40	4.79	75.9	R	130.2
7-2, 16-18	1B	7.22	3.55	5.66	51.8	R	355.5
7-2, 117-120	4B	11.57	2.86	11.23	60.3	R	206.6
7-4, 18-21	2A	6.04	1.54	10.91	67.6	R	56.6
7-4, 87-90	8B	14.51	3.80	10.62	56.8	R	280.7
7-4, 111-114	10A	6.42	3.31	5.38	70.4	R	210.6
7-4, 137-140	11	3.56	4.52	2.19	−56.9	N	348.8
7-5, 70-73	7	2.70	4.61	1.63	−85.3	N	71.4
8-1, 9-11	1A	1.56	4.01	1.08	60.1	R	328.9
8-1, 94-97	2A	3.61	3.32	3.02	56.9	R	80.7
8-2, 50-53	1B	4.31	3.18	3.77	51.2	R	57.6
8-3, 5-8	1	3.63	3.04	3.32	44.0	R	236.9
8-3, 130-133	9B	1.94	3.81	1.41	54.2	R	128.2
8-4, 102-105	6B	3.36	4.30	2.17	47.8	R	50.0
8-5, 60-63	1E	3.80	4.46	2.37	36.8	R	341.2
8-6, 56-59	1E	2.09	4.61	1.26	43.3	R	25.4
8-7, 9-12	1A	2.69	4.15	1.80	40.9	R	350.3
9-1, 9-12	1	4.04	5.92	1.90	51.5	R	7.0
9-1, 142-145	6C	3.06	4.12	2.06	51.6	R	336.8
9-2, 70-73	4B	3.87	5.01	2.15	65.2	R	228.6
9-3, 88-91	1F	2.23	4.81	1.29	82.9	R	160.9
9-4, 103-106	4E	6.19	5.18	3.32	45.5	R	4.5
10-1, 112-115	9B	3.23	4.36	2.06	50.1	R	294.5
10-2, 104-107	1M	3.14	5.24	1.67	54.0	R	8.8
10-3, 94-97	1G	2.26	4.05	1.55	54.4	R	353.7
10-4, 91-94	2A	1.36	2.93	1.29	53.5	R	26.0
10-5, 84-87	1E	1.68	2.84	1.64	49.7	R	355.6
10-6, 36-39	1C	1.94	3.80	1.42	61.0	R	327.2
10-7, 42-45	1C	1.74	3.16	1.53	65.4	R	344.6
11-1, 79-82	2D	1.05	3.12	0.94	54.9	R	36.0
11-2, 103-106	2	1.85	2.04	2.52	60.5	R	228.9
11-3, 13-15	1A	1.50	1.93	2.16	44.8	R	38.0
11-4, 62-64	4	1.47	1.84	2.21	53.7	R	105.2

[a] R = reversed, N = normal.

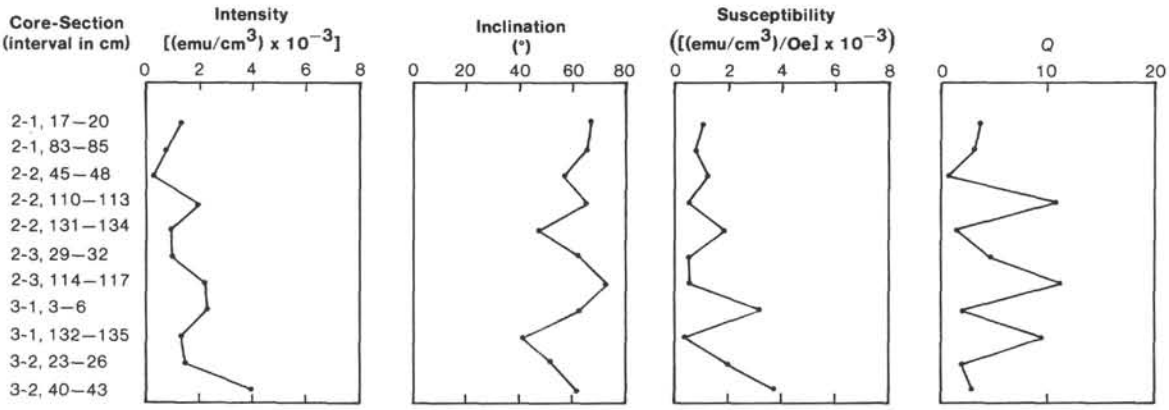

Figure 13. Magnetic properties of basalt samples from Hole 597B.

heat flow instrument, however, is made through a plug on the end of the instrument, and there is very little room for the plug and cable between the end of the instrument and the bottom of the core-barrel connecting sub, which screws in on top of the cutting shoe.

Both of the failures that occurred at Hole 597 are related to this battery-instrument connection. One failure occurred when the connecting sub caused the battery plug to become bent over and forced partially out of the socket. The other occurred when the connecting sub pinched the cable and shorted it out. There may also have been a short circuit on the heat flow tool caused by the abrasion of the insulating potting compound on a lower part of the tool.

We repaired the heat flow tools by insulating the abraded portion and straightening the bent pins in the plug. We spent a considerable amount of time carefully sanding the heat flow instruments and their battery packs in order to ensure an easy fit into the slots in the cutting shoe.

We attempted to measure heat flow at Hole 597A six times to make sure we had a good heat flow measurement at the site. Four attempts were made with the Von Herzen VLHPC probe, and two good measurements were obtained. Two attempts were made with the Barnes/Uyeda/Kinoshita sampling tool, with no usable results.

The Von Herzen tool worked at depths of 14.2 and 33.4 m. The other two measurement attempts failed. One failure resulted from the improper handling of the tool in the lab and on deck. The instrument is designed so that if a delay in the start of the data acquisition is programmed, the tool will not start the program if it is kept on its side for 1 min. after the delay program is activated. The tool then has to be vertical for 5 min. before the regular program (including the programmed delay) is activated. We did not handle the tool within the proper time limits, and it went through the data acquisition cycle on deck instead of in the hole. We do not understand the second failure. The instrument appeared to operate correctly, but it failed to output data properly. Only 30 values were transmitted before the tool stopped functioning, and all the subsequent attempts to recover data were unsuccessful. Both of these failures occurred with temperature tool number 5, which had checked out correctly during bench tests and programmed tests.

The two attempts to acquire heat flow data with the Barnes/Uyeda/Kinoshita sampler in Hole 597A were unsuccessful. On the first attempt, a switch in the sampler broke, so no temperature data were obtained. On the second attempt, the timer was set for too short a delay, and we sampled water and temperature in the pipe, not in the sediment.

The two temperature measurements successfully obtained with the Von Herzen VLHPC probe were corrected to *in situ* temperatures by following the procedures of Horai and Von Herzen (1985). The results are shown in Figure 16. The two sediment temperatures and the known bottom water temperature of 1.55°C give a consistent gradient of 0.115°C/m. The sediment thermal conductivity of samples from Hole 597A was measured with a needle-probe apparatus, but the output from this apparatus was could not be reduced at sea, so the thermal conductivity for the surficial sediments at this site, 0.77 W/m-K, was used to calculate heat flow. The resulting heat flow is 89 mW/m^2. This value is plotted in Figure 17 along with the heat flow results from the site survey.

The value we obtained is in good agreement with the data from the site survey. If the change in thermal conductivity with increasing depth is assumed to be constant, the measurement at Hole 597A extrapolates to a sediment-basement temperature of 7.3°C. This value compares with the extrapolations from the site survey data of 4.7°C in the northeast to 9.2°C in the southwest.

The mean of all the heat flow values at this site is 71.3 mW/m^2, with a standard deviation of 21.1 mW/m^2. The theoretical value for 25-Ma crust is 55 mW/m^2. The small number of measurements precludes a decision as to whether the crust is sealed from fluid exchange with the ocean, although variability of over a factor of 2 across the site does suggest that circulation is continuing within basement.

DOWNHOLE LOGGING

The downhole logging program at Site 597 had high priority on Leg 92. Site 597, a re-entry hole with high basalt recovery in crust formed at a fast-spreading ridge, will provide a valuable comparison with other deep re-entry holes that have been logged, such as Hole 504B,

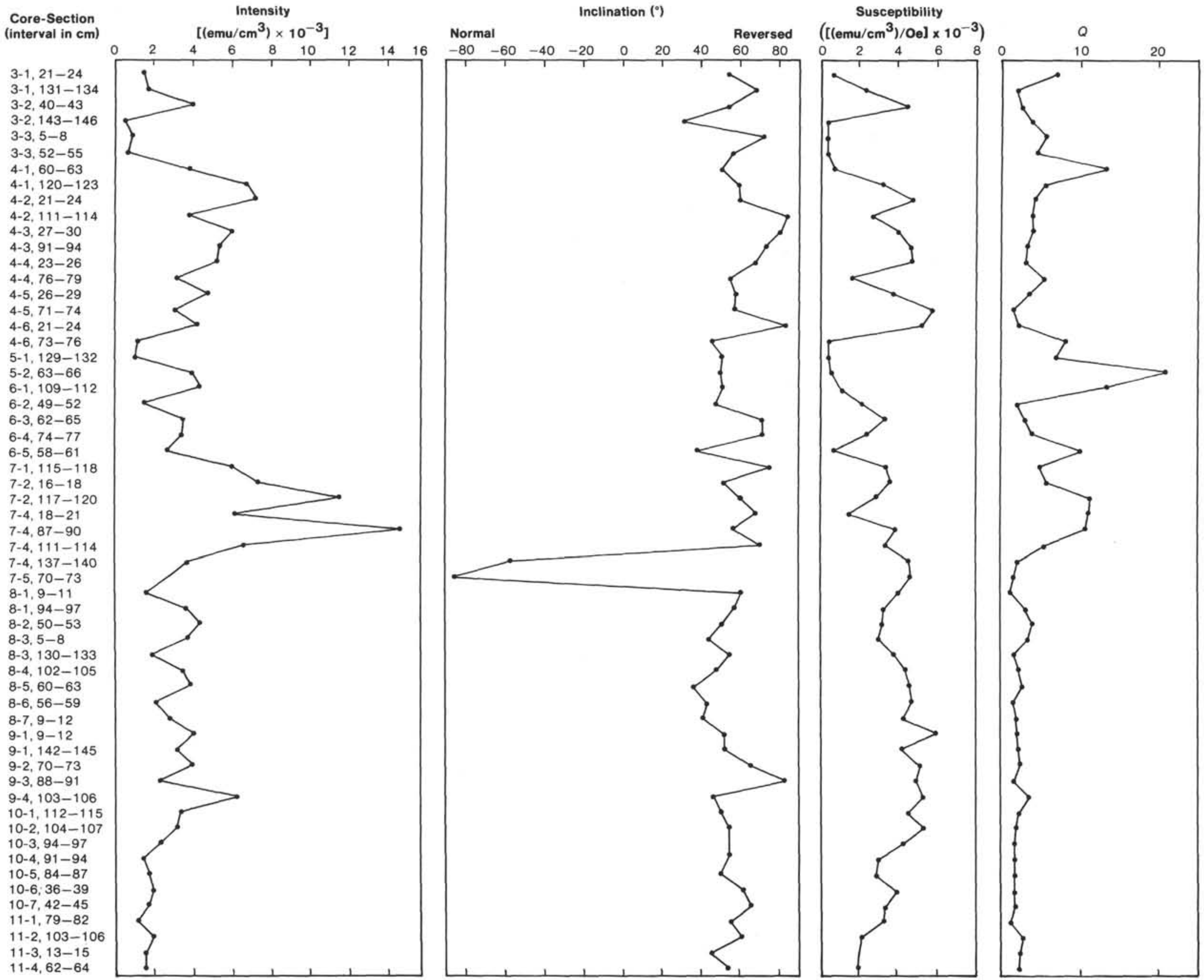

Figure 14. Magnetic properties of basalt samples from Hole 597C.

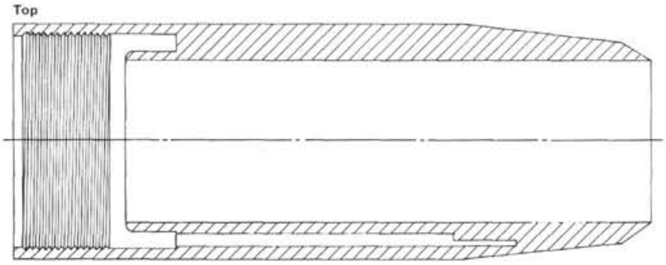

Figure 15. Cutting shoe of the VLHPC for downhole temperature measurement. The shoe is made of maraging iron 250. The slot is for the temperature recorder, with a small hole at the bottom for the thermistor. A similar slot exists for the battery pack.

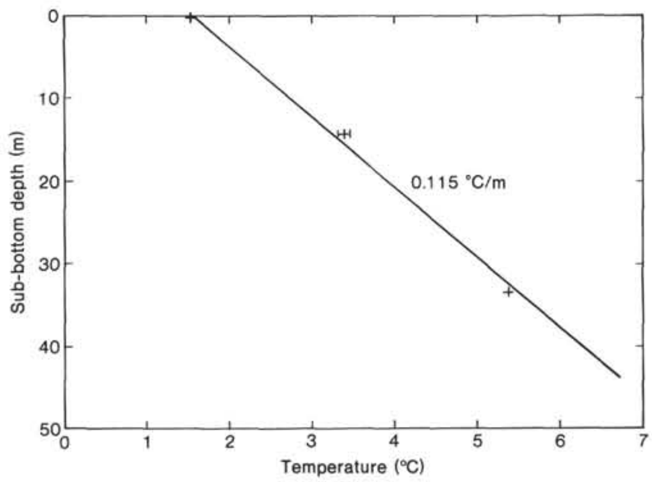

Figure 16. Temperature versus depth at Hole 597A.

on the moderately fast-spreading Costa Rica Rift, and Hole 395A, on the slowly spreading Mid-Atlantic Ridge.

Geophysical logging of DSDP boreholes has previously been performed by contract logging companies using standard oil field techniques. These techniques were developed primarily for use in holes drilled through sedimentary rocks, and therefore they are not necessarily optimum for characterizing the properties of rocks in the upper oceanic crust. Nevertheless, the low core recovery in DSDP boreholes (generally no greater than 50%) has encouraged the continued use of these standard logs, which permit intervals of low or no recovery to be characterized in addition to the intrinsic properties of the recovered basalts and the gross properties of the *in situ* material.

Recently, a number of experimental logging and downhole measurement and analytical techniques have been used in deep-sea drill holes. Downhole logging was carried out in two holes at Site 597, Holes 597B and 597C. The 12-channel sonic log was tested in Hole 597B, the pilot hole. A full range of logging tools was used at Hole 597C, including multiple caliper logs, two borehole televiewer (BHTV) logs, and the 12-channel sonic log. The caliper logs and the BHTV logs obtained excellent data. The 12-channel sonic log failed to operate correctly as a result of damage to the internal wiring in the hydrophone section.

Caliper Log

Tool Design and Logging Operation

The caliper logs were run with a three-arm caliper tool built by Comprobe, Inc., of Crowley, Texas (model 2110-3A). This tool is lowered to the bottom of the hole and is then commanded to extend its three caliper arms. These arms are arranged around the tool at 120° intervals and are inclined downward, so that as the tool moves up the hole during the logging run the arms do not catch on projections or irregularities and get stuck. The use of arms in the design permits this tool to detect smaller irregularities in the wall of the borehole than the Schlumberger caliper tool, which uses bowsprings. The range of the arms permits the tool to measure hole diameters from less than 4 in. (10 cm) to greater than 20 in. (51 cm). The change in the resistance of the potentiometer varies the amount of current that passes through the cable, and it is this current variation that is recorded at the surface. The tool must be calibrated while it is attached to the logging cable, since the resistance of the cable affects the current flow and is indistinguishable from the potentiometer signal from the caliper tool.

Four caliper log runs were made in Hole 597C. The multiple runs were made to determine the best speed for the caliper log and to obtain more data about the hole's shape (since the tool is not oriented and the arms contact only a small portion of the hole walls). The first two logs were run at 4800 ft./hr. (0.41 m/s), and the second two were run at 2400 ft./hr. (0.20 m/s). The chart recorder speed was decreased from 10 in./min. (0.42 cm/s) to 5 in./min. (0.20 cm/s) correspondingly to make the records comparable.

The pipe was lowered to determine the depth to which the hole was clear, and a slug of drilling mud was pumped through and clear of the hole. Hole depth was 4290 m below rig floor (130 m BSF), indicating that some 13.5 m of debris had accumulated in the bottom of the hole (it had been drilled to 4303.5 m [143.5 m BSF]). The pipe was raised to 4223 m (63 m BSF) for the first two caliper runs. Depth was monitored by connecting a pair of switches on the wireline meter counter to a computer. This circuit was calibrated so that one revolution of the counter shaft corresponded to 0.5 m of wire movement. We entered the bottom hole depth determined from pipe length into the computer and counted uphole from that value as we ran the log. The logs indicated that the tool entered the mouth of the drill pipe at exactly the correct counter reading, so our depth control was accurate to 0.5 m.

The first two caliper runs were successful, but there was an unexplained offset in the data at 4232 m (72 m BSF) on the second run (Fig. 18) that indicated a sharp reduction in hole diameter. The offset was not apparent on the other runs, and the apparent constriction could have been caused by the arms getting stuck or being struck by a piece of debris from the wall.

We pulled the pipe up to 4208.5 m below rig floor (48.5 m BSF) in order to log as complete a section of the hole as possible, including the sediment-basement contact. The next two logs were run at a speed of 2400 ft./

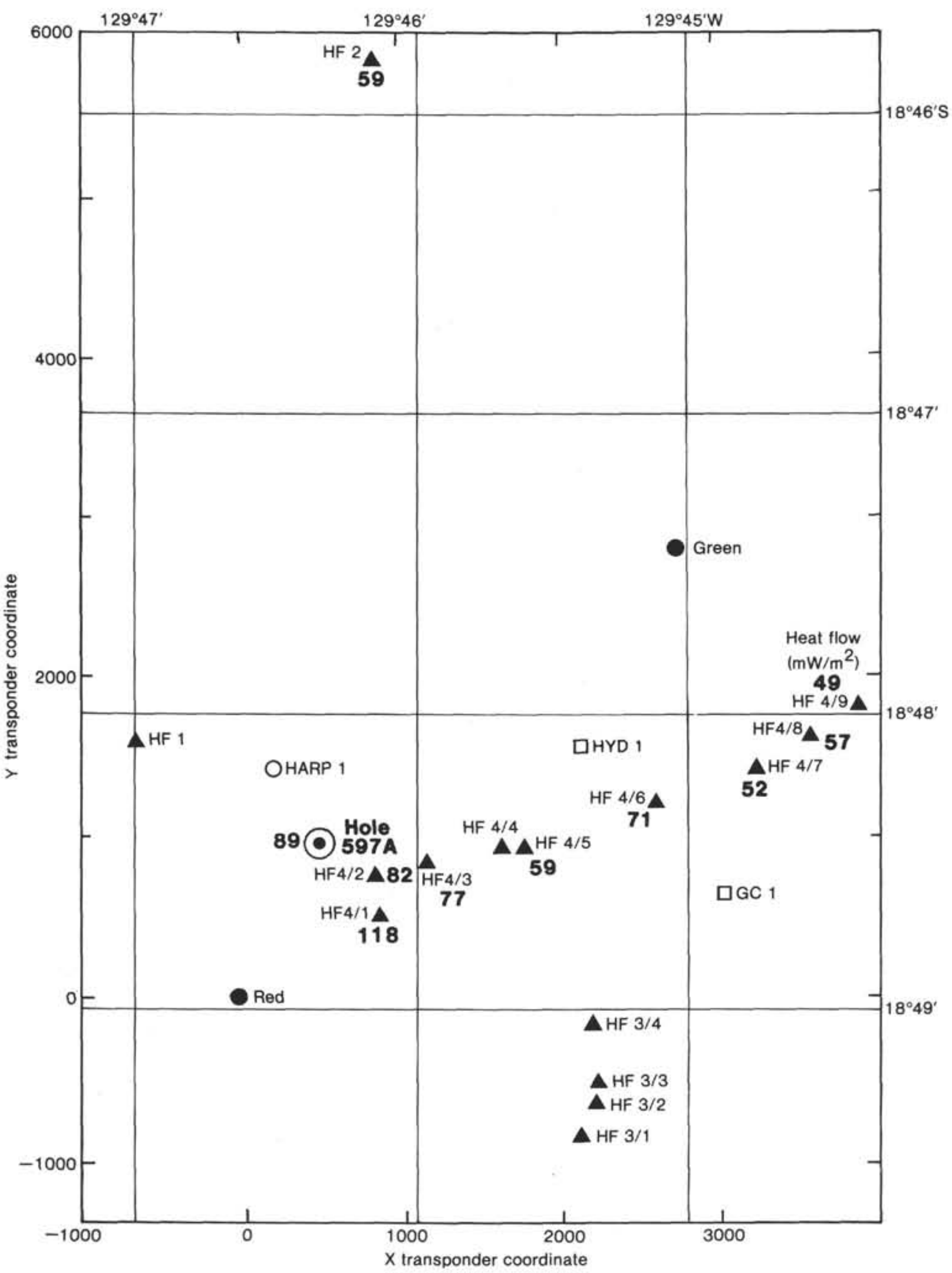

Figure 17. Heat flow values at site survey stations and at Hole 597A. Code numbers for multipenetration heat flow stations (e.g., HF 3/4) indicate the heat flow run and the penetration number. Points marked Red and Green were the locations of long-lived transponders left in the area in order to position the *Glomar Challenger*.

hr. (0.20 m/s) to determine whether slower speeds would permit greater resolution and to avoid anomalies like that at 4232 m (72 m BSF) in run 2. The two slow speed logs were successful and had no problems.

The Comprobe caliper log appears to be a reasonably reliable and very useful tool. It could be improved by using a four-wire resistance connection and by feeding the output directly through an analog-to-digital converter to a computer. The computer could also be used to acquire depths simultaneously. The data would then be available in digital form for use at sea and on shore without the inconvenience and delay of digitizing the chart records. The log could also be played back onto a chart recorder at whatever scale was desired by using a digital-to-analog converter. This arrangement could be set up fairly easily and cheaply, since the HP-1000 computer on board ship is set up to convert seismic signals. Logging would simply add another analog-to-digital channel.

Caliper Log Results

The results of the four logging runs are summarized in Figure 18. This figure was made by tracing the chart

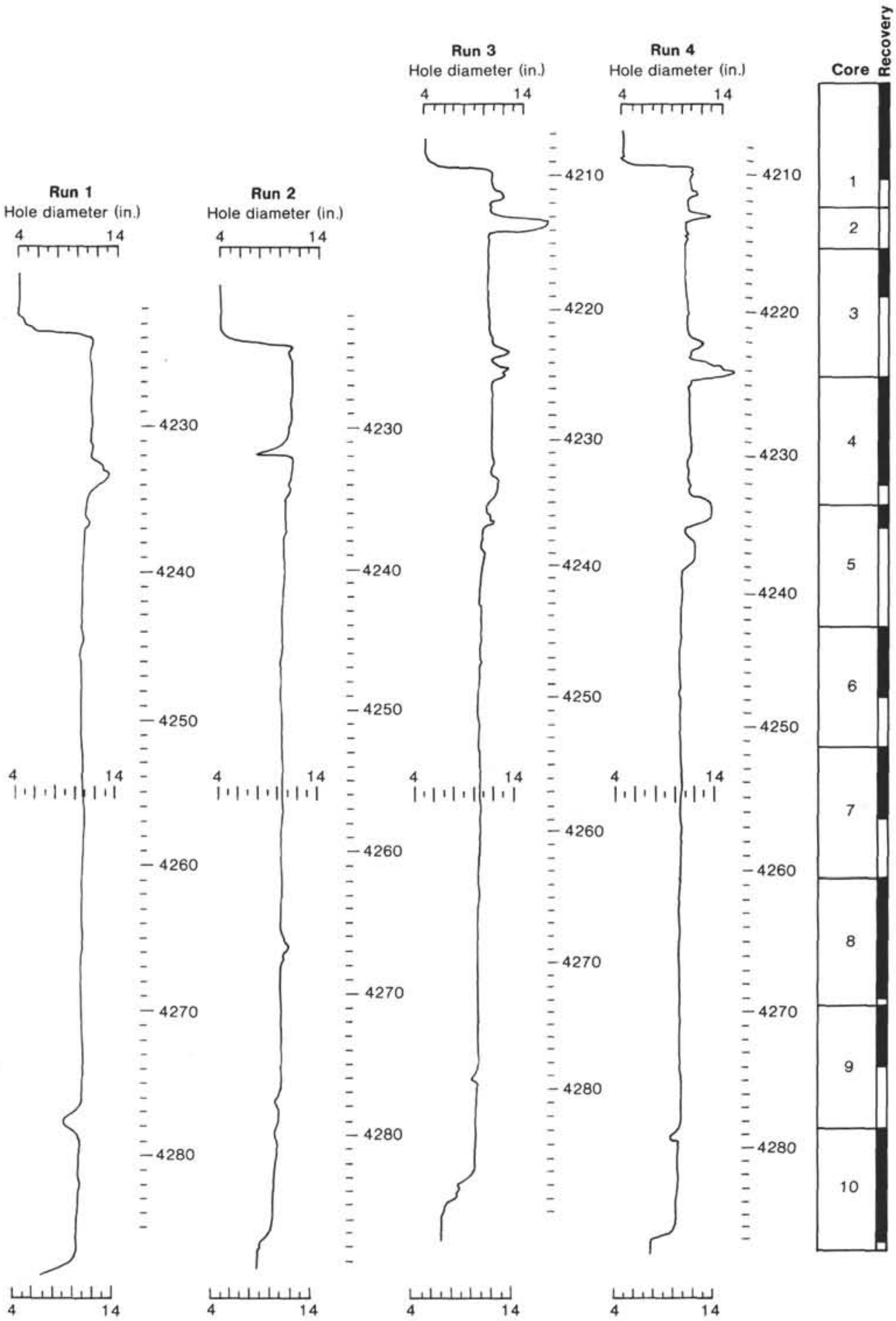

Figure 18. Tracings of the four caliper runs in Hole 597C. Runs 1 and 2 were done at 4800 ft./hr. on the logging winch and 10 in./min. on the chart recorder. Runs 3 and 4 were done 2400 ft./hr. and 5 in./min., respectively. Depths below rig floor for each run are noted to the right of its record. Ticks are at 1-m intervals. Hole diameter scales run from 4 to 14 in. and are corrected for logging cable resistance. The core boundaries shown are drawn with respect to the depth scale for run 4. Core recovery is shown in black.

records and annotating them with the depths from the electronic depth circuit. A hole diameter scale corrected for cable resistance effects had been added. The cored intervals and a bar graph representing the recovery from each core has been drawn next to the depth scale for caliper run 4. The depth scales for the four runs differ slightly as a result of variations in winch speed.

The results of the caliper logs show three important features. The first is that most of the hole is quite uniform in diameter (about 10.7 in. or 27 cm). The second is that there are three areas of larger hole diameter in the upper part of the hole that can be correlated between logs. The three areas of larger diameter each show two maxima in hole diameter, separated by about 2 m. The third feature is that near the bottom of the logged interval (about 4279 m, 119 m BSF), there is a constriction in hole diameter.

The uppermost zone of large hole size is between 4211 (51 m BSF) and 4214 m (54 m BSF), near the base of Core 597C-1 and the top of Core 597C-2. This interval, which is similar in runs 3 and 4, is the depth interval that corresponds to the sediment–basement contact. Holes 597 and 597A recovered basaltic rubble at this contact. The absence of recovery in the lower part of this depth interval in Hole 597C (Core 2) is consistent with the large hole diameter and other evidence of a significant washout of material in this interval.

The second zone of increased hole diameter is near the bottom of Core 597C-3, from 4222 to 4224 m (62 to 64 m BSF). Recovery for Core 597C-3 is 37%. The caliper logs suggest that the material recovered is from the upper part of the cored interval.

There is a much higher rate of recovery (84%) in Core 597C-4 than in the cores immediately above it. The caliper logs show that this core lies between the second and third zones of hole diameter increase. The hole diameter is quite uniform at about 10.5 in. (27 cm) between the two zones.

The third zone of hole diameter increase is near the base of Core 597C-4 and the top of Core 597C-5 (4233 to 4238 m depth, 73 to 78 m BSF). This zone is the only one that was covered by all four of the logging runs, and it is the zone that produces the most variable caliper logs. The increase in diameter in this zone occurs over a greater depth interval than in the zones above. Recovery in Core 597C-5, which is largely from this interval, is only 18%. It seems most likely from the caliper log that the material recovered came from the lower part of the core interval.

The hole diameter is quite uniform below the third zone of hole widening (below 4238 m, 78 m BSF). The logs all show some minor variations in the interval from 4245 to 4248 m (85 to 88 m BSF), but the amount of variation is only about 0.5 in. (1 cm). No variation in hole diameter is apparent thereafter down to 4267 m (107 m BSF), when run 2 shows an increase in diameter of up to 1 in. (3 cm) over a 1-m depth interval.

The final feature of interest is a constriction in hole diameter that is registered in all the caliper runs at about 4278 to 4279 m (118 to 119 m BSF). Runs 2 and 4 show some evidence of a second, smaller constriction about 2 m shallower than the major constriction.

Below 4242 m (82 m BSF; depths represented by Cores 597C-6 through 10), the hole walls are smooth and core recovery is high. The average recovery for these five cores is almost 70%. The lowest two cores show a lower recovery rate (51% and 12%, respectively), but we were unable to log the depth interval for these cores because of debris in the hole. It is not clear how much of the debris represents material from that coring interval. Since the bit was jammed when it came on deck, the debris may also result from the jamming of the drilling bit near the top of Core 597C-12 and the destruction of the material that would have been Core 597C-12.

Borehole Televiewer Log

Tool Capabilities, Design, and Operation

Borehole televiewer (BHTV) logging provides a continuous, complete image of the borehole wall by mapping its ultrasonic reflectivity. A complete map of the borehole shape with depth can be made by displaying the transit time of the ultrasonic signal. Variations in reflectivity caused by void spaces, fractures that intersect the borehole, and textural changes in the rocks can all be mapped. The signals can be immediately photographed to permit visual inspection for features of interest and also stored on video tape to permit later playback and analysis.

The BHTV used on Leg 92 was manufactured by Simplec Corporation and is owned by the U.S.G.S. It was operated as part of a joint U.S.G.S.-Lamont-Doherty Geological Observatory program on board the *Glomar Challenger* on Legs 68, 69, 78B, and 83.

The televiewer operates by emitting a focused ultrasonic beam at one of two frequencies: 1.2 MHz (which produces a 3° beam width) and 500 kHz (which produces a 6° beam width). The transducers emitting the beam also act as receivers and are mounted on an assembly that rotates at a nominal speed of 180 rotations/min. (3 rotations/s). The tool emits ultrasonic pulses at 580-μs intervals (about 1700/s), and as a result it emits about 600 pulses per rotation. A fluxgate magnetometer is also attached to the transducer assembly, and it provides a synchronizing pulse when it is pointed toward magnetic north. The compass pulse, a firing circuit synchronizing pulse, and the received signal data are all transmitted to the surface through the logging cable.

At the surface, these signals are both recorded on video tape and displayed for immediate use. The compass pulse is used to trigger a three-axis oscilloscope to make a horizontal sweep (the oscilloscope has horizontal, vertical, and intensity axes). The firing synchronization pulse is used to adjust the blanking of the signal data, which modulates the intensity of the oscilloscope beam. Using the firing synchronization pulse (i.e., data within a time-gated window) to modulate the beam's intensity ensures that beam intensity will not be adjusted to compensate for a large-amplitude reflection from the plastic boot surrounding and protecting the rotating transducer assembly. The time delay of the window photographed can be adjusted so that only the signal returned from the borehole wall is in the photograph, and the time width of this window can be adjusted. The contrast of the image is controlled by adjusting the level of the blanking. The higher the level of the signal, the more intense the oscilloscope beam and the whiter the photograph.

The BHTV records represent the cylindrical borehole as an unwrapped cylinder with magnetic north at the edges of the image and south in the middle. The compass pulse initiates the scan, which proceeds clockwise from north. The hole diameters as determined from the caliper log indicate that the photographs have a horizontal exaggeration of about 1.7 times.

The experimental arrangement of the televiewer has evolved somewhat since earlier cruises. We used a supplemental DC power supply that doubled the amount of DC power available downhole. We also operated the AC power supply at its maximum rating. This overcame the high power losses in the 30,000-ft. (9.1-km) logging cable. The high pressure–low temperature conditions downhole cause the oil in the tool to become more viscous, which makes it difficult for the transducer assembly to rotate. The power increase helped overcome this problem also and guaranteed maximum torque in the rotating mechanism. It would be advisable in the future to redesign both of the downhole power supply circuits in order to provide a safe margin of operating capability. During our logging runs, it was apparent that the televiewer was rotating its transducer assembly at only about 40% of its normal rate. Thus, the data run off the right margin of the photographs, and as a result only about 350° of the hole circumference are shown. Reprocessing the BHTV records will allow the data to be displayed in a more coherent manner, however.

Tests conducted on deck indicated that the BHTV system was vulnerable to interference from the ship's regular radio and amateur radio transmissions, particularly when the radios operated at high power outputs. This is not surprising in view of our being connected to a 9-km cable, part of which was sitting on deck. We arranged for restricted transmissions while we ran the televiewer logs to eliminate this interference.

We lowered the BHTV to just above the bottom of the hole and tested it before we began the logging run. We used the same kind of depth control for the televiewer logging runs as we had used for the caliper runs. We did not lower the BHTV tool to the bottom of the hole because of the possibility of damaging the plastic window around the rotating transducer head. We started the computer's depth counter circuit at the bottom of the hole, and we used it to provide logging marks that were read aloud on deck and recorded on the audio channel of the video tape recorder. These values were also used to time Polaroid films on the oscilloscope.

The depth marks shown in the BHTV records (Figs. 19 and 20) have been corrected for the depth offset that results from wireline stretch. Experience has shown that when relatively lightweight tools like the re-entry tool or our logging tools are attached to the logging cable, the wireline stretches about 5 or 6 m in about 4000 m. We observed that according to the wireline counter we reached the mouth of the drill pipe at a depth of 4203.5 m (43.5 m BSF) during both BHTV logging runs. The mouth of the drill pipe was being held up (above the bottom of the hole) at 4208.5 m (48.5 m BSF), so the wireline stretched 5 m. The corresponding correction to our starting depths, which were at an indicated depth of 4282 m (122 m BSF), puts the start of the BHTV logs at 4287 m (127 m BSF), almost the same depth as the start of the caliper logs.

Borehole Televiewer High-Frequency Log Results

The first BHTV log run was made with the high-frequency transducer (1.2 MHz) and with the downhole instrument set at a gain level of 4 (out of 6 possible positions) throughout the log. The tool was raised from the bottom of the hole to the top, but we will describe results from the top down. The Polaroid photographs of the high-frequency log are reproduced in reduced form in Figure 19. These are real time records, and they can be filtered during later playback. In all the televiewer images from Hole 597C, the signal strength is very high, which means that the walls of the hole are very reflective. The blanking was decreased considerably when the tool rose above 4272 m (112 m BSF). The logging was done with nearly constant gain about 4272 m. This means that almost all of Figures 19A, 19B, and half of 19C are as bright as the part of Figure 19C between 4272 m and 4273 m (112 to 113 m BSF). The decrease in the returned signal strength below 4272 m (112 m BSF) is real and significant.

The televiewer entered the drill pipe at 4208.5 m (48.5 m BSF). The 2.5-m interval below that depth shows banding with indistinct edges. The area of low reflectivity centered on south may correspond to the small washout recorded by the caliper at 4211 m (51 m BSF). There is a sharply defined band of low reflectivity ranging from north through east to south from 4312.5 to 4213 m (52.5 to 53 m BSF) that probably correlates to the major washout found in the caliper run from 4213 to 4214 m (53 to 54 m BSF).

The borehole below this washout is smooth and reflective. The first visible fracture is at 4213.7 m (53.7 m BSF) and dips to the southeast. Just below this fracture occurs the first of several holes in the next several meters, all centered roughly to the south. The hole is smooth again from 4218 to 4223 m (58 to 63 m BSF). Two fractures dipping to the northwest occur at 4223 and 4223.5 m (63 and 63.5 m BSF).

The depth interval from 4223 (63 m BSF) to 4232 m (72 m BSF) shows prominent vertical banding, and it is hard to pick out possible fractures. It is possible that the dark area centered on south from 4224 to 4225 m (64 to 65 m BSF) is the washout found by the caliper at 4224 m (64 m BSF). The meter below 4232 m (72 m BSF) has a very poor return and probably corresponds to the washout found by the caliper at 4233 m (73 m BSF).

The banding in the signal changes dramatically at 4235 m (75 m BSF), and this probably indicates the washout found by the caliper at 4236 m (76 m BSF). Below this depth the banding, which may indicate either a somewhat irregular hole or a somewhat off-center position for the televiewer, returns.

The borehole appears to become considerably smoother from 4240 to 4242.5 m (80 to 82.5 m BSF). Irregular banding or holes reappear below this depth and continue to 4245.5 m (85.5 m BSF). A major dark area appears at 4246 m (86 m BSF) but does not correspond to anything found on the caliper logs. The hole is quite smooth from 4247 to 4251 m (87 to 91 m BSF). Occasional holes are visible in the next few meters down to 4256 m (96 m BSF). Several fractures are recognizable in this interval. One dips to the southeast at 4252 m (92 m BSF). There is a concentrated area of fractures just below 4253 m (93 m BSF), where there may be as many as nine subparallel fractures in a 2.5-m interval, all dipping to the southeast. The fractures are spaced about 20 cm apart in the upper part of this sequence; the spacing increases to about 50 cm in the lower part.

Strong banding reappears at 4256 m (96 m BSF) and continues for about 12 m below this depth. It is possible to make out numerous fractures in this interval, but we will have to enhance the playback to count them accurately or see their directions of dip. The hole becomes smoother at 4266.5 m (106.5 m BSF) and remains so for about 1 m; then the banding shows up again. The banding continues, with varying intensity, down to 4272 m (112 m BSF). As mentioned earlier, the blanking signal was changed at that depth, so the banding, while still present, looks drastically different.

The intensity of the returned signal drops rapidly below 4275 m (115 m BSF). There is only one moderately strong band below 4276 m (116 m BSF). The banding stops at 4281 m (121 m BSF), and a mottled signal of about equal brightness is present for the next 4 m. A single band is present for the 1-m interval below 4285 m (125 m BSF). The last meter of the record probably just shows the record acquired in the time before the tool started moving.

Borehole Televiewer Low-Frequency Log Results

The low-frequency televiewer operates at 500 kHz and has a beam width of approximately 6°. The operational procedure for low-frequency televiewer logging is essentially the same as that for high-frequency televiewer logging.

The record (Fig. 20) is similar to that produced by the high-frequency run. The upper part of the hole, above 4272 m (112 m BSF) is very reflective, whereas the lower part gives essentially no return. The decrease in reflectivity is even more extreme than in the high-frequency run.

The mouth of the drill pipe was at 4208.5 m (48.5 BSF) for the low-frequency BHTV logging run. The record below the drill pipe indicates a generally smooth borehole wall down to 4230 m (70 m BSF). There are some features of interest in this interval. There are two holes in the meter just below the mouth of the drill pipe. A small hole runs from east to south at 4208.7 m (48.7 m BSF), and a larger hole (or washout) goes completely around the borehole at 4209 m (49 m BSF). There are a number of subhorizontal features that may be low-angle fractures. These are visible at 4211 m (51 m BSF) and in the interval from 4212.5 to 4215 m (52.5 to 55 m BSF).

A fracture at 4214.5 m (54.5 m BSF) dips very slightly to the southeast, whereas one at 4214.7 m (54.7 m BSF) dips more steeply to the northwest.

The change in record brightness at 4216.5 m (56.5 m BSF) reflects a change in the setting of the blanking control. There is an unusual bright patch in the record from 4218.5 to 4219 m (58.5 to 60 m BSF) on the northwest side of the hole.

A high-angle fracture dips to the north at 4220 m (60 m BSF). Below this fracture, a hole on the south side of the borehole encountered at 4221.5 m (61.5 m BSF) corresponds to the widening found by the caliper at the same depth. A broader hole found at 4222.5 m (62.5 m BSF) also matches the caliper record. Several small holes are visible in the next few meters.

The returned signal becomes very patchy and irregular in the region from 4230 to 4234 m (70 to 74 m BSF). This corresponds to the area of washouts and holes found by the caliper log from 4231 to 4234 m (71 to 74 m BSF). A similar patchy zone is found near 4236.5 m (76.5 m BSF). Both of these zones are in the depth range of Core 597C-5, which had only 18% recovery. The patchy character of the return probably indicates the presence of a nonhomogeneous rock layer.

The borehole wall is smooth below 4237 m (77 m BSF). Several faint traces that may be fractures are visible. Two circular features are visible on the south side of borehole between 4242 and 4243 m (82 and 83 m BSF) that could be pillow rims or the intersection of slightly scalloped near-vertical fractures that do not cross the width of the borehole.

Numerous fractures are visible in the record from 4243 m (83 m BSF) down. Three parallel, steeply dipping fractures spaced about 15 cm apart occur at 4243 m (83 m BSF). All dip to the north. A less steeply dipping subparallel fracture occurs about 50 cm deeper, and a similar set of three fractures occurs near 4246.5 m (86.5 m BSF). Subparallel fractures spaced about 50 cm apart are visible for the next 5 m.

A fracture at 4254.5 m (94.5 m BSF) dips slightly to the south, altering this sequence of north-dipping fractures. There are a few indistinct fractures in the next few meters below this that appear to dip either north or south.

A fracture visible at 4260 m (100 m BSF) dips steeply to the east. Several indistinct fractures are visible in the few meters beneath this depth. Three subparallel fractures, all dipping to the south, occur between 4263.7 and 4264.5 m (103.7 and 104.5 m BSF).

The record from 4264 m (104 m BSF) to 4269 m (109 m BSF) is too bright to show any details. The decrease in signal intensity below 4269 m (109 m BSF) is real and corresponds to a loss of signal strength that occurs in the high-frequency televiewer runs at the same depth.

The zone of very low reflectivity below 4270 m (110 m BSF), a major feature of the BHTV logging runs, is difficult to explain. This zone corresponds to the interval sampled by Cores 597C-9 and -10. The recovery in these cores, 49 and 92%, respectively, is comparable to or better than the recovery in cores elsewhere in the borehole. Nowhere above 4270 m (110 m BSF) did we encounter such a great signal loss. Physical property measurements on samples of recovered core indicate that the only clear differences in the interval of Cores 597C-9 and -10 are increases in density and sonic velocity. The product of these two properties is acoustic impedance, which determines reflectivity. The amount of energy reflected at an interface is a function of the mismatch in acoustic impedances of the two materials, and the reflection coefficient is given by the difference in the two impedances di-

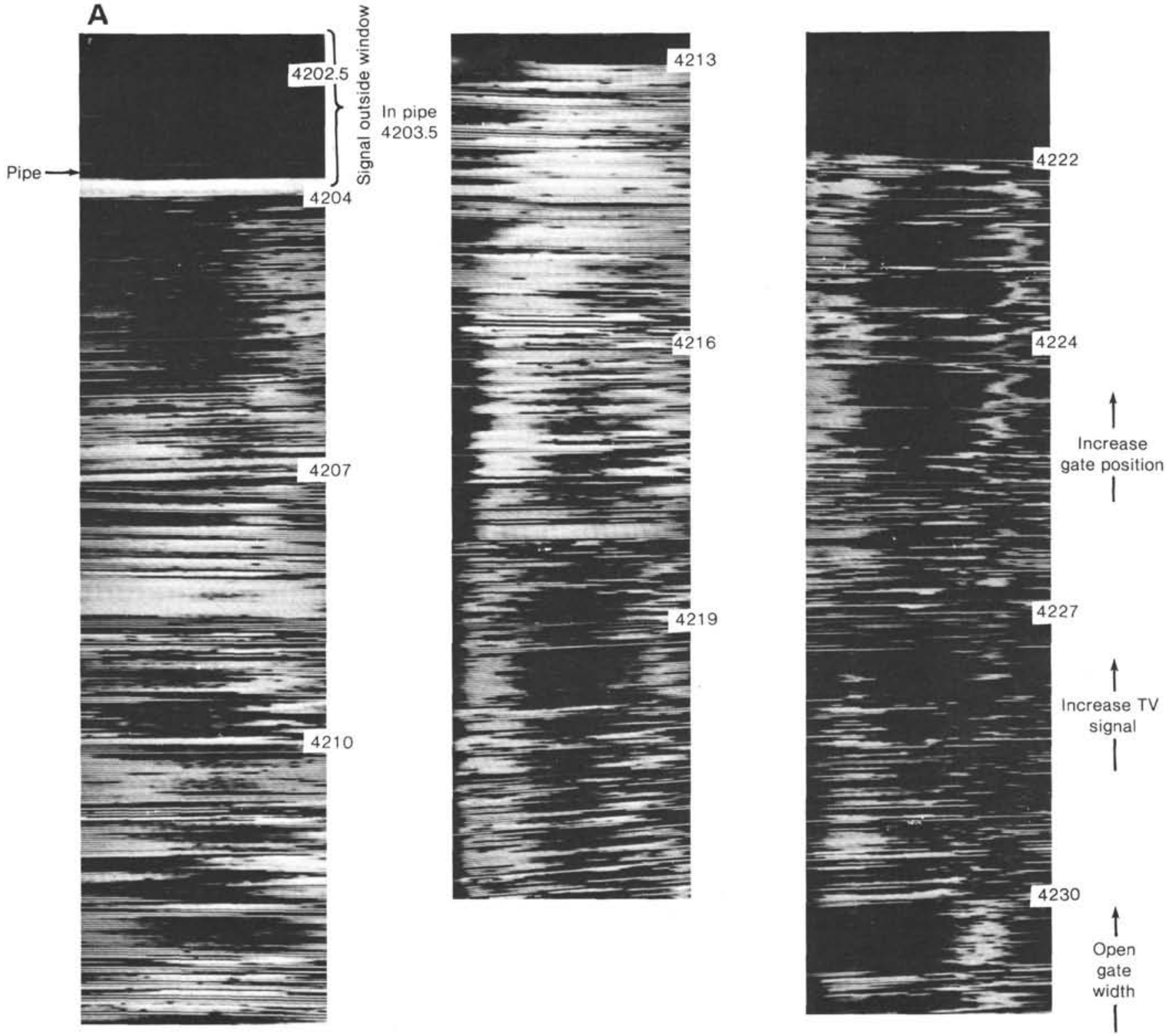

Figure 19. The high-frequency (1.2-MHz) borehole televiewer (BHTV) log for Hole 597C. The depths in the figure are in corrected meters below the rig floor (see text). Areas of high reflectance are bright and areas of low reflection are dark. Changes in gain and blanking are noted by the records. A. Upper part of hole. B. Middle part of hole. C. Lower part of hole. Note the change in the blanking signal at 4272 m (112 m BSF). All the records above this depth are as bright as the record between 4272 and 4273 m (112 and 113 m BSF). The decrease in signal strength at the bottom of the hole is discussed in the text.

vided by the sum of the two impedances. A downhole plot of the acoustic impedance, Z, and the reflection coefficient derived from it, R (Fig. 21), shows that the area below 4270 m (110 m BSF) does not differ greatly in acoustic impedance. The small change that does occur results in a reflection coefficient about 1.5% higher, not lower, in the zone of low reflected signal. The low-frequency BHTV logging run recorded essentially zero reflectance, whereas the high-frequency BHTV run did get a weak signal return. The low-frequency BHTV is at 500 kHz, and the high-frequency BHTV is at 1.2 MHz; the wavelengths are 3 and 1.25 mm, respectively. A difference in surface texture in the holes could conceivably affect reflectivity at these wavelengths.

We are left with several possible explanations for the zone of low reflectivity. (1) The BHTV tool might have malfunctioned. This seems unlikely for two reasons. First, the zone appears in both the high- and low-frequency records, which were made with separate transducers. Second, we raised and lowered the tool across the normal/low reflectance boundary several times when we first tested the tool and also between the two logging runs. The boundary was always found at the same depth. (2) The borehole might have a drastically lower reflectivity below 4270 m. The physical property measurements on the samples of recovered core contradict this idea. The high recovery rate suggests that we have representative samples. (3) The borehole might be much wider, reduc-

B

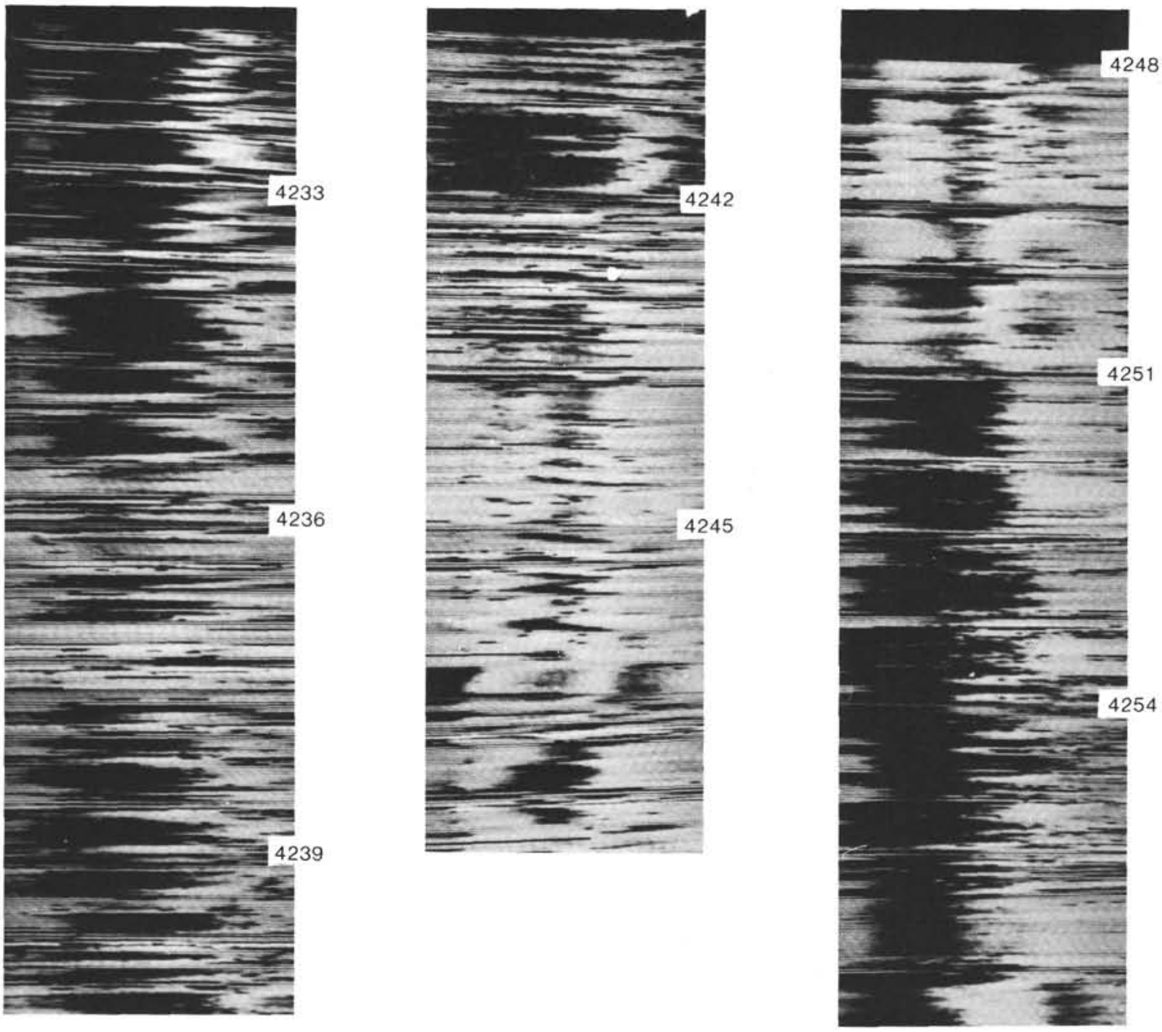

Figure 19 (continued).

ing signal strength. The caliper log contradicts this idea. (4) There may be a large concentration of suspended particles in the borehole fluid that makes the fluid acoustically opaque. Nearly 2 days elapsed between fluid circulation in the hole and the BHTV logging runs, which would be ample time for the particles suspended in the fluid during the drilling process to settle toward the bottom of the hole. Nevertheless, we feel that this is the most reasonable explanation for the extreme decrease in reflectivity at the bottom of Hole 597C.

Twelve-Channel Sonic Log

Borehole sonic logs have proven to be useful for characterizing the *in situ* properties of the rocks surrounding DSDP boreholes. These logs provide a detailed survey of the changes with increasing depth of the elastic wave velocities of the rocks. The sonic logs give reliable results where the rock is homogeneous, but where fractures or other discontinuities occur, substantial amounts of energy are lost from the transmitted wave. Therefore, velocity measurements in areas of fracturing are much less reliable. Much of the upper oceanic crust is fractured or otherwise nonhomogeneous, so conventional sonic logs are unreliable over the very intervals of the borehole where accurate velocity measurements are the most desired, that is, regions of low basalt recovery.

This problem was particularly evident in the results from Hole 504B on Leg 83, which was logged by using a Schlumberger long-spacing sonic logging tool. Void spaces and fractures are common in the upper part of Hole 504B, and the sonic velocity measurements were quite variable. The lower parts of the hole were much more homogeneous, and excellent compressional and shear wave velocity measurements were obtained. Physical properties inferred from the logs, such as porosity and clay content, are in agreement with other measurements obtained at the site.

We used a multiple-receiver long-spacing sonic logging tool developed at the Lamont-Doherty Geological Observatory and the U.S.G.S. in order to improve the quality of the sonic log data obtained in DSDP boreholes. The tool incorporates a single source and 12 re-

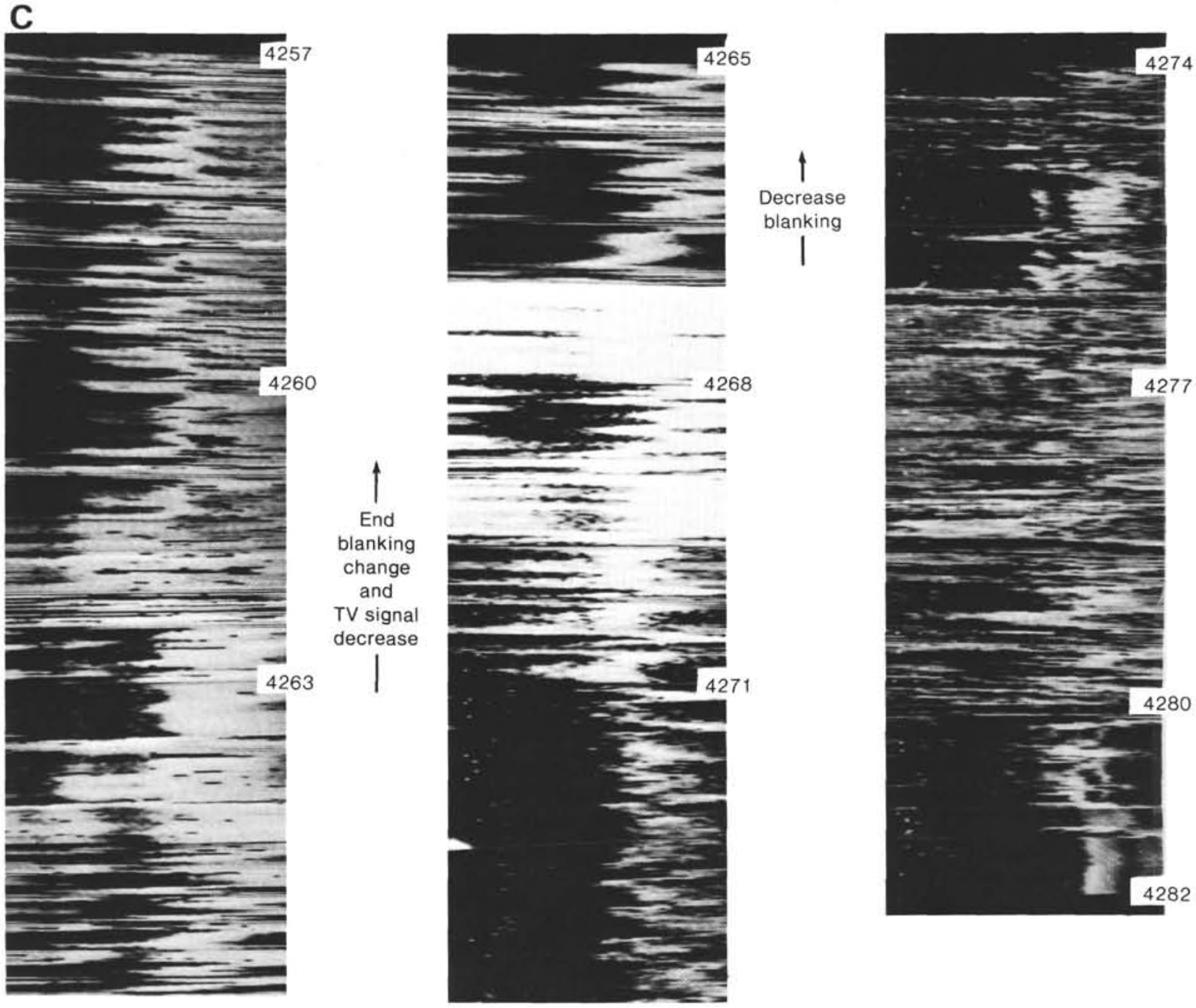

Figure 19 (continued).

ceivers spaced 1 ft. (30 cm) apart. The spacing between the source and the nearest receiver is adjustable. The tool is triggered repeatedly as it is drawn up the borehole, and the seismic wave arrivals at successive receivers are transmitted to the surface. The entire arriving waveform is recorded for each receiver position, resulting in a 12-channel mini-refraction survey. Each suite of 12 records can therefore be analyzed by using standard techniques, and the velocities of both the compressional and shear arrivals can be determined by waveform matching over the entire receiver spread. Data density is limited only by the time required to run the log and the finite size of the storage media. This technique results in a dramatic improvement in the accuracy and reliability of our measurements of *in situ* sonic velocities.

The long-spacing sonic tool operates in the frequency range from 5 to 20 kHz, so the wavelength of the recorded energy is somewhat less than 1 m. Structural and constructional features such as pillows have dimensions on the order of a few meters or less, so the sonic wave energy is particularly sensitive to the presence of such features. The amplitude and frequency spectra of the arrivals can therefore be analyzed to get additional data on these features.

Tool Description

The logging tool that was used is manufactured by the Simplec Corporation of Crowley, Texas. The downhole tool consists of two packages connected by a length of logging cable attached to the two sections by means of standard Gearhart-Owen cable heads. The tool runs on seven-conductor logging cable. The uppermost package contains power supplies and interface electronics that allow the downhole tool to receive data through the logging cable. The electronics are enclosed in a steel pressure case with an outer dimension of about 3.4 in. (8.5 cm). The sonic source is at the lower end of the upper assembly. The lower assembly contains control electronics and a preamplifier section in a short steel pressure case. The receiver string is attached below this section. The 12 receivers are clamped to a steel cable and enclosed in a semi-rigid rubber hose that is filled with oil to protect the receivers from pressure.

Experimental Methods

The experimental technique at Site 597 is to run the sonic tool through the drill pipe to the total depth of the hole and then to log slowly upward. Typical logging speeds are 600 ft./hr. (0.05 m/s) or less. Each signal is generated by a single source pulse, and the receivers are selected in sequence from the surface. Gain settings are also selected from the surface. The receiver numbers and gain settings are selected in one of two modes. The logging tool surface panel can be used to select the receivers and each receiver gain individually. A digital interface also allows the user to run the logging from a computer keyboard and have the receivers selected in arbitrary order. The use of a computer allows the gains to be adjusted individually to compensate for changes in the properties of the rock adjacent to the borehole.

The depths at which the suite of arrivals is recorded can be chosen in either of two ways. The suite can be recorded continuously at selected time intervals as the tool moves upward in the hole, using a depth count generated by the computer. Alternatively, the log can be run with the tool stationary in the hole, so that the user can select the depths at which data are obtained. These methods may be varied by changing the controlling computer program. For instance, the source pulse can be fired, either by the computer at preselected time intervals or by manually depressing a key on the terminal keyboard. The variations are limited only by the imagination of the programmer–operator.

The arrivals at each receiver are digitized at the surface and stored on floppy diskettes for later analysis. Both the compressional and shear velocities are determined during the postcruise analysis of the recorded waveforms. The current control program could be expanded to permit real time analysis of the logging data during the run, however.

Operations

Before deploying the sonic logging tool in the re-entry hole, we tried to test the tool in Hole 597B, the pilot hole. Hole 597B was suitable for testing the sonic logging tool because it penetrated about 27 m of basalt and core recovery in the lower 20 m was quite high. To test the tool, the drill pipe was raised to provide about 15 to 20 m of open hole. The logging tool was assembled and lowered into the drill pipe past a wiper. The wiper sealed the top of the pipe and permitted the pipe to be pressurized so the tool could be pumped down the drill pipe to the bottom. The weight indicator on the logging cable was not operating during this logging run, so it was difficult to obtain accurate information about the descent of the tool. The absence of descent information contributed to the difficulty (described below) we had in trying to get the tool out of the pipe and into the open hole.

The tool was tested before it was run down the hole. The connecting cable between the upper and lower sections had become damaged during tool assembly. The cable was replaced and the tool operated correctly. The tool was then reinserted and run down the drill pipe. The tool was tested as it was being pumped down the pipe, and it did not seem to be functioning correctly. We could not run the tool out of the pipe and into the open hole below. Because of our attempts to run the tool out of the pipe, the entire upper assembly was forced down past the connecting cable, and it became wedged over the receiver string, damaging both the cable and the rubber hose containing the receivers. The tool stopped working at that time, and the logging run was terminated.

We repaired the sonic tool while the re-entry hole was being drilled. The receiver string was repaired by shortening the upper section and removing the first receiver. The connecting cable was replaced, and a short section of steel pipe was run over the cable to make the connection between the upper and lower pressure cases rigid. The steel pipe made the reconnection of the upper and lower assemblies difficult and might have increased the amplitude of the energy being conducted along the tool body. It was also possible that this configuration would cause significant interference in the refracted arrivals traveling along the hole. Nevertheless, it was decided that the connecting cable was too fragile to forgo the additional support provided by the connecting pipe. Two other pipe sections were welded to the weight hung below the receiver string to increase the weight of the tool and to act as a guide as the tool was lowered out of the bottom of the pipe. The entire tool was run through the bottom hole assembly (which included a packer section and two drill collars) to ensure that it would not hang up in the hole.

The re-entry hole, 597C, was drilled to a total depth of 4303.5 m (143.5 m BSF), 91 m below the sediment–basalt contact. The drill string was lowered to about 5 m below this contact in order to keep the logging tool from being damaged as it emerged from the drill pipe. The tool was run into the pipe after it was checked to verify that the source was being triggered. No arrivals were recorded during the tool's descent through the drill pipe, in contrast to our experience in the pilot hole. We ran the tool out of the pipe and into the formation to ensure that it could be run through the packer section without mishap.

We were unable to get any arrivals while we were in the open hole, so we abandoned the logging attempt and retrieved the tool. The tool was examined in the electronics shop upon retrieval and no damage was found to either of the electronics packages or to the connecting cable. No signals were being generated by the receivers, and the hose around the receiver string had collapsed at one point. It was decided that repairs could not be made rapidly enough to log Hole 597C in the time remaining for the site.

Comments and Suggestions

The full-wave sonic tool should be redesigned to withstand the logging conditions encountered at sea, which are more severe than in boreholes on land. The parts of the tool that are flexible need to be stiffened or otherwise strengthened. The flexible receiver array should probably be replaced by a more rigid array and protected by a rubber boot. The receiver array should also be modified to permit easy servicing of the internal connections and easy draining and refilling with oil.

It is absolutely essential for the weight indicators for the logging system to be working for any logging attempt. The total depth–weight indicators currently being used on the *Challenger* are unreliable and require

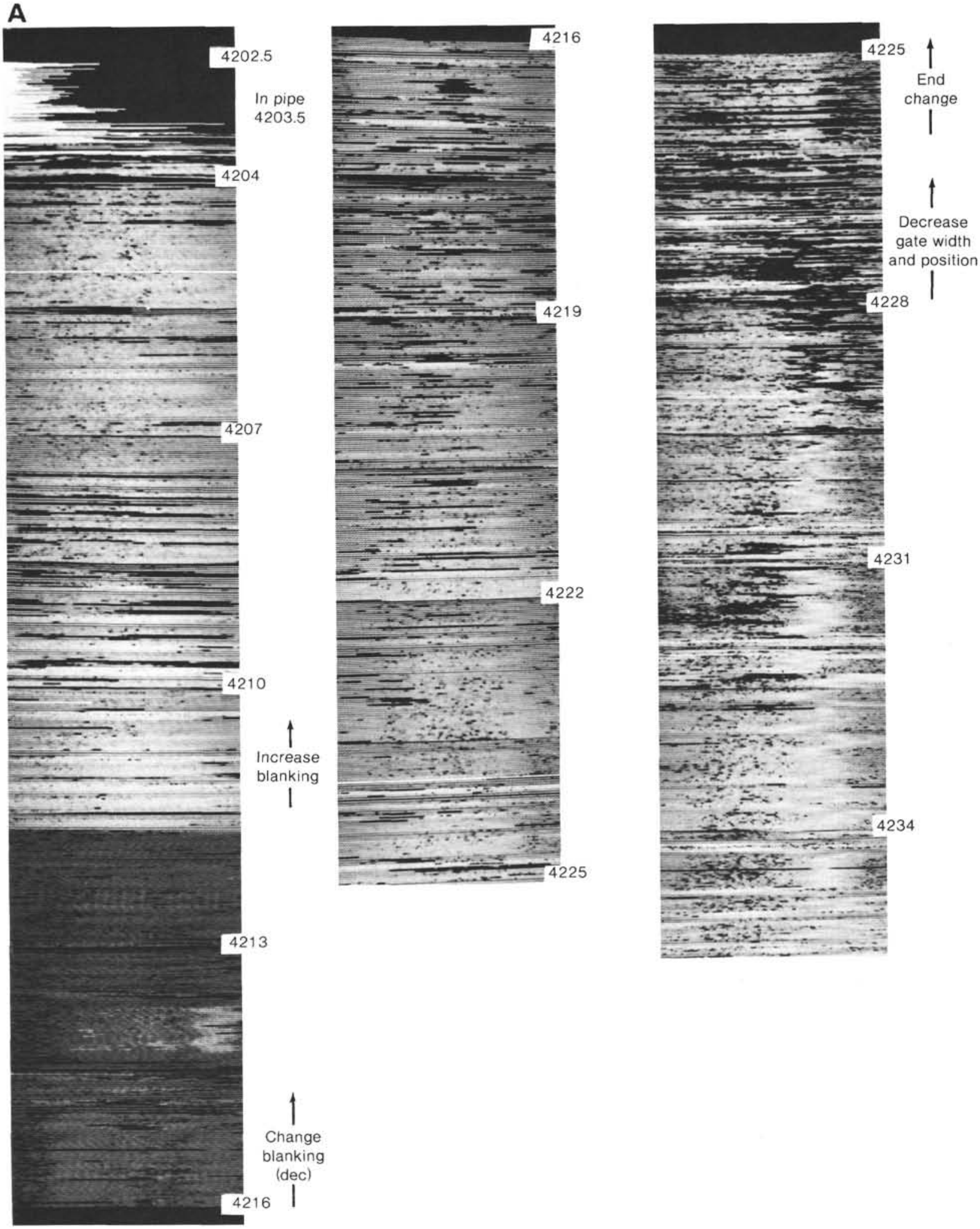

Figure 20. Low-frequency (500-kHz) BHTV records from Hole 597C. The hole appears to be more uniform than in the high-frequency records. Details as noted in the caption for Figure 19. A. Top part of hole. B. Middle part of hole. Note circular structures and fractures (horizontal sinusoidal features) from 4242 to 4245 m (82 to 85 m BSF). C. Lower part of hole. Note the change in blanking at 4263 m (103 m BSF). The entire hole above this depth is as bright as the portion shown here. Note the tremendous decrease in signal strength below about 4270 m (110 m BSF).

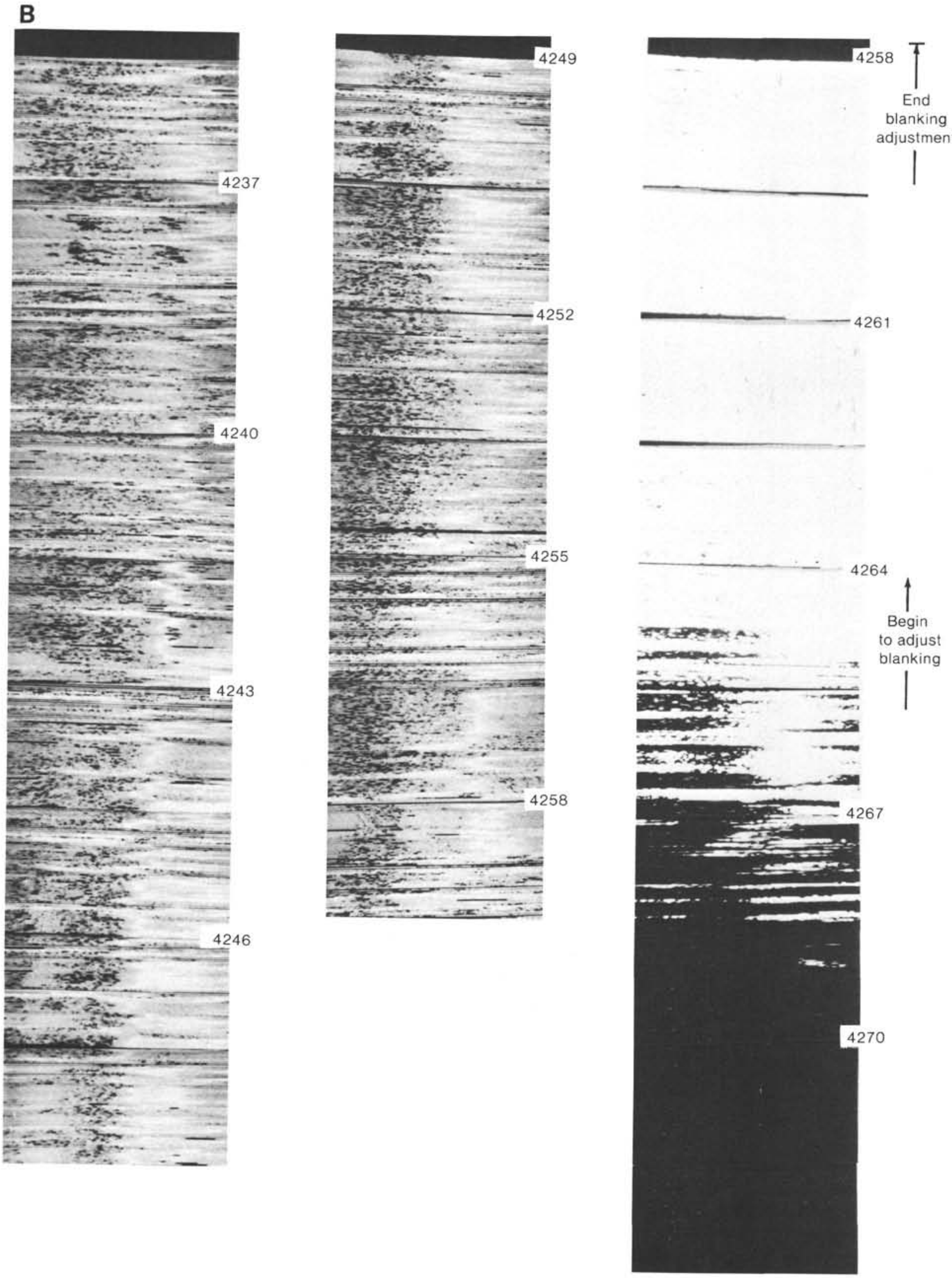

Figure 20 (continued).

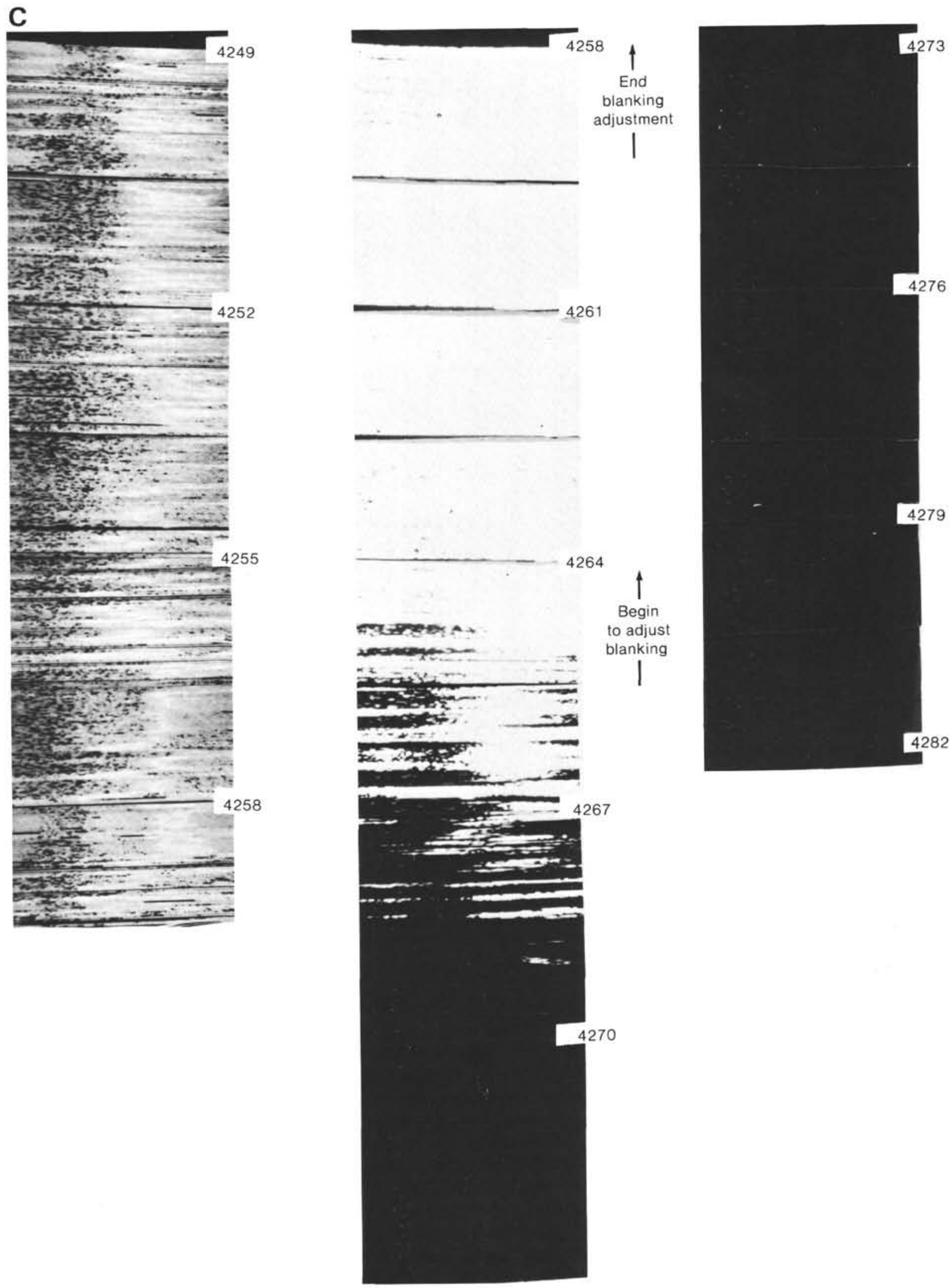

Figure 20 (continued).

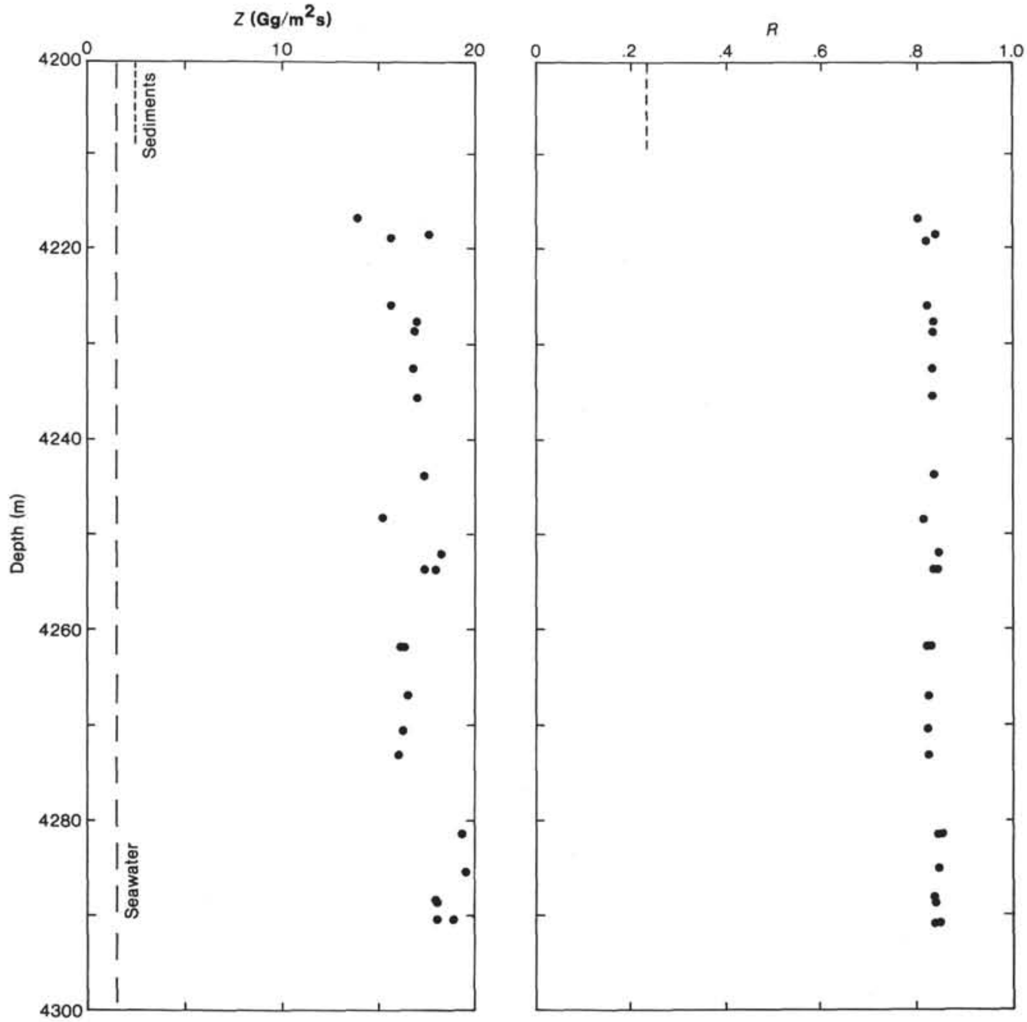

Figure 21. Acoustic impedance (*Z*) and calculated reflection coefficients (*R*) versus depth for Hole 597C. Acoustic impedance is the product of density times the sonic velocity.

constant attention from the electronics technicians. They should either be rebuilt at the factory or replaced. The damage to the receiver string during the logging attempt in Hole 597B probably could have been avoided if we could have seen the decrease in weight that occurred when the tool hung up at the pipe mouth. The failure of the receiver connections at Hole 597C might also have been avoided, because we would not have had to rebuild the receiver hose.

PACKER EXPERIMENT

We attempted one packer experiment to determine the permeability and *in situ* formation pressure at Hole 597C. The experiment was only partially successful, because the packer deflated prematurely.

Tool Design

The packer used on the *Glomar Challenger* is built by the Lynes Corporation. It was originally designed to prevent the escape of hydrocarbons from a drill hole. The packer consists of an inflatable steel-belted radial rubber element on the outside of the drill pipe and has an internal plumbing system that permits the packer element to be inflated and deflated by using pumps on the surface. The packer section is set into the bottom hole assembly at the distance above the bit that the experiment is to be run. The packer is seated by dropping a safety go-devil or sampler go-devil down the pipe until it seats in the packer assembly and seals off the pipe beneath. The pumps then pressure up the drill pipe above the go-devil, inflating the packer with water and sealing off the outer annulus between the drill pipe and the borehole wall. When the pressure exceeds 1000 lb/in^2 (6.9 MPa), a piston slides into the packer assembly and the packer becomes sealed off from the drill pipe.

In situ formation pressure can be determined while the packer is inflated. A Kuster Corporation model K-3 pressure gauge hangs beneath the go-devil and measures the pressure in the sealed lower section of borehole. We used two K-3 pressure gauges with a connecting sub between them in Hole 597C to ensure the acquisition of at least one good record.

After a sufficiently long record of *in situ* formation pressure has been obtained, the drill pipe pressure is increased to 1800 lb/in^2 (12.4 MPa), blowing a shear plug in the go-devil and resulting in the free exchange of water between the drill pipe and the previously sealed section of borehole. The decay of this pressure pulse is monitored to determine permeability.

After determining permeabilities, a slug test is performed by generating a pressure pulse with the Byron Jackson (BJ) pump and permitting the pulse to decay. This test may be repeated one or more times. If the formation is sufficiently permeable, a flow test may be performed by pumping at a given rate and observing the level at which the pressure stabilizes. The flow test may be run at different flow values to test for nonlinear behavior and possible leakage past the packer.

Finally, a steel ball is dropped down the pipe, which seats in the go-devil. The pressure is then increased until a packer deflate plug shears, after which pressure is decreased, allowing the packer to deflate.

Operations and Results

The excellent core recovery from Hole 597C gave us high hopes for a successful packer test. We decided to seat the packer at the depth where recovery had been highest (Core 597C-10, 4283 m below rig floor, 123 m BSF), so the BHA was made up with two drill collars below the packer. No drill bit was put on the assembly, since the purpose of the pipe trip was to perform logging and the packer experiment. Holes were cut in the pipe to ensure that water would circulate freely in the borehole after we set the end of the pipe on the bottom of the hole.

The pipe was lowered into the hole after the logging runs. The bottom seemed to be reached at about 4297 m (370 m BSF), some 6 to 7 m above the bottom of the hole. This apparent bottom supported a weight of over 15,000 lb (6804 kg), so we decided that the obstruction could not be a ledge. The pipe was picked up and lowered again to double check the depth, and it encountered bottom again at the same place. We concluded that the hole had filled with debris to that level, and the packer experiment proceeded. We pumped to 1400 lb/in^2 (9.7 MPa) to inflate the packer. The driller noticed an increase in drill string weight, so the pipe pressure was vented off. The bumper subs were pounding (an indication that they were fully extended) and the pipe sank about 6 m, making it necessary for us to break out the circulating head and put on another stand of pipe before resuming the experiment. We pumped up again in order to make sure the packer was set, since we were not sure the packer had inflated the first time. We then waited to observe *in situ* formation pressures. After these pressures were recorded we increased pressure to shear the go-devil plug. The pressure decayed very rapidly. We then attempted to pump the pressure up to 150 lb/in^2 (1.0 MPa, less than 80% of the overburden pressure) for a slug test but were unable to exceed 100 lb/in^2 (0.7 MPa) despite going to high flow rates. We shut the BJ pump down and picked up the drill string for a pull test on the packer. There was no increase in weight to indicate that the packer was seated, so we pulled the pipe out of the hole.

The records from the two Kuster K-3 pressure gauges that we used with the safety go-devil are shown in Figures 22A and B. More details are visible in the original records. Records of surface pressure, drill string weight, and circulating fluid pressure were also used to interpret results of the experiment.

The results suggest that part of the drill pipe hung up on the ledge that appears in the caliper log at 4279 m (119 m BSF). When the packer inflated it may have centered the drill string, allowing the drill string to bypass the ledge and causing the packer assembly to slide down 6 m. The center of the packer assembly was then at a depth of about 4267 m (107 m BSF).

The Totco drilling records indicate that the rate at which the pipe slipped increased approximately exponentially. The Kuster pressure gauges recorded constant pressure. The record acquired during this slippage was therefore equivalent to a constant pressure permeability test rather than a slug test with decaying pressure.

A second permeability test results from the decay of the pressure pulse generated by blowing out the shear plug. The decay was too rapid to be clearly visible in the Kuster gauges, but it was monitored by the surface pressure gauge. This very brief record indicates that permeability is very high in Hole 597C (over 100 milidarcys, or $1 \times 10^{-13}m^2$). The results of this test are uncertain, since the overpressure plug blew and caused the packer to deflate less than 1 min. after the shear plug had been blown from the surface. Furthermore, the data from the surface pressure gauge are not used for this part of the record under normal circumstances.

The Kuster records are unambiguous about the formation pressure and show a clear shift upward once the shear plug was blown. The formation was underpressured by about 5 bars (74 lb./in.^{2} or 0.5 MPa).

The packer element was undamaged when the bottom hole assembly returned to the rig floor, and examination showed that the packer deflate plug had sheared.

We conclude that the hole conditions in Hole 597C are excellent for conducting packer experiments in the future, because the packer element was not damaged even after slipping in the hole. The details of the caliper log should be checked before the packer is set, however. We were somewhat misled by the problems we encountered in recalibrating the caliper tool after the run. It was only after the experiments were over and we had time to analyze the caliper runs closely that we became convinced that the fine details in the caliper logs were real. We also suggest converting the system from the analog Kuster pressure recorders to a digital recorder. The microprocessor unit for the Von Herzen VLHPC temperature tool consists of a microprocessor, analog-to-digital converter, and memory. It is designed to permit the recording of data other than temperatures and is very compact. We suggest acquiring at least two of these units along with suitable pressure transducers and pressure cases for use with the packer system. It would be far easier to read the data directly into the computer than it is to digitize the carbon-black-on-brass records of the Kuster gauges. The digital units also provide great versatility in terms of sampling rate and programming.

SUMMARY AND CONCLUSIONS

The coring at Site 597 produced two important sets of samples for the interpretation of hydrothermal pro-

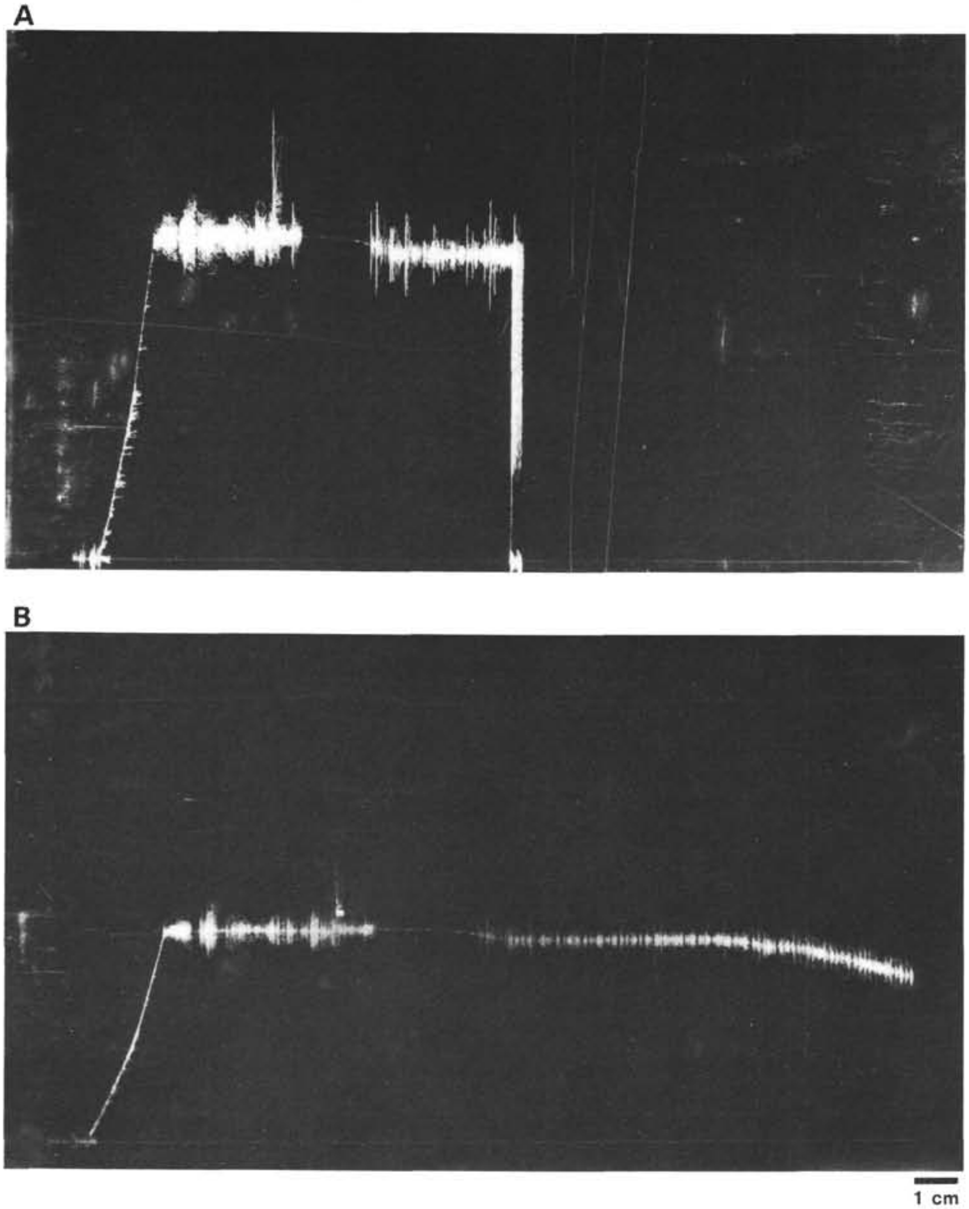

Figure 22. A. Pressure versus time record for Kuster model K-3 pressure gauge (S/N 9942:0 to 9950 lb/in.^{2}, 0 to 68.6 MPa), and K-3 clock (S/N 13105) for the packer experiment in Hole 597C. The vertical line at the right shows when the clock stopped operating. B. Pressure versus time record for Kuster model K-3, 9945 pressure gauge (S/N 9949:0 to 15,400 lb/in.^{2}, 0 to 106.2 MPa), and K-3 clock (S/N 13106) for the packer experiment in Hole 597C.

cesses. The first is a lower Miocene to upper Oligocene clay-bearing nannofossil ooze that was recovered at Holes 597 and 597A. It contains a good record of the sedimentation from 15 to 28.3 Ma that can be used to interpret hydrothermal activity. The second is the basalt from Hole 597C, where we drilled 91 m into crust generated at a fast-spreading rise crest and recovered 48.5 m of rock. The basalts are essentially all massive flows and show three distinct stages of alteration.

Sediment

Two sedimentary units were recovered from Holes 597 and 597A. At Hole 597C only the lowermost unit was recovered. Unit I is 1.4 m of Pleistocene to middle Miocene zeolitic clay. Unit IIA is about 40 m of clay-bearing nannofossil ooze that averages 80% calcium carbonate and 20% iron oxides and hydroxides, RSO (reddish yellow, semiopaque objects), and poorly crystalline clays. Unit IIB comprises the lower 7 to 10 m of the section. It is clayey nannofossil ooze made up of the same components as Unit IIA except the carbonate content is only 65 to 70%. Foraminifers comprise a few percent of Unit IIB but are present only in trace amounts in Unit IIA. A single, probably correlative, ash layer occurs 3 to 6 m above basalt in Holes 597, 597A, and 597C. The sedimentary column is of generally uniform porosity (about 65%), grain density (2.62 g/cm^3 corrected for salt content), and sonic velocity (1.52 km/s).

Unit I spans Pleistocene to early middle Miocene time with a linear sedimentation rate (LSR) of 0.1 mm/10^3

yr. The temporal record of such low LSR materials commonly includes numerous lacunae. Sedimentation rates increase downcore to values of about 7.7 mm/10^3 yr. Mass accumulation rates (MAR), calculated from LSR, porosity, and grain density values, range from about 5 to 750 mg/($cm^2 \times 10^3$ yr.). In the lower portion of the site, where the poorly crystalline to amorphous, iron-rich (inferred hydrothermal) component accounts for up to 30% of the sediment, the MAR exceeds 200 mg/($cm^2 \times 10^3$ yr.).

The decrease of nearly two orders of magnitude in LSR that occurred about 17 Ma apparently corresponds to the submergence of Site 597 through the early Miocene calcium carbonate lysocline, then at about 3700 m.

Analysis of interstitial waters from both squeezed and *in situ* samples revealed no evidence of fluid advection through the sediment column but suggests that the dissolution of $CaCO_3$ may be continuing in the uppermost 10 m of sediment.

Rock

Igneous basement was recovered from all four holes at Site 597. Recovery represented 2 m of basalt fragments at Hole 597; 25 cm of basalt–glass breccia at Hole 597A; 5.4 m of basalt (out of 24.6 m drilled) at the pilot Hole 597B; and 48.5 m of basalt (of 91 m drilled) at Hole 597C, the re-entry hole. The penetration and recovery at Hole 597C make it the most successful hole drilled into fast-spreading oceanic crust.

The basalts are olivine-poor tholeiites containing plagioclase, clinopyroxene, magnetite, glass, and olivine. They are medium to fine grained, moderately vesicular (in basalt Unit I), and fractured. Massive flows appear to dominate the entire sequence; only one small fragment, possibly a pillow margin, with a glassy rim was recovered. Three units, which are distinguished on the presence or absence of olivine and on the basis of chemical composition, can be discerned within the basalt sequence. Unit I is 48 m thick (52.5 to 100.5 m BSF), contains olivine, and is characterized by vesicular subspherulitic to intersertal texture in the upper part and subophitic texture toward the base. Unit II is about 21 m thick (100.5 to 121.3 m BSF), olivine free, and dominated by intergranular and poikilophitic textures. Unit III, 22 m thick (121.3 to 143.5 m BSF) has similar textures but contains ubiquitous olivine.

Three stages of basalt alteration have been identified. The first is late magmatic, possibly deuteric, alteration in which saponite has replaced olivine and basalt groundmass and filled vesicles. The second is characterized by the presence of dark green smectite, chlorite, pyrite, chalcopyrite, and native copper. This alteration stage is clearly associated with veins. The presence of celadonite may characterize the transition between stages two and three; the third is late-stage oxidative alteration that has resulted in the presence of calcite, aragonite, zeolite, iron oxides, and a brown smectite. This type of alteration is pervasive in Unit I and vein related in basalt Units II and III.

The basalts in Hole 597C have sonic velocities typical of crustal Layer 2—about 5.8 km/s above Core 597C-10 and about 6.3 km/s in the fresh rocks from Cores 597C-11 and -12. Paleomagnetic studies show the basalts to be reversely magnetized and therefore probably from the reversed interval between Anomalies 8 and 9. This would suggest an age of about 28.6 Ma for Site 597 (Harland et al., 1982), an age consistent with the nannofossil zonation of the basal sediments. A brief period of normal polarity may be recorded in the basalts of Core 597C-7. NRM intensities are about 1.6×10^{-3} emu/cm^3. Magnetic inclination values are high (nearly 60° before alternating field demagnetization and 45° afterwards); the expected inclination for Site 597 (18.8°S) is about 34°. Unusually high magnetic inclinations also characterize the basalts from DSDP Sites 319 and 320 (Ade-Hall and Johnson, 1976), also on crust generated at the Mendoza Rise. As yet there is no satisfactory explanation for these high inclinations.

Four downhole experiments were attempted in the reentry hole. Caliper and televiewer logs were successful and showed variations in formation fracturing that can be associated with both the recovery and the petrology of basalt. The large decrease in televiewer reflectivity at 4270 to 4274 m (110 to 114 m BSF) indicates that a combination of drilling mud and fine drilling debris fills the lower 30 m of Hole 597C, even though water was circulated to clear the hole. A 12-channel sonic log was unsuccessful at both Holes 597B and 597C. A packer experiment was only partially successful because the packer deflated prematurely.

At the end of our time at Site 597, while awaiting the rendezvous with the French naval ship *Papenoo*, we tested a wireline re-entry system under development. Re-entry was not achieved, but it was obvious that with the proper (bottom-mounted) navigational and guidance equipment the operation could easily become routine.

REFERENCES

Ade-Hall, J. M., and Johnson, H. P., 1976. Paleomagnetism of basalts, Leg 34. *In* Yeats, R. S., Hart, S. R., et al., *Init. Repts. DSDP*, 34: Washington (U.S. Govt. Printing Office), 513–532.

Archie, G. E., 1942. The electrical resistivity log as an aid in determining some reservoir characteristics. *Trans. Am. Inst. Min. Metall. Eng.*, 146:54–62.

Arrhenius, G., 1963. Pelagic sediments. *In* Hill, M. N. (Ed.), *The Sea* (Vol. 3): New York (Wiley Interscience), 655–727.

Bass, M. N., 1976a. Rare and unusual minerals and fossils(?) in sediments of Leg 34. *In* Yeats, R. S., Hart, S. R., et al., *Init. Repts. DSDP*, 34: Washington (U.S. Govt. Printing Office), 611–624.

________, 1976b. Secondary minerals in oceanic basalts, with special reference to Leg 34, Deep Sea Drilling Project. *In* Yeats, R. S., Hart, S. R., et al., *Init. Repts. DSDP*, 34: Washington (U.S. Govt. Printing Office), 393–432.

Bender, M. L., Hudson, A., Graham, D. W., Barnes, R. O., Leinen, M., and Kahn, D., 1985. Diagenesis and convection reflected in pore water chemistry on the western flank of the East Pacific Rise, 20 degrees south. *Earth Planet. Sci. Lett.*, 76:71–83.

Berger, W. H., and Winterer, E. L., 1974. Plate stratigraphy and fluctuating carbonate line. *Spec. Publ. Int. Assoc. Sedimentol.*, 1: 11–48.

Blow, W. H., 1969. Late middle Eocene to Recent planktonic foraminiferal biostratigraphy. *In* Brönnimann, P., and Renz, H. H. (Eds.), *Proc. First Int. Conf. Planktonic Microfossils* (Geneva, 1967): Leiden (E. J. Brill), pp. 199–421.

Boyce, R. E., 1976. Definitions and laboratory techniques of compressional sound velocity parameters and wet-water content, wet-bulk density, and porosity parameters by gravimetric and gamma ray attenuation techniques. *In* Schlanger, S. O., Jackson, E. D., et al., *Init. Repts. DSDP*, 33: Washington (U.S. Govt. Printing Office), 931-958.

Broecker, W. S., and Broecker, S., 1974. Carbonate dissolution on the western flank of the East Pacific Rise. *In* Hay, W. W. (Ed.), *Studies in Paleoceanography.* Spec. Publ., Soc. Econ. Paleont. Mineral., 20:44-57.

Carvalho, H. da S., Purwoko, Siswoyo, Thamrin, M., and Vacquier, V., 1980. Terrestrial heat flow in the Tertiary basin of central Sumatra. *Tectonophysics*, 69:163-188.

Donnelly, T. W., 1976. Tertiary explosive volcanic activity in the eastern equatorial Pacific Ocean: Sites 320 and 321, DSDP Leg 34. *In* Yeats, R. S., Hart, S. R., et al., *Init. Repts. DSDP*, 34: Washington (U.S. Govt. Printing Office), 605-609.

Gieskes, J. M., 1973. Interstitial water studies, Leg 15—alkalinity, pH, Mg, Ca, Si, PO_4, and NH_4. *In* Heezen, B. C., MacGregor, I. D., et al., *Init. Repts. DSDP*, 20: Washington (U.S. Govt. Printing Office), 813-830.

Handschumacher, D. W., 1976. Post-Eocene plate tectonics of the eastern Pacific. *In* Sutton, G. H., Manghnani, M. H., and Moberly, R. (Eds.), *The Geophysics of the Pacific Basin and its Margin.* Monogr. Am. Geophys. Union, 19:177-202.

Haq, B. U., 1984. Jurassic to Recent nannofossil biochronology: an update. *In* Haq, B. U. (Ed.), *Nannofossil Biostratigraphy:* Stroudsburg, Pa. (Hutchinson Ross Publ. Co.), pp. 358-378.

Harland, W. B., Cox, A. V., Llewellyn, P. G., Pickton, C. A. G., Smith, A. G., and Walters, R., 1982. *A Geologic Time Scale:* Cambridge (Cambridge University Press).

Horai, K., and Von Herzen, R. P., 1985. Measurement of heat flow on Leg 86 of the Deep Sea Drilling Project. *In* Heath, G. R., Burckle, L. H., et al., *Init. Repts. DSDP*, 86: Washington (U.S. Govt. Printing Office), 759-777.

Mammerickx, J., Herron, E., and Dorman, L., 1980. Evidence for two fossil spreading ridges in the southeast Pacific. *Geol. Soc. Am. Bull.*, Pt. I, 91:263-271.

Manheim, F. T., and Waterman, L. S., 1974. Diffusimetry (diffusion coefficient estimation) on sediment cores by resistivity probe. *In* von der Borch, C. C., Sclater, J. G., et al., *Init. Repts. DSDP*, 22: Washington (U.S. Govt. Printing Office), 663-670.

Moore, T. C., Jr., van Andel, T. H., Sancetta, C., and Pisias, N., 1978. Cenozoic hiatuses in pelagic sediments. *Micropaleontol.*, 24(2):113-138.

Okada, H., and Bukry, D., 1980. Supplementary modification and introduction of code numbers to the low-latitude coccolith biostratigraphic zonation (Bukry, 1973; 1975). *Mar. Micropaleontol.*, 5: 321-325.

Quilty, P. G., Sachs, H., Benson, W. E., Vallier, T. L., and Blechschmidt, G., 1976. Sedimentologic history, Leg 34 Deep Sea Drilling Project. *In* Yeats, R. S., Hart, S. R., et al., *Init. Repts. DSDP*, 34: Washington (U.S. Govt. Printing Office), 779-794.

Rea, D. K., 1981. Tectonics of the Nazca-Pacific divergent plate boundary. *In* Kulm, L. D., Dymond, J., Dasch, E. J., Hussong, D. M., and Roderick, R. (Eds.), *Nazca Plate: Crustal Formation and Andean Convergence.* Mem. Geol. Soc. Am., 154:27-62.

Sayles, F. L., Manhein, F. T., and Waterman, L. S., 1973. Interstitial water studies on small core samples—Leg 15. *In* Heezen, B. C., MacGregor, I. D., et al., *Init. Repts. DSDP*, 20: Washington (U.S. Govt. Printing Office), 783-804.

Srinivasan, M. S., and Kennett, J. P., 1981. Neogene planktonic foraminiferal biostratigraphy and evolution: equatorial to sub-Antarctic, South Pacific. *Mar. Micropaleontol.*, 6:499-533.

Tracey, J. I., Jr., Sutton, G. H., et al., 1971. *Init. Repts. DSDP*, 8: Washington (U.S. Govt. Printing Office).

van Andel, T. H., Heath, G. R., and Moore, T. C., 1975. Cenozoic history and paleoceanography of the central equatorial Pacific Ocean. *Mem. Geol. Soc. Am.*, 143.

Von Herzen, R. P., and Maxwell, A. E., 1959. The measurement of thermal conductivity of deep-sea sediments by a needle probe method. *J. Geophys. Res.*, 64:1557-1563.

Windom, H. L., 1969. Atmospheric dust records in permanent snowfields: implications to marine sedimentation. *Geol. Soc. Am. Bull.*, 80:761-782.

SITE 597 HOLE CORE 1 CORED INTERVAL 0.0–4.6 m

TIME – ROCK UNIT	BIOSTRATIGRAPHIC ZONE	FORAMINIFERS	NANNOFOSSILS	RADIOLARIANS	DIATOMS	SECTION	METERS
Pleistocene	NN19/20	C	CP			1	0.5, 1.0
?			B				
			AM				
lower Miocene	CN4/3					2	
						3	
lower Miocene	N7 (F) CN2–4	FP	A/ MP			4, CC	

GRAPHIC LITHOLOGY

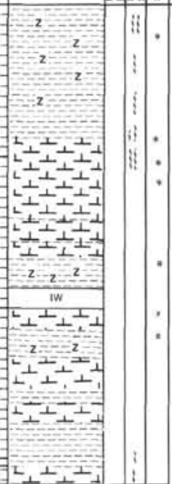

LITHOLOGIC DESCRIPTION

Section 1:
0-21 cm: Zeolitic clay, very dusky red (2.5YR 2.5/2)
21–140 cm: 2.5YR 2.5/2 grading to dark reddish brown (5YR 3/3)

CLAY-BEARING NANNO OOZE
Section 2: CLAY-BEARING NANNO OOZE
0–140 cm: Dark yellowish brown (10YR 4/4) grading to yellowish brown (10YR 5/6)
114–116 cm: 5YR 3/3
121 cm: 5YR 3/3
130 cm: 5YR 3/3

Section 3:
0–36 cm: Dark brown (7.5YR 4/4) zeolitic clay
36–41 cm: Dusky red (2.5YR 3/2)
41–66 cm: Yellowish brown (10YR 5/8)

CLAY-BEARING NANNO OOZE

66–100 cm: Dark brown (7.5YR 4/4)
100–114 cm: 7.5YR 4.5/4
114–125 cm: 7.5YR 4/4
125–131 cm: Strong brown (7.5YR 5/6)

DARK BROWN CLAY

131–140 cm: 7.5 YR 3/2

Core Catcher:
0–8 cm: Strong brown (7.5YR 5/8)
8–24 cm: Dark brown (7.5YR 4/4)

SMEAR SLIDE SUMMARY (%):

	1, 35 D	2, 110 D
Composition:		
Quartz	TR	TR
Feldspar	TR	TR
Mica	TR	–
Heavy minerals	TR	–
Clay	85	<10
Volcanic glass	<3	–
Palagonite	~5	<5
Zeolite	≥10	–
Calc. nannofossils	–	85
Opaques	–	Some

SITE 597 HOLE CORE 2 CORED INTERVAL 4.6–14.2 m

TIME – ROCK UNIT	BIOSTRATIGRAPHIC ZONE	FORAMINIFERS	NANNOFOSSILS	RADIOLARIANS	DIATOMS	SECTION	METERS
lower Miocene			AV				
	CN2					1	0.5, 1.0
						2	
	N7 (F)					3	
						4	
						5	
	CN2					6	
	N7 (F)	AM	AM			7, CC	

GRAPHIC LITHOLOGY

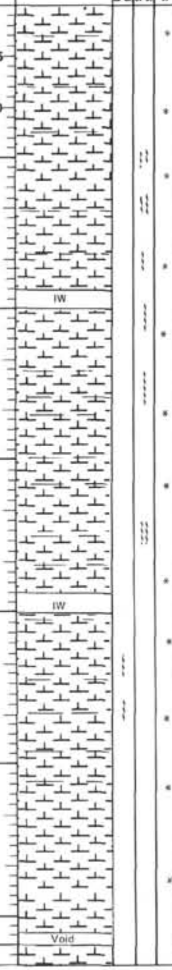

LITHOLOGIC DESCRIPTION

CLAY-BEARING NANNOFOSSIL OOZE

Section 1:
0–150 cm: Dark reddish brown (5YR 3/4)

Section 2:
0–60 cm: Yellowish red (5YR 4/6)
60–90 cm: Dark reddish brown (5YR 3/4)
90–140 cm: Yellowish red (5YR 3/6)

Section 3:
0–150 cm: Reddish brown (5YR 4/4)

Section 4:
0–140 cm: Yellowish red (5YR 4/6)

Section 5:
0–151 cm: Brown (7.5YR 5/4)

Section 6:
0–5 cm: Brown (7.5YR 5/4)
5–150 cm: Reddish yellow (7.5YR 6/6)

Section 7:
0–15 cm: 7.5YR 6/6

Core Catcher:
0–13 cm: 7.5YR 6/6

SMEAR SLIDE SUMMARY (%):

	2, 110 D	5, 30 D	6, 120
Composition:			
Quartz	–	TR	TR
Feldspar	–	TR	TR
Mica	–	TR	TR
Clay	15	>15	10–15
Volcanic glass	–	TR	TR
Palagonite	–	TR	–
Zeolite	TR	–	–
Calc. nannofossils	85	80	85
Opaques	–	TR	–

Information on core description sheets, for ALL sites, represents field notes taken aboard ship under time pressure. Some of this information has been refined in accord with post-cruise findings, but production schedules prohibit definitive correlation of these sheets with subsequent findings. Thus the reader should be alerted to the occasional ambiguity or discrepancy.

SITE 597 HOLE CORE 3 CORED INTERVAL 14.2–23.8 m

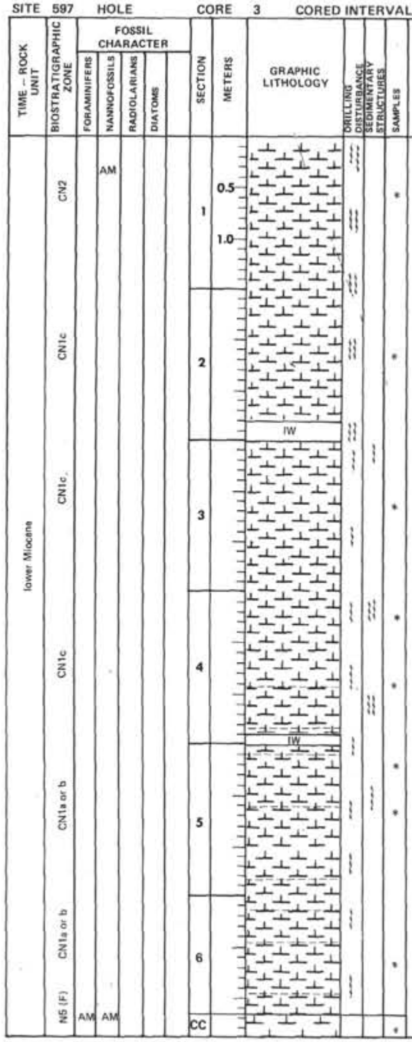

LITHOLOGIC DESCRIPTION

NANNOFOSSIL OOZE

Section 1:
0–150 cm: Reddish yellow (7.5YR 6/6)

Section 2:
0–140 cm: Reddish yellow (7.5YR 6/6)

Section 3:
0–11 cm: Strong brown (7.5YR 5/6)
11–34 cm: Reddish yellow (7.5YR 6/6)
34–85 cm: Strong brown (7.5YR 5/6)
85–150 cm: Reddish yellow (7.5YR 6/6)

Section 4:
0–140 cm: Strong brown (7.5YR 5/6)

CLAY-BEARING NANNO OOZE

Section 5:
0–150 cm: Strong brown (7.5YR 5/6)
Layers of brown (7.5YR 4/4) at 50–90, 110–122, and 136–140 cm

Section 6:
0–114 cm: Brown (7.5YR 4/4)
Slightly darker at 47–51 cm

Core Catcher:
Brown (7.5YR 4/4)

SMEAR SLIDE SUMMARY (%):

	2, 70	4, 30	6, 70
Texture:			
Clay	–	TR	10
Composition:			
Quartz	TR	–	–
Clay	TR	–	–
Calc. nannofossils	99	>95	90
Red-brown oxides	0.5	–	–

SITE 597 HOLE CORE 4 CORED INTERVAL 23.8–33.4 m

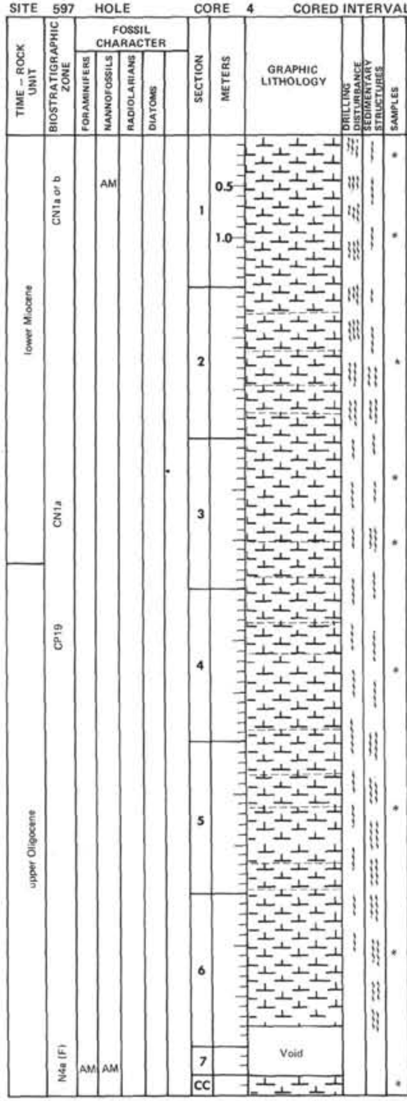

LITHOLOGIC DESCRIPTION

CLAY-BEARING NANNOFOSSIL OOZE

Section 1:
0–150 cm: Brown (7.5YR 4/4)

Section 2:
0–45 cm: Brown (7.5YR 4/4)
45–140 cm: Dark brown (7.5YR 3/4)

Section 3:
0–150 cm: Dark brown (7.5YR 3/4) grading to brown (7.5YR 4/4)

Section 4:
0–140 cm: Brown (7.5YR 4/4)

Section 5:
0–150 cm: Brown (7.5YR 4/4) grading to brown (7.5YR 5/4)

NANNOFOSSIL OOZE

Section 6:
0–115 cm: Brown (7.5YR 4/4)
115–124 cm: Dark brown (7.5YR 4/2)

Core Catcher:
Very dark brown (7.5YR 3/2)

SMEAR SLIDE SUMMARY (%):

	2, 75	4, 30	6, 60
Composition:			
Clay	20	>15	<40
Palagonite	TR	TR	–
Calc. nannofossils	80	80	>90
Opaques	–	1–2	–

Core 5, 33.4–43.0 m: no recovery.

SITE 597 HOLE CORE 6 CORED INTERVAL 43.0–52.6 m

TIME – ROCK UNIT	BIOSTRATIGRAPHIC ZONE	FORAMINIFERS	NANNOFOSSILS	RADIOLARIANS	DIATOMS	SECTION	METERS
upper Oligocene	CP19		CA/M			1	0.5, 1.0
						2	
						3	
						4	
						5	
	CP19					6	
	N4a (F)	RP	FP			CC	

GRAPHIC LITHOLOGY / DRILLING DISTURBANCE / SEDIMENTARY STRUCTURES / SAMPLES

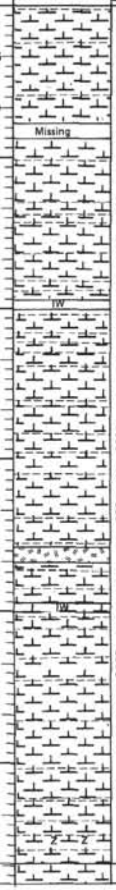

LITHOLOGIC DESCRIPTION

CLAYEY NANNOFOSSIL OOZE

Section 1: CLAYEY NANNOFOSSIL OOZE
0–42 cm: Brown (5YR 3/3)
42–49 cm: Chocolate brown (5YR 2.5/2)
49–116 cm: Brown (5YR 3/3)

NANNOFOSSIL CLAY

130–150 cm: Nannofossil clay, brown (5YR 3/3)

CLAYEY NANNO OOZE TO NANNO CLAY

Section 2:
0–47 cm: Dark reddish brown (5YR 2.5/2)
47–68 cm: Black (5YR 2.5/1)
68–140 cm: Dark reddish brown (5YR 3/2)

Section 3:
0–110 cm: Dark reddish brown (10YR 3/3)
110–120 cm: Dark reddish brown (10YR 2.5/2)
120–150 cm: Dark reddish brown (5YR 3/3)

Section 4:
0–17 cm: Dark reddish brown (5YR 3/4)
17–29 cm: Dark reddish brown (5YR 2.5/2)
29–64 cm: Dark reddish brown (5YR 3/4)
64–91 cm: 5YR 3/2
91–95 cm: 5YR 4/6
95–131 cm: 5YR 3/4
131–140 cm: 5YR 2.5/2

Section 5:
0–28 cm: 5YR 2.5/2
28–46 cm: 5YR 3/4
46–82 cm: 5YR 3/3
82–105 cm: 5YR 3/2
105–113 cm: 5YR 3/4
113–148 cm: 5YR 2.5/3

Section 6:
0–8 cm: 5YR 3/4
8–27 cm: 5YR 2.5/2
27–46 cm: 5YR 3/2
46–80 cm: 5YR 3/2
80–97 cm: 5YR 2.5/3

SMEAR SLIDE SUMMARY (%):

	2, 100	4, 92	5, 107
	D	M	D
Texture:			
Silt	50	95	30
Clay	50	5	70
Composition:			
Quartz	–	–	<5
Feldspar	–	2	TR
Heavy minerals	–	5	–
Clay	45–55	–	30
Volcanic glass	–	80	–
Palagonite	–	6	–
Zeolite	–	<5	–
Foraminifers	TR	TR	<5
Calc. nannofossils	45–55	5	60
Fe-Mn oxy. hydrox.	TR	–	~3

SITE 597 HOLE CORE 7 CORED INTERVAL 52.6–52.7 m

TIME – ROCK UNIT	BIOSTRATIGRAPHIC ZONE	FORAMINIFERS	NANNOFOSSILS	RADIOLARIANS	DIATOMS	SECTION	METERS
upper Oligocene		RF/P	AM			1	

GRAPHIC LITHOLOGY / DRILLING DISTURBANCE / SEDIMENTARY STRUCTURES / SAMPLES

LITHOLOGIC DESCRIPTION

DRILLING BRECCIA

Sediment color is dark brown (7.5YR 3/2). Contains silty chalk fragments.

SITE 597 HOLE CORE 8 CORED INTERVAL 52.7–54.7 m

TIME – ROCK UNIT	BIOSTRATIGRAPHIC ZONE	FORAMINIFERS	NANNOFOSSILS	RADIOLARIANS	DIATOMS	SECTION	METERS
upper Oligocene	CP19		AM			1	0.5, 1.0
	N4a (F)	RF/P				2	

GRAPHIC LITHOLOGY / DRILLING DISTURBANCE / SEDIMENTARY STRUCTURES / SAMPLES

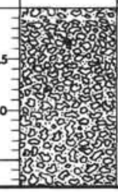

LITHOLOGIC DESCRIPTION

DRILLING BRECCIA

Mixture of dark brown (7.5YR 3/2) sediment.

BASALT FRAGMENTS

Basalt medium- to fine-grained, almost non-porphyritic (<1% phenocrysts). 1% by volume vesicles lined with green smectite. Igneous mineralogy almost entirely plagioclase, clinopyroxene, and iron-oxides.

SITE 597 HOLE A CORE 1 CORED INTERVAL 0.0–4.6 m

TIME – ROCK UNIT	BIOSTRATIGRAPHIC ZONE	FOSSIL CHARACTER: FORAMINIFERS	NANNOFOSSILS	RADIOLARIANS	DIATOMS	SECTION	METERS	GRAPHIC LITHOLOGY	DRILLING DISTURBANCE	SEDIMENTARY STRUCTURES	SAMPLES	LITHOLOGIC DESCRIPTION

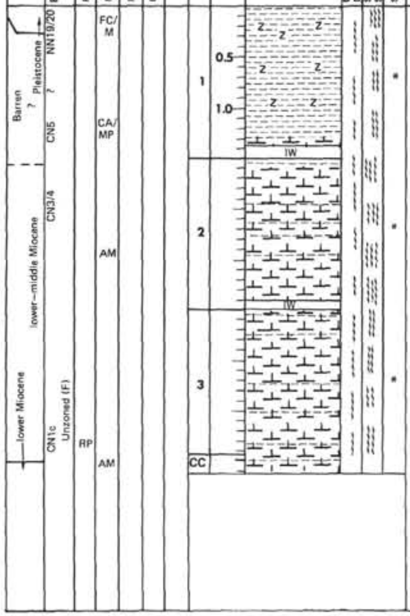

Section 1:
0–133 cm: ZEOLITIC PALAGONITIC CLAY, dark reddish brown (5YR 2.5/2) grading to dark reddish brown (5YR 3/3)
133–140 cm: CLAY-BEARING NANNO OOZE, dark brown (7.5YR 4/4)

Section 2:
0–55 cm: Dark brown (7.5YR 3/4)
55–83 cm: Brown (7.5YR 4/4)
83–140 cm: Brown (7.5YR 5/4)

Section 3:
0–43 cm: Strong brown (7.5YR 4/6) grading to brown (7.5YR 5/4)
43–48 cm: Brown (7.5YR 4/4)
48–65 cm: Lighter (slightly)
65–77 cm: Brown (7.5YR 4/4)
77–147 cm: Slightly lighter color

Core Catcher:
0–20 cm: Brown (10YR 4/4)

SMEAR SLIDE SUMMARY (%):

	1, 70	2, 70	3, 70
Texture:			
Sand	5	–	–
Silt	20	80	75
Clay	75	20	25
Composition:			
Quartz	TR	–	–
Feldspar	1–2	–	TR
Clay	70	15–20	25
Volcanic glass	5	1	1
Palagonite	>10	3	3
Zeolite	15	–	–
Foraminifers	–	TR	–
Calc. nannofossils	80+	80+	70

SITE 597 HOLE A CORE 2 CORED INTERVAL 4.6–14.2 m

TIME – ROCK UNIT	BIOSTRATIGRAPHIC ZONE	FOSSIL CHARACTER: FORAMINIFERS	NANNOFOSSILS	RADIOLARIANS	DIATOMS	SECTION	METERS	GRAPHIC LITHOLOGY	DRILLING DISTURBANCE	SEDIMENTARY STRUCTURES	SAMPLES	LITHOLOGIC DESCRIPTION

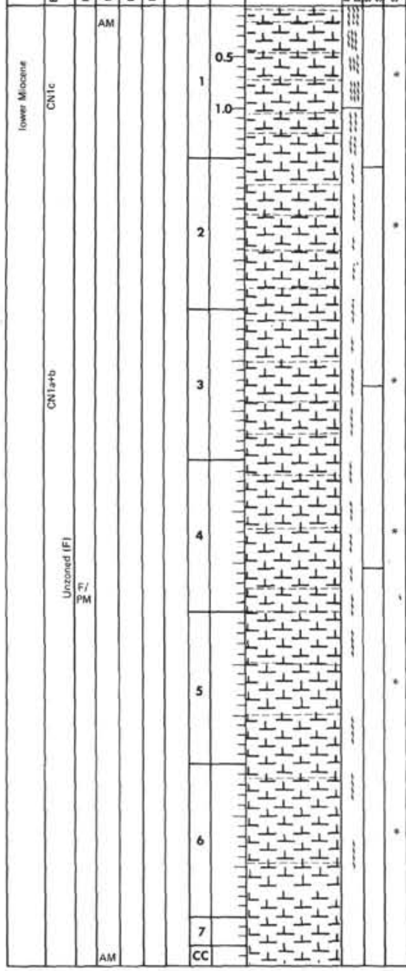

Section 1: CLAYEY NANNOFOSSIL OOZE
0–37 cm: Dark brown (10YR 3/4)
37–45 cm: Dark reddish brown (5YR 3/2)
45–150 cm: Dark brown (10YR 3/4)

Section 2: CLAYEY TO CLAY-BEARING NANNO OOZE
0–9 cm: Brown (7.5YR 4/4)
9–150 cm: Brown (7.5YR 5/4) grading to brown (7.5YR 4/4)

Section 3: CLAY-BEARING NANNOFOSSIL OOZE
0–71 cm: Brown (7.5YR 4/4)
71–150 cm: Brown (7.5YR 5/4)

Section 4:
0–104 cm: Brown (10YR 5/4) grading to brown (10YR 4/4)
104–150 cm: Brown (10YR 5/4)

Section 5: CLAY-BEARING NANNO OOZE TO NANNO OOZE
0–150 cm: Brown (10YR 5/6) grades to 10YR 6/6

Section 6:
0–150 cm: Reddish yellow (7.5YR 6/6)

Section 7: NANNO OOZE
0–52 cm: 7.5YR 6/6

Core Catcher:
0–22 cm: 10YR 6/6

SMEAR SLIDE SUMMARY (%):

	2, 70	4, 60	6, 70
Composition:			
Feldspar	TR	–	TR
Clay	25	15–20	10
Volcanic glass	–	TR	–
Palagonite	2	>1	TR
Foraminifers	–	TR	TR
Calc. nannofossils	70	75	85

SITE 597 HOLE A CORE 3 CORED INTERVAL 14.2–23.8 m

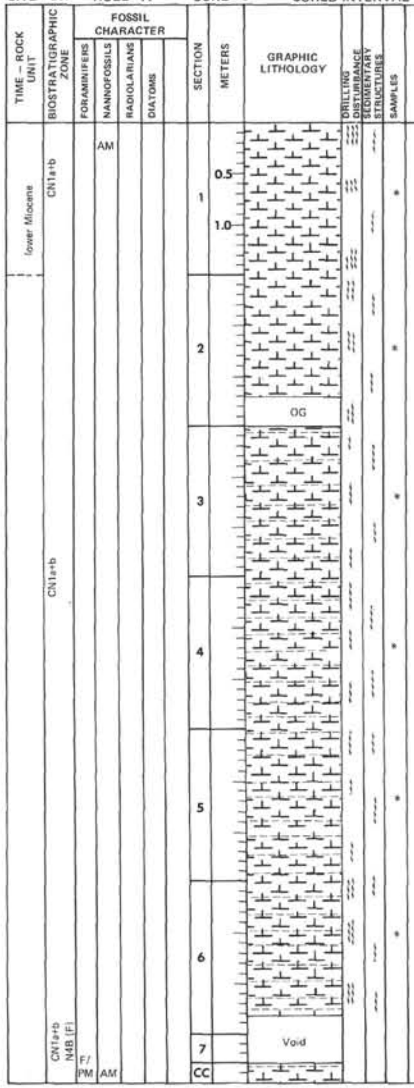

LITHOLOGIC DESCRIPTION

Section 1:
0–150 cm: NANNOFOSSIL OOZE, brown (7.5YR 5/4) grading into strong brown (7.5YR 5/8)

Section 2:
0–120 cm: NANNOFOSSIL OOZE, brown (7.5YR 4/4)

Section 3:
0–150 cm: CLAY-BEARING NANNO OOZE, brown (7.5YR 4/4)
36–40, 74–83, and 123–132 cm: Slightly darker color

Section 4:
0–150 cm: CLAY-BEARING NANNO OOZE, brown (7.5YR 4/4)
53–59, 86–90, and 113–118 cm: Slightly darker color

Section 5:
0–150 cm: CLAY-BEARING NANNO OOZE, brown (7.5YR 4/4)
0–10 and 92–97 cm: Slightly darker color

Section 6:
0–131 cm: CLAY-BEARING TO CLAYEY NANNO OOZE, brown (7.5YR 4/4)
21–25, 68–72, and 112–118 cm: Slightly darker color

Core Catcher:
0–14 cm: Brown (7.5YR 4/4)

SMEAR SLIDE SUMMARY (%):

	2, 70	4, 70	6, 50
Texture:			
Silt	85	80	75
Clay	15	20	25
Composition:			
Feldspar	TR	–	–
Clay	10	15	25
Volcanic glass	TR	–	–
Palagonite	TR	1	1–2
Foraminifers	–	1	1
Calc. nannofossils	85	80	70

SITE 597 HOLE A CORE 4 CORED INTERVAL 23.8–33.4 m

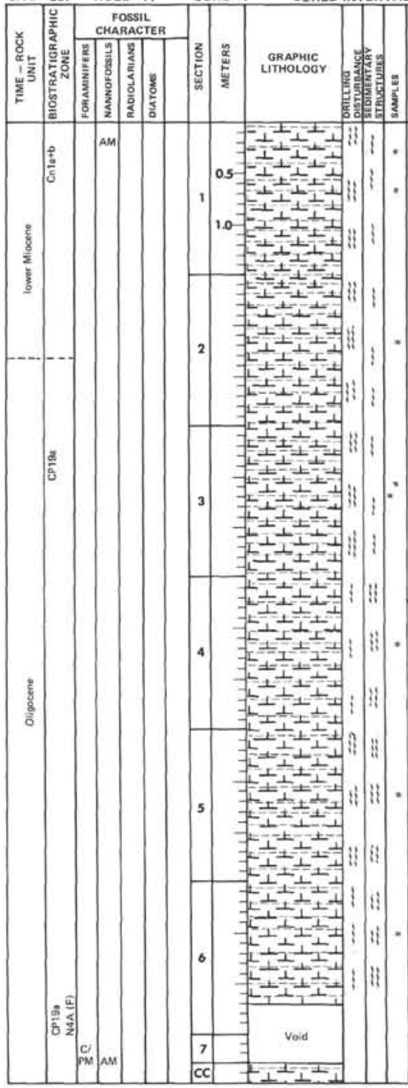

LITHOLOGIC DESCRIPTION

Section 1:
0–150 cm: CLAY-BEARING NANNO OOZE, brown (7.5YR 4/4)

Section 2:
0–140 cm: CLAY-BEARING NANNO OOZE, brown (7.5YR 4/4)

Section 3:
0–150 cm: CLAY-BEARING NANNO OOZE, brown (7.5YR 4/4)
51–55 cm: Slightly darker color

Section 4:
0–150 cm: CLAY-BEARING NANNO OOZE, brown (7.5YR 4/4)
55–63 cm: Slightly darker color

Section 5:
0–150 cm: CLAY-BEARING NANNO OOZE, brown (7.5YR 4/4)
143–150 cm: Slightly darker color

Section 6:
0–120 cm: Dark brown (7.5YR 3/2) CLAY-BEARING NANNO OOZE

Core Catcher:
Dark brown (7.5YR 3/2)

SMEAR SLIDE SUMMARY (%):

	1, 30	3, 60	5, 70
	D	D	D
Texture:			
Silt	80	75	80
Clay	20	25	20
Composition:			
Clay	15	20	10
Palagonite	–	TR	–
Calc. nannofossils	85	80	90

SITE 597 HOLE A CORE 5 CORED INTERVAL 33.4–43.0 m

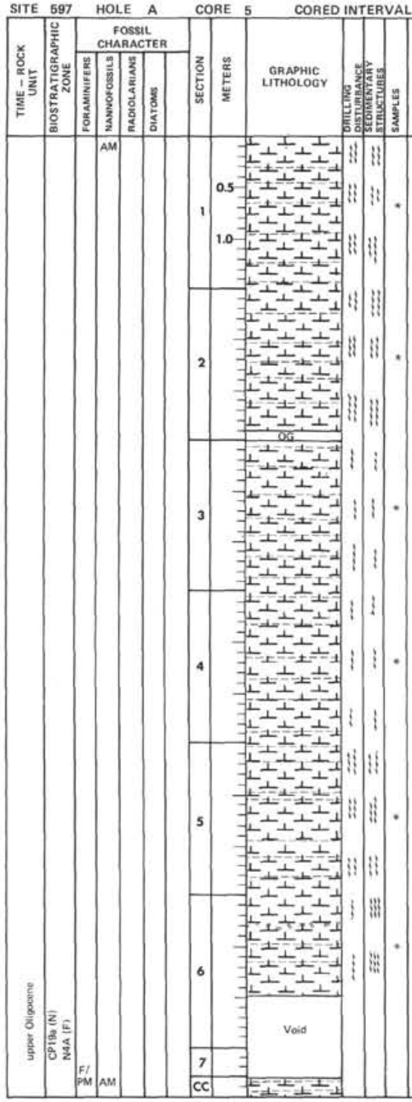

LITHOLOGIC DESCRIPTION

Section 1:
0–147 cm: CLAY-BEARING NANNO OOZE, brown (7.5YR 4/4) silty clay
137–147 cm: Slightly darker color

Section 2:
0–140 cm: CLAY-BEARING NANNO OOZE, brown (7.5YR 4/4)

Section 3:
0–150 cm: CLAY-BEARING NANNO OOZE, brown (7.5YR 4/4)
29–32, 66–72, and 125–129 cm: Slightly darker

Section 4:
0–150 cm: CLAY-BEARING NANNO OOZE, dark reddish gray (5YR 4/2)

Section 5:
0–150 cm: CLAY-BEARING TO CLAYEY NANNO OOZE, dark reddish brown (5YR 3/4)
0–4, 83–86, 111–114, and 133–137 cm: Slightly darker color

Section 6:
0–95 cm: CLAY-BEARING NANNO OOZE, dark reddish brown (5YR 3/4)
7–11 cm: Slightly darker color
33–34 cm: Slightly lighter color, zeolitic, palagonitic ash

Core Catcher: Dark reddish brown (5YR 3/4)

SMEAR SLIDE SUMMARY (%):

	2, 70 D	4, 70 D	6, 50 D
Texture:			
Silt	65	75	75
Clay	35	25	25
Composition:			
Clay	15	15	15
Foraminifers	–	TR	TR
Calc. nannofossils	85	85	85
Opaques	TR	–	–

SITE 597 HOLE A CORE 6 CORED INTERVAL 43.0–47.6 m

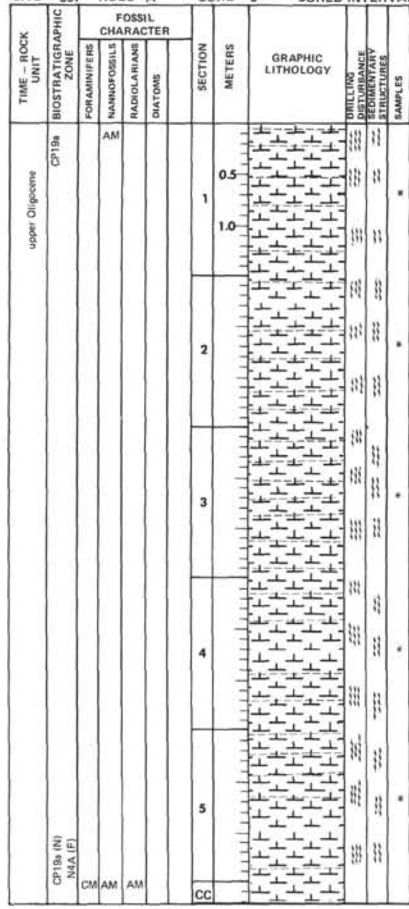

LITHOLOGIC DESCRIPTION

Section 1:
0–150 cm: CLAYEY NANNO OOZE, dark reddish brown (5YR 3/4) with yellowish red (5YR 5/8) smeared blobs at 142–146 cm, probably fall in
Entire section soupy

Section 2:
0–150 cm: CLAY-BEARING TO CLAYEY NANNO OOZE, dark reddish brown (5YR 3/4) with yellowish red (5YR 5/8) smeared blobs at 67–73 and 113–150 cm
Entire section soupy

Section 3:
0–150 cm: CLAYEY NANNO OOZE, dark reddish brown (5YR 3/4) with yellowish red (5YR 5/8) smeared blobs at 0–60 cm
123–127, 133–137, and 145–150 cm: Slightly darker bands
0–60 cm: Very soupy

Section 4:
0–150 cm: CLAYEY NANNO OOZE, dark reddish brown (5YR 3/4) with yellowish red (5YR 5/8) smeared blobs at 125–150 cm

Section 5:
0–150 cm: CLAYEY NANNO OOZE TO NANNO CLAY, dark reddish brown (5YR 3/4) with yellowish red (5YR 3/4) smeared blobs at 5–33 cm
Entire section soupy

Core Catcher:
0–7 cm: Dark reddish brown (5YR 3/4)

SMEAR SLIDE SUMMARY (%):

	1, 70 D	3, 70 D	5, 70 D
Texture:			
Silt	65	65	50
Clay	35	35	50
Composition:			
Quartz	TR	–	–
Feldspar	TR	TR	–
Clay	35	35	–
Palagonite	<1	1–2	1
Zeolite	1–2	TR	TR
Foraminifers	5	5	5
Calc. nannofossils	60	60	45
Fe-Mn oxy. hydrox.	–	–	TR

SITE 597 HOLE A CORE 7 CORED INTERVAL 47.6–48.6 m

Core Catcher: 21 cm of fragments of basalt glass breccia.

It contains angular clasts, up to 2 cm across, of fresh basaltic glass covered by 2-mm rinds of palagonite. The matrix is pink to white in color and comprises fine-grained phillipsite, calcite, and minor iron oxyhydroxide, and it contains drusy cavities partially filled by well crystallized calcite.

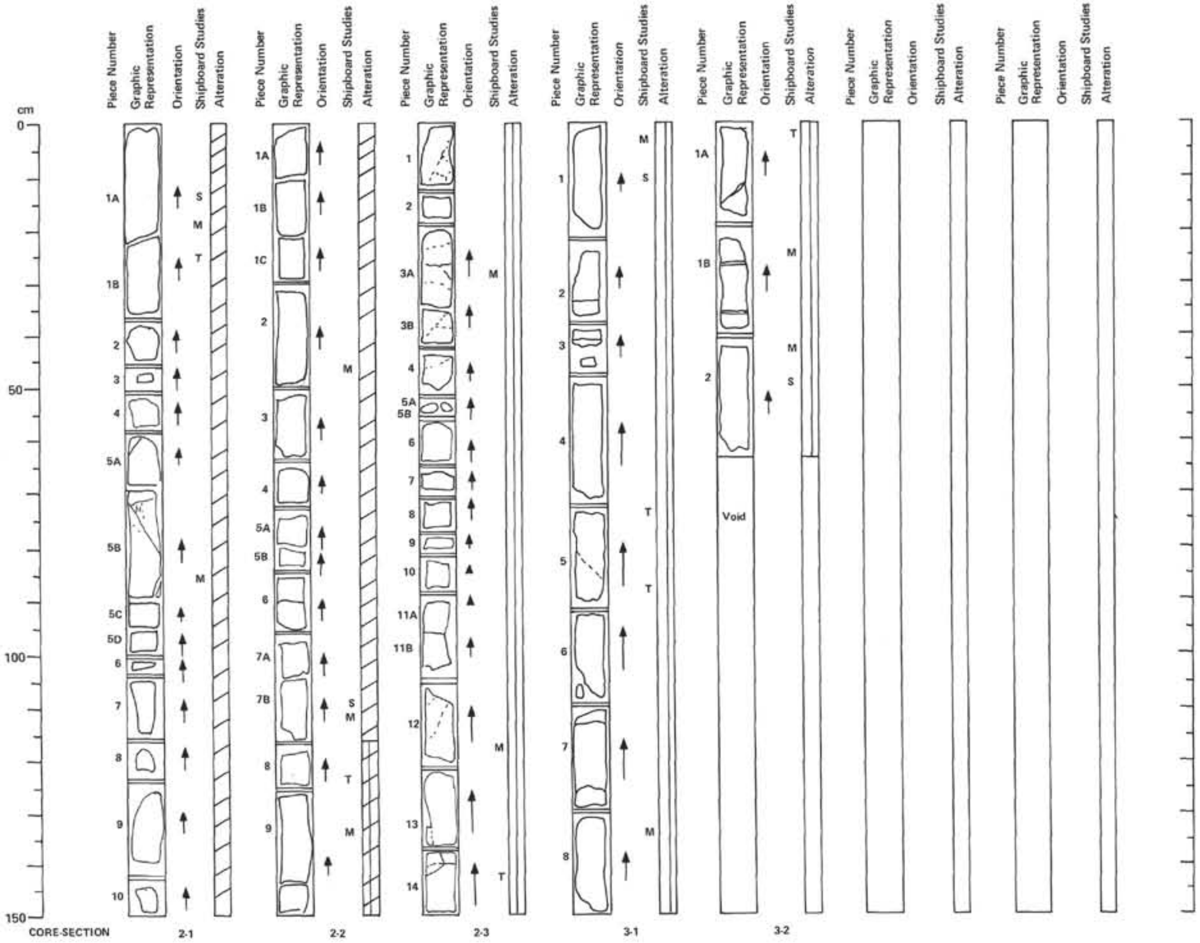

92-597B-2 Depth: 54.4–63.5 m

Macroscopic description

(i) Rock type: Basalt – fine- to medium-grained, predominantly aphyric but with rare microphenocrysts of clinopyroxene. Mineralogy = plagioclase and clinopyroxene (and oxides). No igneous contacts within section.

(ii) Alteration: Slight to moderate alteration; patchy brown oxidative alteration at margins of some fragments and around some veins. Pieces 1A and 1B are least altered.

(iii) Vesicles: Highly vesicular ranging from 10–20% by volume up to 1 mm in diameter – subspherical. Most vesicles filled though empty vesicles common in Pieces 8–10. Fillings: brown-stained ?zeolite, calcite, green smectite (Piece 7 only). In zoned vesicles calcite occupies center.

(iv) Veins: Rare, brown iron oxide/?clay-filled (esp. Piece 5B) or calcite-filled (esp. Pieces 7–9).

Thin section description

Piece 1B, 25–26 cm: Aphyric basalt. The basalt is made up of zoned ($\sim An_{60}$–An_{70}) *plagioclase laths and rare* clinopyroxene crystals set in a finer-grained variolitic matrix of plagioclase and clinopyroxene and some interstitial grains of iron oxide and cryptocrystalline $\sim pl_{65}\ cpx_{34}\ mt_{1}$. Vesicles $\sim$15% by volume, subspherical containing pale brown cryptocrystalline material (?smectite ?zeolite) and sometimes an inner core of calcite. Brown material replaces the finer grained material in matrix (deeper brown where close to magnetite). Possible incipient alteration of feldspar.

Section 2: BASALT (?massive flow)

Macroscopic description

(i) Rock type: Basalt – fine- to medium-grained, aphyric containing clinopyroxene and plagioclase. No igneous contacts within section.

(ii) Alteration: Moderate alteration. Oxidative alteration common but variable involving replacement of clinopyroxene by orange-brown Fe-oxide-hydroxides and staining of feldspars. Celadonite appears in Pieces 8 and 9 and occurs with zeolite in matrix as well as vesicles.

(iii) Vesicles: Highly vesicular throughout ($\sim$20% by volume), vesicles ranging up to 1 mm diameter. Filling variable from 0–100%. In Pieces 1–7, zeolite (and Fe-oxide) and calcite common, in Pieces 8 and 9 blue-green celadonite and zeolite common. One vesicle in Piece 9 has celadonite rim, and zeolite and pyrite in center.

(iv) Veins: Rare calcite veins in Pieces 1–7; celadonite and zeolite and pyrite and calcite veins from upper and lower edges of Pieces 8 and 9.

Thin section description

Piece 8, 122–123 cm: Aphyric basalt. The basalt is made up of plagioclase feldspar (zoned $\sim An_{60}$–An_{70}) and augitic pyroxene with a small proportion of iron-oxide. The texture is normally intersertal, locally ophitic reaching a maximum grain size of about 1.5 mm. Vesicles make up about 2% by volume and are completely filled by pale brown cryptocrystalline material (?smectite). This same brown material replaces about 20% of the rock, variably pseudomorphing pyroxene.

Section 3: BASALT (?massive flow)

Macroscopic description

(i) Rock type: Basalt – fine- to medium-grained, slightly porphyritic (<2%) to aphyric. Phenocrysts and microphenocrysts (< 1.5 mm) are of clinopyroxene; mineralogy = clinopyroxene and plagioclase and Fe-oxides. No igneous contacts within section.

(ii) Alteration: Strong, pervasive alteration dominated by replacement of primary minerals by celadonite, green smectite (esp. Pieces 3A and B), *zeolite and orange Fe-O-OH. Details of alteration vary down section as seen in dark* 'alteration fronts' rich in celadonite which give rock a patchy dark-pale gray appearance. Pseudomorphing of pyroxenes by the various alteration minerals is common.

(iii) Vesicles: Approximately 5% by volume, usually filled wholly or partially. Celadonite most common filling but also iron-oxide, zeolite, and calcite. Zoning common, often celadonite rim and calcite growing into center; also zeolite rim and calcite center. Orange iron-oxide-hydroxide alteration outside vesicles.

(iv) Veins: Very thin black celadonite veins occur throughout. Calcite veins rarer but thicker (<1.5 mm) (esp. Piece 14).

Thin section description

Piece 14, 144–145 cm: Aphyric basalt. The basalt is made up of plagioclase (50–60%), clinopyroxene (40–50%) and a few per cent iron-oxide. Both plagioclase (ave. An_{65}) and clinopyroxene are zoned. The texture varies from intersertal to ophitic/poikilitic. There are about 3% spherical vesicles containing mainly a yellow brown fibrous material (?smectite) with a small amount of red-brown Fe-oxide and opaques. This material also pseudomorphs *some clinopyroxene grains. Both feldspars and clinopyroxenes may have suffered incipient alteration.*

92-597B-3 Depth: 63.5–72.6 m

Section 1: BASALT (massive flow?)

Macroscopic description

*(i) Rock type: Fine- to medium-grained basalt, aphyric with trace microphenocrysts of clinopyroxene; min*eralogy: clinopyroxene and plagioclase and Fe-oxides (except Piece 1 and Piece 5 at bottom). No igneous contact within section.

(ii) Alteration: Strong alteration with variations down section, generally with replacement of primary minerals by green-blue smectite(?) and orange-red Fe-oxides. Piece 1 is dark-pale gray, with no red Fe-oxides, but mainly with dark alteration minerals. Piece 5 has an 'alteration front' – its top has Fe-oxides and its bottom is like Piece 1. There is rare pseudomorphing of pyroxene by alteration minerals.

(iii) Vesicles: <1% by volume; filled with green-blue smectite in Piece 1 and bottom of Piece 5 – otherwise filled with Fe-oxides or zeolites.

(iv) Veins: Rare. Piece 3 filled with calcite; Piece 7 at top (112 cm) filled with celadonite (1–1.5 mm).

Thin section description: Slightly porphyritic basalt containing plagioclase, clinopyroxene, opaque iron oxide and cryptocrystalline interstitial material, ~1% plagioclase phenocryst and 2% plagioclase glomerocrysts (2–3 mm size). Variolitic texture (radiating plagioclase laths and interstitial pyroxene and 'magnetite' and cryptocrystalline matrix). Between varioles texture varies from intersertal to ophitic. Grain size of groundmass from <0.1–1 mm. All cryptocrystalline matrix and parts of some pyroxenes are altered to yellow-green clay. Otherwise minerals quite fresh. Further oxidative alteration converts this to a yellow-brown clay and medium iron oxide (?hematite). Minor vesicles, contain some clay minerals and calcite if near vein. Calcite vein (late) cuts rock. Very low birefringent cryptocrystalline material near vein, probably zeolite.

Piece 5, 87–89 cm: Basalt (slightly plagioclase-phyric). The basalt is made up of about 60% plagioclase, about 40% clinopyroxene and a few per cent Fe-oxides. It contains ~2% plagioclase phenocrysts which are 2–3 mm across, strongly zoned with outer sodic margins and includes glomerocrysts. The groundmass has an intersertal to ophitic texture of grain-size 0.1–1 mm although the largest poikilitic clinopyroxenes reach 2 mm. There are about 1% vesicles containing a bright green clay mineral (plane polarized light) and an opaque mineral. Alteration includes about 5% replacement of groundmass (esp. clinopyroxene) by the bright green and a yellow-green clay mineral. Most crystals are cloudy possibly indicative of further incipient alteration.

Section 2: BASALT (massive flow?)

Macroscopic description

(i) Rock type: Fine- to medium-grained basalt; aphyric with trace microphenocrysts of clinopyroxene; mineralogy: clinopyroxene and plagioclase (and Fe-oxides in Pieces 1A and 1B).

(ii) Alteration: Moderate to strong alteration with variations down section, with replacement of primary minerals by green-gray smectite(?), zeolite and orange-red Fe-oxides. Piece 1A shows oxidative alteration (Fe-oxides). Piece 1B shows an 'alteration front' – its top has dark green-blue alteration minerals and its bottom has Fe-oxides. Piece 2 has green-blue-gray smectite and zeolite. There is pseudomorphing of primary minerals by alteration minerals (Fe-oxides in Piece 1).

(iii) Vesicles: <1% by volume. Piece 1B bottom and Piece 1A filled partly with Fe-oxide rim and calcite in center or fully filled with Fe-oxides. Piece 2 and 1B top filled with green-blue smectite(?) ≲1 mm diameter.

(iv) Veins: Rare; filled commonly with Fe-oxides; sometimes with adjacent altered zones.

It seems that Pieces 1A and 1B should not be placed together.

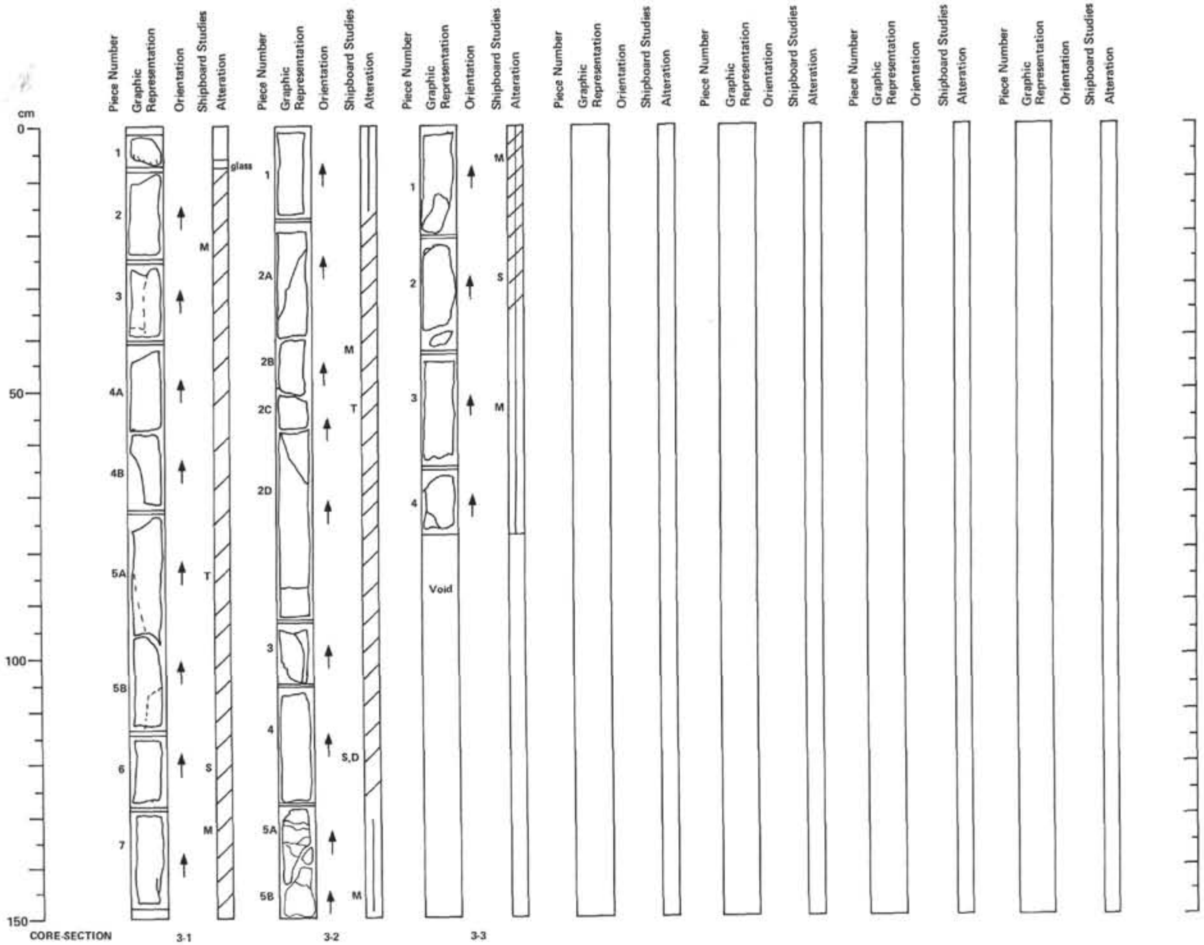

92-597C-3 | Depth: 55.5–64.5 m

Section 1:

Macroscopic description

Piece 1 is a fine-grained basalt with a 3 mm thick glassy margin containing fresh glass inside a palagonitized rim. There is a thin vesicular zone inside the glassy margin containing a white-yellow mineral, not calcite (?zeolite ?smectite). The remainder contains clinopyroxene plagioclase and a yellow-brown ?smectite and about 3% of microvesicles. One 'hole' about 3 mm across and rimmed with iron oxide could have been a pseudomorphed phenocryst (?olivine).

Pieces 2–7:

(i) Rock type: Fine- to medium-grained basalt, predominantly aphyric (rare microphenocrysts of plagioclase and clinopyroxene) containing clinopyroxene, plagioclase and oxide as primary minerals. No igneous contacts within section.

(ii) Alteration: Moderate alteration represented by clay minerals (?smectite) partly pseudomorphing pyroxene. Patchy brown oxidative alteration zones throughout. Outside zones the clay mineral is green-blue, inside it is yellow-brown.

(iii) Vesicles: General increase in vesicularity from Piece 2 (~3% by volume) to Piece 7 (~15% by volume). Vesicles generally subspherical, maximum size 1.5 mm. Vesicle filling variable: in non-oxidative zones it is blue-green clay ± calcite ± dark green clay; in oxidative zones it is yellow brown clay ± calcite. At border, yellow-brown clay replaces blue-green clay; around pyrite veins dark green clay replaces blue-green clay. Zeolite may also be present.

(iv) Veins: Not strongly veined. Thickest (<1 mm) are of calcite rimmed by yellow-brown clay and have variable orientation. Very thin horizontal veins contain sulfide and dark green clay ±? manganese oxide.

Thin section description

Pieces 5A, 83–84 cm: Aphyric though with 2–5% plagioclase glomerocrysts. Mineralogy: plagioclase 50%, clinopyroxene ~35%, magnetite ~5%, glass ≈10%. Texture ~50% subspherulitic, the remainder intersertal and intergranular. Interstitial glass replaced by medium-brown clay; minor alteration of feldspar by yellowish material. Vesicular (~5–7% vesicles), mostly partially filled. In unoxidized part of the core, outer zone is medium brown clay, inner zone is bright green clay. In oxidized part both are overprinted by reddish-brown clay/oxide. Groundmass clay is overprinted in the same way.

Section 2:

Macroscopic description

(i) Rock type: Fine- to medium-grained basalt; aphyric with trace microphenocrysts of clinopyroxene and plagioclase (+ Fe-oxides in Pieces 1, 2D, 3, and 5). No igneous contact within section. Mineralogy: clinopyroxene and plagioclase.

(ii) Alteration: Moderate alteration with variations down section; with pseudomorphic replacement of primary minerals by light green-blue clay minerals (smectite?) and orange-red Fe-oxides; zeolite. Pieces 1 and 5: oxidative alteration with mainly orange Fe-oxides. Pieces 2A–2D top, 4, and 3 bottom: light green-blue alteration minerals. Alteration fronts in Pieces 2B, 2D, and 3.

(iii) Vesicles: Piece 1: ~5% by volume, 1–5 mm diameter; partly filled with patchy brown-orange clay minerals, with red Fe-oxide rims and sometimes with calcite in the centers. Pieces 2–5: <1% by volume, ~1 mm diameter, filled with light green-blue alteration minerals except Piece 5, sometimes with orange rims (Piece 2D bottom and Piece 3 top), some filled with calcite.

(iv) Veins: Rare (except Piece 5); ~1–1.5 mm thick; filled commonly with dark alteration minerals, some with calcite (esp. Piece 5 with 5–8 mm vein). Some veins have adjacent red-orange altered zones.

Thin section description

Piece 2C, 50–51 cm: Range of grain size from <0.1–2 mm but no isolated phenocrysts, only a few glomerocrysts of plagioclase. Texture ranges from subvariolitic (~50% of slide) to intersertal and intergranular. Mineralogy is plagioclase feldspar, clinopyroxene and magnetite plus ~10% interstitial glass (totally replaced – so possibly originally cryptocrystalline. Magnetites ~3% are small (< 0.2 mm) and interstitial. Plagioclase has usual range of forms: skeletal microlites, long curved microlites, laths. Alteration is restricted to interstitial glass and comprises a dark reddish-brown clay minerals which makes up 5–10% of the rock. Small pyroxenes between microlites are unaffected. Vesicles make up ~2% of the rock and are partly to completely filled by the brown clay. One thin ?pyrite vein also evident.

Thin section description

Aphyric basalt though containing 1–2% of glomerocrysts of plagioclase. Primary mineralogy = ~60% plagioclase, 40% clinopyroxene, and ~3% oxide. Texture is mainly ophitic and the grain size from cryptocrystalline to 2.5 mm. The largest grains are poikilitic clinopyroxene. Approximately 10% of the slide is microcrystalline containing evidence of variolitic texture and possibly some glass (though now replaced by yellow sericite). Approximately 5% yellow smectite in slide, mainly replacing microcrystalline groundmass, ~1–2% of vesicles containing yellow smectite rim and calcite ± brown Fe-oxide core.

Section 3:

Macroscopic description

(i) Rock type: Fine- to medium-grained basalt; aphyric with rare microphenocrysts of clinopyroxene. No igneous contact within section. Mineralogy: clinopyroxene and plagioclase (+ trace Fe-oxides).

(ii) Alteration: Moderate alteration down section, with replacement of primary minerals by light yellow-patchy brown clay (?)minerals, zeolite and few orange-red Fe-oxides.

(iii) Vesicles: <1% by volume, ≤1 mm diameter; some empty with light yellow rims; others filled with yellow-brown clay ± calcite, possibly also with zeolites.

(iv) Veins: Rare, <1 mm, some with calcite, mainly filled with dark (green?) alteration minerals.

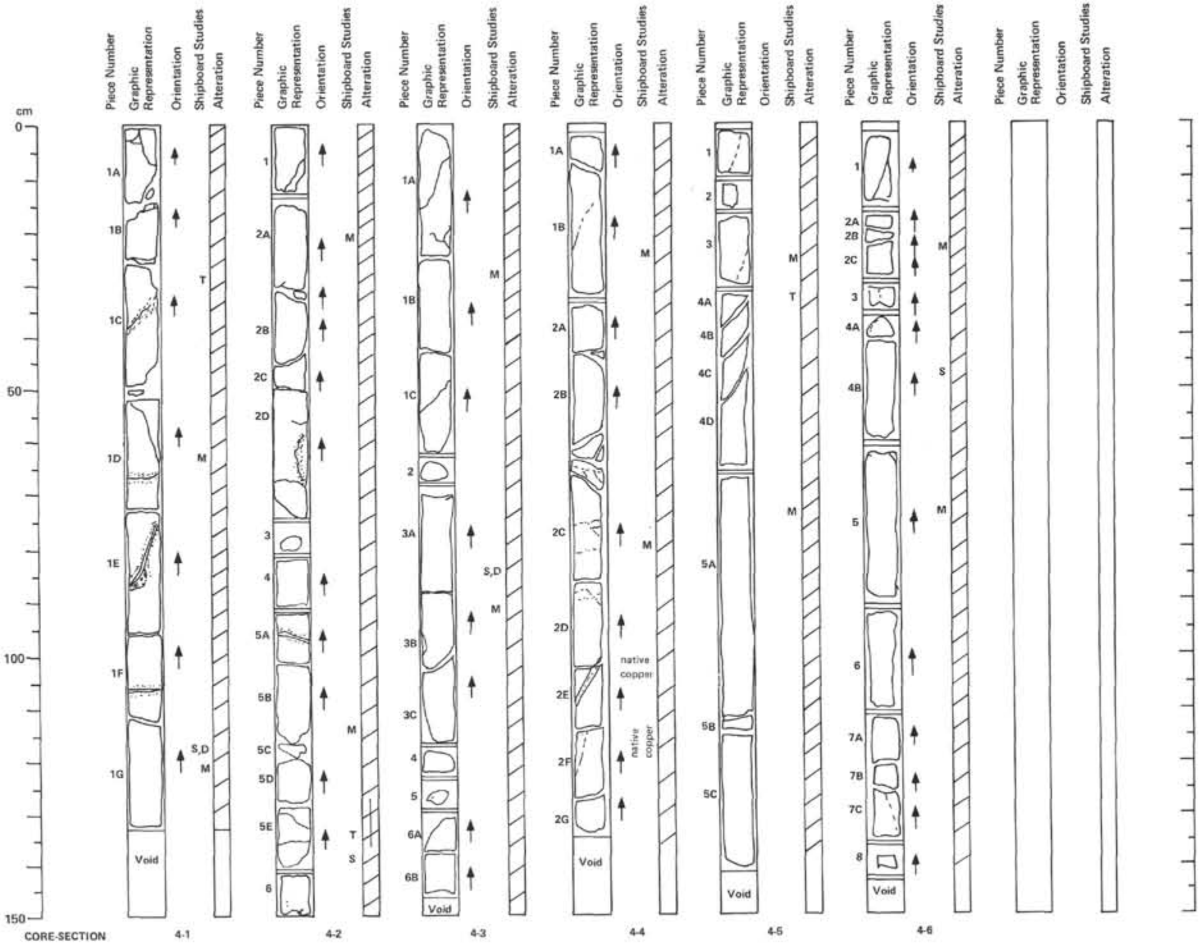

92-597C-4

Depth: 64.5–73.5 m

Section 1:

Macroscopic description

(i) Rock type: Fine- to medium-grained basalt; aphyric with trace microphenocrysts of pyroxene and plagioclase. No igneous contact within section. Mineralogy: clinopyroxene and plagioclase (+ traces of oxides).

(ii) Alteration: Moderate alteration with variations down section. Alteration fronts in Pieces 1A, 1B, and 1C; darker parts seem to be more altered then light parts; in darker parts there are dark green-blue alteration minerals (smectite?); trace zeolite; patchy brown-orange alteration at margins of veins. Replacement of primary minerals by different secondary minerals. Native copper near some veins (esp. Pieces 1C–E) (copper disseminated <0.1 mm); calcite rare.

(iii) Vesicles: Trace, <0.1% by volume; some filled with dark green smectite(?), some nearly empty with light yellow rims, no calcite-filling; <1 mm diameter; some with light green transparent crystals (copper minerals?).

(iv) Veins: Common – two types: a) with dark green smectite filling and adjacent alteration next to it;<1 mm thick; b) with white to light brown filling (no calcite or only traces) and nearly oxidative alteration (Fe-oxides) near to it; 1–6 mm; native copper occurs in vicinity of this type.

Thin section description

Piece 1B, 26–27 cm: Glomeroporphyric texture. Glomerocrysts comprise plagioclase (6% total volume, 1.5–3 mm crystal size) and clinopyroxene (2% total volume 1.5–2.5 mm crystal size, augite composition). Some feldspar zoned (sodic rim). Groundmass contains feldspar laths, some skeletal, and spherulites (0.2 mm typical diameter) of feldspar with interstitial clinopyroxene and magnetite and a small proportion of interstitial glass, now smectite. Some feldspars have cores of brown glass. Alteration of glass to yellow-green (p. p. light) smectite, which is brown in the vicinity of magnetite. Magnetites throughout have oxidized rims. No vesicles or veins. Quite a fresh rock by MORB standards.

Section 2:

Macroscopic description

(i) Rock type: Fine- to medium-grained basalt; aphyric with rare microphenocrysts of clinopyroxene and plagioclase. Mineralogy: clinopyroxene and plagioclase (+ traces of Fe-oxides). No igneous contact within section.

(ii) Alteration: Slight to moderate alteration with some variations down section (Fe-oxides in Pieces 2D, 5A, and 5E). Alteration fronts mostly in vicinity of veins; darker parts more altered than lighter parts; darker parts with dark green alteration minerals which sometimes replace primary minerals (smectite); zeolite; native copper near veins (esp. Pieces 5E and 2D). Piece 5E strongly altered with abundant green smectite(?) in matrix.

(iii) Vesicles: Trace, <1% by volume, different fillings: dark green opaque; light green transparent; white (no calcite); different copper minerals(?); pyrite: blue-green. Some with Fe-oxide rims and green-blue minerals in center, <1mm diameter.

(iv) Veins: Rare, <1 mm thick. Mainly two types: a) with dark green filling or light green alteration minerals (smectite?) and traces of calcite; without any visible halo and b) white to light brown to yellow minerals with Fe-oxide oxidation halos; native copper next to the veins (esp. Pieces 2D and 5E). Pyrite in veins (esp. Piece 5E).

Thin section description

Piece 5E, 133–134 cm: Slightly plagioclase-phyric basalt. Approximately 5% plagioclase phenocrysts (2–3 mm) forming large glomerocrysts. Groundmass texture variable. Coarser areas have ophitic – intersertal texture. Finer-grained areas have sub-variolitic texture. Interstitial material now contains green smectite and (Ti)-magnetite: green smectite possibly once glass. Alteration of 'glass' means that slide contains ~5% bottle green (p. p. light) smectite but minerals generally unaltered. Smectite is brown-green where locally oxidized. Thin calcite vein cuts section.

Section 3:

Macroscopic description

(i) Rock type: Fine- to medium-grained basalt; aphyric with trace microphenocrysts of clinopyroxenes and plagioclase. Mineralogy: clinopyroxenes and plagioclase. No igneous contact within section.

(ii) Alteration: Slight to moderate alteration with a few variations down section; almost no Fe-oxides except near veins. Replacement of primary minerals by zeolite(?) and smectite.

(iii) Vesicles: Trace <0.1% by volume, spherical, 1–1.5 mm diameter; nearly all filled with light blue-green alteration minerals, or sometimes blue smectite.

(iv) Veins: Rare, 1 mm thick filled with dark green material. One vein in Piece 1A has brown-orange (Fe-oxide?) alteration minerals next to it (±1 cm halo).

Section 4: Basalt (mainly aphyric) massive flow

Macroscopic description

(i) Rock type: Basalt, fine- to medium-grained with sparse (≤1%) microphenocrysts of plagioclase and clinopyroxene (~1.5 mm). Primary mineralogy = plagioclase and clinopyroxene (+ oxide). No igneous contacts. Color: gray to green-gray.

(ii) Alteration: Slight to moderate alteration mainly represented by variable alteration of pyroxene to dark green clay. Pieces 2C–2F exhibit oxidative alteration and contain yellow-brown clay. Alteration front in Piece 6.

(iii) Vesicles: Rare (≤1%) spherical vesicles ~1 mm diameter filled with clay. Color zoning in some from almost black margins to pale green cores.

(iv) Veins: Rare and irregular. Very thin veins contain dark green clay and (later???) brown clay with alteration halos. A few contain dark green clay only – one of these between Pieces 2E and 2F contains native copper. One vein of variable thickness (average ~5 mm) in Pieces D and E appears to contain a fibrous mineral (zeolite?), yellow-brown clay, calcite, a black-dark red/brown mineral (mica) and native copper.

Section 5: Basalt, massive flow

Macroscopic description

(i) Rock type: Basalt, fine- to medium-grained with sparse (≤1%) microphenocrysts of plagioclase and clinopyroxene (~1–5 mm). Primary mineralogy = plagioclase and clinopyroxene. No igneous contacts. Uniform gray color.

(ii) Alteration: Least altered so far but still shows green/blue-green clay replacement of pyroxene in places. Little oxidative alteration except around vein.

(iii) Vesicles: Rare (≤1%) subspherical vesicles containing black-dark gray clay.

(iv) Veins: Two veins only, one in Piece 1 and a smaller vein in Piece 3. The vein in Piece 1 comprises an outer brown clay(?) zone, then an inner zone going from black to dark green at the center. Width ~1 mm, orientation ~20° to vertical. Small subvein as above but no brown material. Contacts between Pieces 4A, 4B, 4C, and 4D also dark green vein material.

Thin section description

Piece 4A, 33–34 cm: Aphyric though with glomerophyric clusters of (mainly) plagioclase of > average grain size. Texture varies from spherulitic to intersertal and intergranular. Magnetites (~5%) are small and interstitial. Other minerals are plagioclase and clinopyroxene. Smaller plagioclase crystals sometimes have internal zones of glass. All glass is altered to a darkish brown ?clay mineral. No vesicles or veins.

Section 6: BASALT (massive flow)

Macroscopic description

(i) Rock type: Basalt, fine- to medium-grained with sparse (≤1%) microphenocrysts of plagioclase and clinopyroxene (~1.5 mm). Primary mineralogy: plagioclase and clinopyroxene (+ oxide). No igneous contact. Color: gray with brown patches.

(ii) Alteration: Slight to moderate alteration. In Pieces 1–4 and parts of Pieces 5–8, main effect is replacement of pyroxene by blue-green clay. In Pieces 5–8 variable oxidation replaces the blue-green with yellow-brown clay. Oxidation front evident within Pieces 5–8 in part sharp, in part showing mottling.

(iii) Vesicles: Very rare, subspherical clay-filled 0.5–1 mm diameter.

(iv) Veins: Two types of veins, both vertical or subvertical. First type seen in Pieces 1–5 contains dark green clay, very thin (??? + zeolite?). Second type in Piece 7 is ~1 mm thick containing white platy ??zeolite with calcite in central vug. Associated with a marginal yellow brown clay zone and a brownish alteration halo extending ~1.5 cm into surrounding rock.

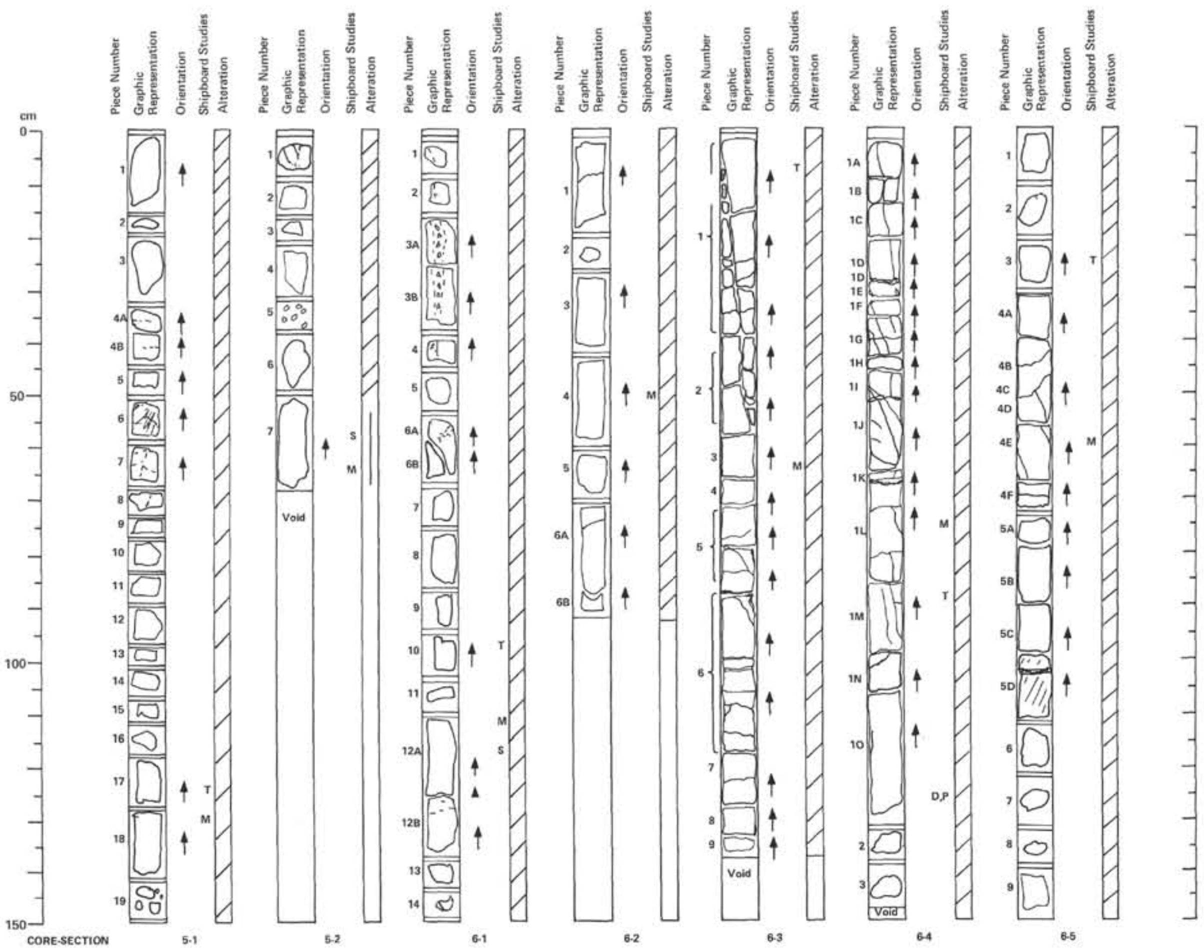

92-597C-5 Depth: 73.5–82.5 m

Section 1:

Macroscopic description

(i) Rock type: Basalt, fine- to medium-grained with sparse (<1%) microphenocrysts of plagioclase and clinopyroxene (~1.5 mm). Primary mineralogy: plagioclase and clinopyroxene (+ oxide). No igneous contact. Gray-brown color throughout.

(ii) Alteration: Moderate oxidative alteration throughout. Brownish crystalline material (stained zeolite more likely than smectite) common in groundmass and ?replacing feldspar. Pyroxene appears fresh. Calcite also in groundmass.

(iii) Vesicles: Rare, small containing brown material (see ii) and calcite.

(iv) Veins: Sparse thin veins in fragments but also at fragment margins. Contents calcite, probable zeolite and brownish smectite or iron-oxide staining.

Thin section description

Piece 17, 127–128 cm: Ophitic-poikilophitic texture of clinopyroxene enclosing plagioclase laths. Intersertal texture in places, the spaces filled by euhedral-subhedral magnetite and glass/cryptocrystalline material. Grain size from <0.1–2.5 mm. Glass altered to golden-yellow palagonite and brown smectite/oxide.

Section 2:

Macroscopic description

(i) Rock type: Basalt, fine- to medium-grained with sparse microphenocrysts of plagioclase and pyroxene. Pieces 6 and 7 may contain a significant percentage of microphenocrysts of pyroxene but this is difficult to assess owing to alteration. Plagioclase and clinopyroxene are the main minerals as before. No igneous contacts, gray-brown color.

(ii) Alteration: Moderate to intensive. All except Piece 6 have brown oxidative weathering. Where dark green clay is present this has partly reacted to a brown material, and pyroxenes and groundmass are partly replaced. Piece 4 does not show this alteration type. The main alteration mineral is green-white.

(iii) Vesicles: < 1% spherical vesicles in most of section. Contents are dark green clay rimmed by yellow-brown oxides and/or clay except in Piece 4 where they are filled by green-white clay. All 100% filled. Pieces 6 and 7 may contain more vesicles (see i).

(iv) Veins: Sparse. Piece 1 shows interesting relationship in which vein containing calcite/zeolite cuts vein containing dark green clay. Both have brown oxidized margins.

92-597C-6 Depth: 82.5–91.5 m

Section 1:

Macroscopic description

(i) Rock type: Basalt, fine- to medium-grained. Sparsely microphyric with ~5% feldspar and trace pyroxene microphenocrysts about 2–3 mm across. Groundmass and clinopyroxene and plagioclase (+ oxides). No igneous contacts. Color: gray.

(ii) Alteration: Moderately altered though irregular variation in intensity (Piece 12A freshest). Most alteration is oxidative in which yellow-brown oxides/clays pseudomorph pyroxene to various degrees. Some zeolite may be present.

(iii) Vesicles: Sparsely vesicular (~1%) containing orange-brown iron oxide/clay, calcite, pale brown clay. Spherical and irregular up to 1 mm diameter.

(iv) Veins: Pieces 1–4 contain a thick vein (1 cm maximum width) containing small angular fragments of wall rock and pinkish-brown iron-oxide and/or clay, zeolite, calcite and a pale green ?clay and a dark mineral, possibly mica. Other smaller veins also present.

Thin section description

Piece 10, 94–95 cm: Aphyric though with glomerophyric clusters that contain plagioclase, olivine and minor clinopyroxene. Approximately 60% of the rock has a spherulitic texture, the remainder is intersertal, sometimes intergranular. Plagioclase varies from <0.1–2 mm and from microlites to tabular laths. Clinopyroxenes vary from 0.1–1 mm. Olivines are sub-euhedral, and include one 2 mm crystal and a number of 0.1–0.5 mm crystals. Magnetite (~3%) are small and interstitial. All olivines are totally replaced by yellow clay and orange-brown oxide in rims and fractures. All glass (or cryptocrystalline material) is replaced by brown clay. No veins or vesicles in section.

Section 2: BASALT (massive flow)

Macroscopic description

(i) Rock type: Fine- to medium-grained basalt. Aphyric with rare microphenocrysts of feldspar and pyroxene (1–3 mm across). Mineralogy: clinopyroxene and plagioclase (±oxides). No igneous contact within section.

(ii) Alteration: Moderately altered with irregular variation down section. Alteration is mainly oxidative in which yellow to light brown oxides/clays(?) pseudomorph pyroxene in lighter gray parts; in darker gray parts the alteration minerals may be the same, but only the color changes to red-orange-brown (alteration may be more intensive).

(iii) Vesicles ≪0.1% by volume, 1 mm diameter, filled with orange-brown Fe-oxides or Fe-clays.

(iv) Veins: Trace; <1 mm thick; filled with light brown Fe-oxides/smectite.

Section 3: BASALT (massive flow)

Macroscopic description

(i) Rock type: Fine- to medium-grained basalt. Aphyric with microphenocrysts of feldspars and pyroxene (2–3 mm across). Mineralogy: clinopyroxene and plagioclase (±oxides). No igneous contact within section.

(ii) Alteration: Moderately altered with irregular variation down section, esp. near veins. Alteration is oxidative with red-brown material which pseudomorphly replaces pyroxene. In the less altered Pieces 2 bottom, 3, and 4 the alteration minerals (zeolites?–smectites?) are light yellow to light orange. Near viens red-brown Fe-oxides and sometimes calcite, are common.

(iii) Vesicles: <0.1% by volume, 1–2 mm diameter. All filled with material from light yellow to brown-red, no calcite.

(iv) Veins: Common esp. in Pieces 1, 2, 5, and 6; ~1 mm thick, filled with green to yellow-red smectite and calcite. Red Fe-oxide halos.

Section 4: BASALT (massive flow)

Macroscopic description

(i) Rock type: Fine- to medium-grained basalt; aphyric with microphenocrysts of plagioclase and clinopyroxene (1–2 mm across). Mineralogy: clinopyroxene, plagioclase (+ oxides). No igneous contact within section.

(ii) Alteration: Moderately altered with variations down section. Replacement of primary minerals by alteration material with different colors, from white to red-brown. Pieces 1A–1E; light brown to yellow minerals (also Fe-oxides). Pieces 1F–1I: yellow-brown, light green and dark green minerals. Pieces 1J–1O: only light to dark green alteration minerals. No "brown" colors, but white zeolites in matrix. Piece 1O has an alteration front – the bottom of Piece 1O and Pieces 2 and 3 have no colored alteration products, while the top of Piece 1O has light green minerals.

(iii) Vesicles: Nearly no vesicles.

(iv) Veins: Common in Pieces 1A–1N; rare in Pieces 1O, 2, and 3; <1 mm–1.5 mm thick; filled with zeolites, different colored smectites(?) and calcite. Color depends on alteration zone (white, green, red-brown Fe-oxides halos in Pieces 1A–1E). Some well crystallized minerals of zeolite(?).

Section 5: BASALT (massive flow)

Macroscopic description

(i) Rock type: Fine- to medium-grained basalt; aphyric with microphenocrysts of plagioclase and pyroxene (2–3 mm across). Mineralogy: clinopyroxene, plagioclase (+ oxides). No igneous contact within section.

(ii) Alteration: Moderately altered with variations down section. Pseudomorphic replacement of primary minerals (pyroxenes) by alteration minerals. Different alteration stages: light green to dark green to light brown to red-brown. Some blue-green alteration products (smectite). Fe-oxides Pieces 4A–4F, some calcite is common.

(iii) Vesicles: Trace <1% by volume, <1 mm diameter filled with Fe-oxides or dark green smectite(?). Empty vesicles in Piece 1 with ~1% by volume (vugs?).

(iv) Veins: Trace, <1–2 mm thick. White minerals in Piece 4B (less calcite). Light brown filling in Pieces 5B and 5C. Others filled with dark green materials. Piece 5D shows one side of a vein with filling materials (may be 2–3 mm thick), some well crystallized partly calcite.

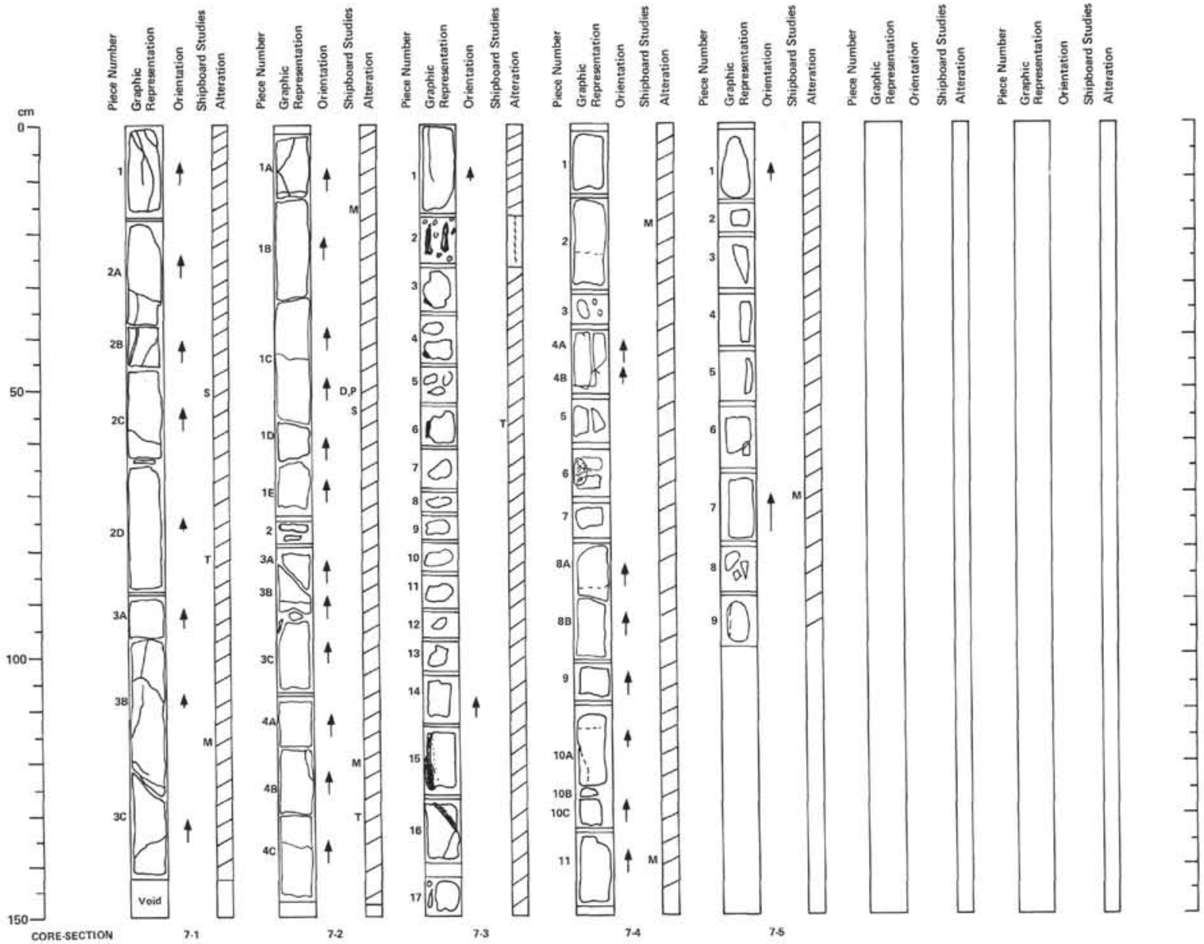

92-597C-7

Depth: 91.5–100.5 m

Section 1: BASALT (massive flow)

Macroscopic description

(i) Rock type: Fine- to medium-grained basalt; aphyric with microphenocrysts of plagioclase and clinopyroxene (~1 mm across); some changes in grain size (e. g. Piece 2A bottom, fine-grained). Mineralogy: clinopyroxene, plagioclase (+ oxides). No igneous contact within section.

(ii) Alteration: Moderately altered with variations within section. Pseudomorphic replacement of pyroxenes by light to dark green alteration minerals (smectite?). Alteration faults in Pieces 2A and 2D, with changes from light green to red-light brown (Fe-oxides) altered material.

(iii) Vesicles: Trace, < 1% by volume, 1–2 mm diameter, filled with green smectite. Sometimes in oxidation zones with brown material.

(iv) Veins: Numbers of veins vary down section. Filled with green or yellow-white minerals, most with adjacent oxidation halos.

Section 2: BASALT (massive flow)

Macroscopic description

(i) Rock type: Fine- to medium-grained basalt. Aphyric with microphenocrysts of plagioclase and pyroxene (~1–2 mm across). Some changes in grain size (esp. Pieces 1A, 1E, and 4C with some fine-grained parts). Mineralogy: clinopyroxene, plagioclase.

(ii) Alteration: Moderately altered with trace variations down section. Pseudomorphic replacement of pyroxenes by light green alteration minerals (in matrix and phenocrysts). Some light brown alteration minerals in vicinity of some veins (Fe-oxides).

(iii) Vesicles: Trace (<0.1%). Filled with light green and green-blue opaque minerals; ~1 mm diameter.

(iv) Veins: Rare, dark green and some with light green filling, common light brown (Fe-oxides?) veins with oxidation halos.

Thin section description

Piece 4C, 129–130 cm: Basalt. Variable grain size from < 0.1 mm to 4 mm but not obviously porphyritic. One glomerocryst of plagioclase and clinopyroxene. Texture of small spherulites (subspherulitic texture) of plagioclase and pyroxene and larger plagioclase laths and pyroxene grains in intergranular relationship and interstitial glass and material. Yellowish green smectite replaces glass (or ?crytocrystalline material) and some pyroxene. Brown alteration product replaces smectite, edges of pyroxene and effects slight alteration of plagioclase. No vesicles or veins.

Section 3:

Macroscopic description

(i) Rock type: Fine- to medium-grained basalt. Aphyric with trace microphenocrysts of feldspar and clinopyroxene. Mineralogy: clinopyroxene, plagioclase (+ oxides). No igneous contact within section.

(ii) Alteration: Moderately altered. Pseudomorphic replacement of pyroxenes by light green-blue and sometimes by red-brown (Fe-oxides?) alteration minerals.

(iii) Vesicles: Trace, <0.1% by volume, filled with light green minerals, diameter <1 mm.

(iv) Veins: Beside some small veins (~1 mm thick) filled with green-blue material, there are parts of and complete visible veins >1 cm thick, filled with yellow-brown fine-grained material, mainly calcite (XRD), some amorphous minerals and possibly some Fe-oxides (color). Within this vein filling are some unidentified particles (1–2 mm across) which may be smectite and disseminated native copper. Between veins and basalt there are only small reaction zones (≤1 mm) with green-blue or/and red-brown alteration minerals (mainly Fe-oxides). Piece 2 consists mainly of vein-filling material.

Section 4:

Macroscopic description

(i) Rock type: Basalt, fine- to medium-grained, containing sparse microphenocrysts of plagioclase feldspar (1–2% by volume, 2 mm maximum diameter). Groundmass: plagioclase and clinopyroxene (+ oxide). No igneous contact. Color: gray with brown patches.

(ii) Alteration: Moderately altered with blue-green and dark green partial – complete alteration of many clinopyroxene crystals and in patches elsewhere. Sometimes sulfides occur as tiny scattered grains within the clay mineral. Local alteration of green clay to yellow-brown clay minerals.

(iii) Vesicles: Almost non-vesicular.

(iv) Veins: Sparse, up to 1 mm thick. Typical vein at top of Piece 10A is rimmed by yellow-brown clay minerals and has a core of dark green clay minerals which is mottled due to a dark red alteration product. The vein is surrounded by a 1.5 cm brown alteration halo.

Section 5:

Macroscopic description

(i) Rock type: Basalt, fine- to medium-grained, containing sparse (~3%) microphenocrysts of plagioclase feldspar (2–3 mm maximum size). Groundmass: plagioclase and clinopyroxene (+ oxides). No igneous contacts. Color: gray.

(ii) Alteration: Moderate, main alteration product is blue-green clay minerals which partially–totally pseudomorphs some pyroxenes and occurs as patches elsewhere.

(iii) Vesicles: Almost non-vesicular.

(iv) Veins: Vertical vein containing dark green clay mineral forms the left hand edge (as drawn) of Pieces 3–5.

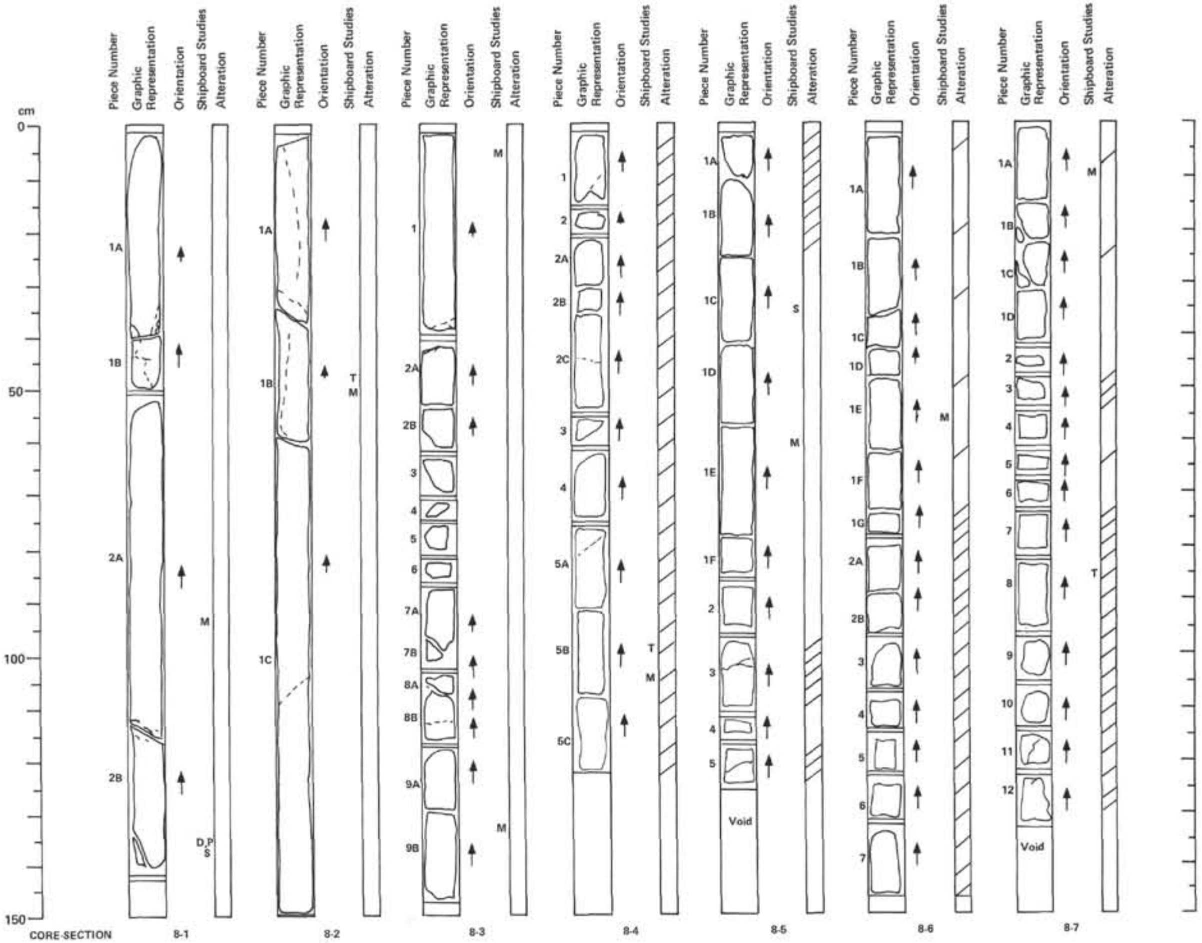

92-597C-8 Depth: 100.5–109.5 m

Section 1:

Macroscopic description

(i) Rock type: Basalt, fine- to medium-grained containing sparse microphenocrysts (2–4 mm) and glomerocrysts of subhedral clinopyroxene (~3% by volume) in a groundmass of plagioclase and clinopyroxene (+ oxide). No igneous contacts. Gray.

(ii) Alteration: Slightly altered with local zones of oxidative alteration but freshest in core so far. Pyroxenes little altered; brown stain to feldspar in oxidative zone.

(iii) Vesicles: Almost non-vesicular.

(iv) Veins: Rare – most common at the base of Piece 1 where they contain pale green to colorless botryoidal calcite and a black material (MnO_2?, smectite?).

Section 2:

Macroscopic description

(i) Rock type: Basalt, fine- to medium-grained. Sparse (1% or less) microphenocrysts of clinopyroxene, 2–3 mm across. Groundmass is plagioclase and clinopyroxene (+ oxide). No igneous contacts. Homogeneous gray.

(ii) Alteration: Slightly altered, with a few patches of oxidative alteration in the top 40 cm and average small proportion of clay minerals throughout.

(iii) Vesicles: Non-vesicular.

(iv) Veins: Rare, up to 1 mm across. Vein at 30–35 cm is most interesting, containing pale green, waxy amorphous ?smectite and calcite. Vein marking Pieces 1A–1B contact contains calcite, black ?MnO_2 and brown iron-oxide (? or smectite).

Thin section description:
Piece 1B, 45–46 cm: Plagioclase laths and magnetite crystals in a generally finer grained matrix of clinopyroxene and plagioclase. Matrix normally has an intergranular texture, sometimes sub-variolitic texture on the pyroxenes and somtimes the plagioclase can be microcrystalline. Zoning in feldspars is seen at all scales of crystal size; pyroxenes are also zoned though to a lesser extent.

Section 3:

Macroscopic description

(i) Rock type: Basalt, fine- to medium-grained with a very slight coarsening of grain size from top to bottom of the section. More-or-less aphyric: very sparse clinopyroxene phenocrysts. Mineralogy: clinopyroxene and plagioclase (+ oxide). Marked variolitic texture in which spherical varioles are surrounded by larger grains of plagioclase and clinopyroxene in intersertal relationship. No igneous texture. Gray with brown patches.

(ii) Alteration: Fairly fresh in the first and last 30 cm; elsewhere slight, irregular oxidative alteration, including minor alteration fronts. Oxidative zones contain minor yellow-brown Fe-oxide (+ smectite? + zeolite?). A small degree of alteration by bluish clay minerals exists.

(iii) Vesicles: Non-vesicular.

(iv) Veins: Rare. Only 1 significant vein at 4 cm between Piece 1 and Piece 2A. Contains blue clay minerals and black ?Mn-oxide and brown ?iron-oxide. Carries 5 cm-wide alteration halo.

Section 4:

Macroscopic description

(i) Rock type: Basalt fine- to medium-grained. Textures as in Core 8, Section 3. No igneous contacts. Gray with brown patches.

(ii) Alteration: Slight increase in alteration of Core 8, Section 3. Dark green clay mineral replacement of pyroxene more common. Oxidative alteration zones mainly around veins marked by replacement of green clay mineral by yellow-brown clay mineral (or iron-oxide?) and possibly by replacement of feldspar by zeolite.

(iii) Vesicles: Almost non-vesicular.

(iv) Veins: Rare. Contain dark green clay mineral (<1 mm thick) with very minor red and yellow brown ?oxide in Piece 2C together with minor calcite and ?zeolite.

Thin section description
Ophitic/poikilophitic texture in which plagioclase laths 0.2–3 mm in largest dimension are enclosed in large anhedral pyroxene (augite) crystals which can reach 10 mm in length. Both feldspar and augite are strongly zoned. Approximately 5% magnetite (subhedral, often skeletal) occurs mainly within pyroxene. Rock is almost completely fresh.

Section 5: BASALT (massive flow)

Macroscopic description

(i) Rock type: Fine- to medium-grained basalt, aphyric with trace microphenocrysts of pyroxene. Mineralogy: clinopyroxene, plagioclase (+ oxides). No igneous contact down section. Fragments with brown patches in Pieces 1A and 1B.

(ii) Alteration: Slight to moderate alteration with variations down section. Piece 1A and top of Piece 1B have brown-red alteration minerals pseudomorphing pyroxene. Alteration front in Piece 1B. Pieces 3 and 5 are more altered than Piece 1C–2 and 4 but contain no brown-colored alteration minerals, which are common in Pieces 1C–2 and 4. Pieces 1C–2 and 4 also show light to dark green alteration products also pseudomorphing pyroxene (smectite?). Pyrite <0.1 mm across in Piece 5.

(iii) Vesicles: Almost no vesicles.

(iv) Veins: Almost no veins down section, except in Pieces 3 and 5. Piece 3 has one vein filled with light green material and one vein filled with calcite. Piece 5 has one vein filled with green alteration material; pyrite occurs near this vein.

Section 6: BASALT (massive flow)

Macroscopic description

(i) Rock type: Fine- to medium-grained basalt. Aphyric with trace microphenocrysts of pyroxene and plagioclase. Gray with brown patches (in Pieces 1G–7 only). No igneous contact within section. Mineralogy: clinopyroxene, plagioclase (+ oxides and sulfides [?]).

(ii) Alteration: Slight (Pieces 1A–1F) to moderate (Pieces 1G–7) alteration with variations within section. Pieces 1A–1F: light green alteration minerals (clay) pseudomorphing pyroxene; disseminated fine-grained pyrite (<0.1 mm across); nearly no Fe-oxides as alteration products. Pieces 1G–7: patchy brown to red-brown Fe-oxides as alteration minerals (+ smectite) pseudomorphing pyroxene; fewer green colored minerals; pyrite disappears; sometimes zeolite replaces feldspar.

(iii) Vesicles: Almost non-vesicular.

(iv) Veins: Almost no veins down section.

Section 7: BASALT (massive flow)

Macroscopic description

(i) Rock type: Fine- to medium-grained basalt. Aphyric with rare microphenocrysts (1–2 mm across) of pyroxene and plagioclase. Gray with brown patches (Pieces 3 and 7–12 only). Mineralogy: clinopyroxenes, plagioclase (+ oxides). No igneous contact within section.

(ii) Alteration: Slight (Pieces 1–2 and 4–6) to moderate (Pieces 3 and 7–12) alteration with variations within section. Pieces 1–2 and 4–6: light green-blue alteration minerals (clay, smectite[?]) pseudomorphing pyroxenes; disseminated fine-grained pyrite? (sulfide minerals) (<0.1 mm across <0.1% by volume); no Fe-oxides. Pieces 3 and 7–12: patchy light brown Fe-oxides (smectite[?]), and red-brown clay alteration minerals, pseudomorphing pyroxene; no pyrite. Rare replacement of feldspar by zeolite down section.

(iii) Vesicles: Non-vesicular.

(iv) Veins: Almost no veins (except Piece 11, vein filled with calcite, oxidation halo next to it).

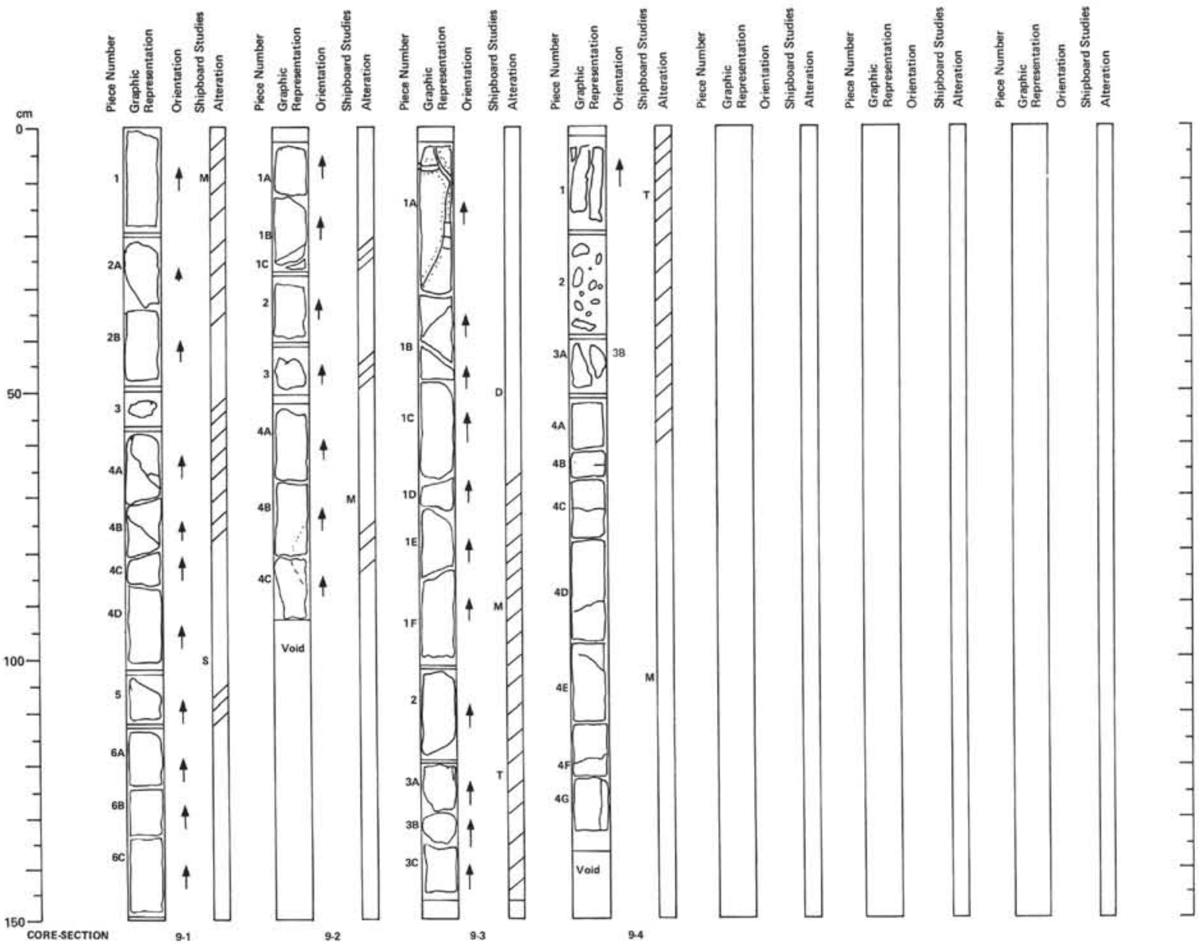

92-597C-9

Depth: 109.5–118.5 m

Section 1: BASALT (massive flow)

Macroscopic description

(i) Rock type: Medium-grained basalt. Phyric with trace microphenocrysts (1–3 mm) of plagioclase and pyroxene. Fragments with brown patches within section. Mineralogy: clinopyroxenes, plagioclase and oxides. No igneous contact down section.

(ii) Alteration: Slight (Pieces 2B, 4C, 4D, 6A–6C) to moderate (Piece 1, 2A, 3, 4A, 4B, and 5) alteration. Pieces 2B, 4C, 4D, 6A–6C: some light green alteration minerals (smectite) pseudomorphing matrix pyroxene. Pieces 1, 2A, 3, 4A, 4B, and 5: patchy light brown Fe-oxides and clay minerals, pseudomorphing pyroxene. Pyrite (<0.1 mm across) in Piece 5.

(iii) Vesicles: Almost non-vesicular.

(iv) Veins: Trace, except Pieces 4A and 4B; 1–1.5 mm thick in Piece 4A filled with green-blue material (celadonite?). Alteration near veins always more intensive; some calcite occurs.

Section 2: BASALT (massive flow)

Macroscopic description

(i) Rock type: Same as Core 9, Section 1. No igneous contact down section.

(ii) Alteration: Slight to moderate (Pieces 1C, 3, 4B, and 4C) alteration. Variation between nearly fresh basalt and slight alteration with light green alteration minerals, pseudomorphing matrix pyroxene. Pieces 1B bottom, 1C, 3, 4B, and 4C have patchy brown Fe-oxides and clay minerals, sometimes pseudomorphing pyroxene. Alteration front in Pieces 4B and 4C.

(iii) Vesicles: Non-vesicular.

(iv) Veins: Rare; filled with brown clay minerals (Piece 1B) or green smectite(?) Piece 4C. Alteration halos next to the veins.

Section 3: BASALT (massive flow)

Macroscopic description

(i) Rock type: Same as Core 9, Sections 1 and 2; no igneous contact within section.

(ii) Alteration: Slight (Pieces 1A–1C) to moderate (Pieces 1D–3C) alteration. Pieces 1A–1C: some green alteration minerals, pseudomorphing matrix pyroxene. No strong alteration next to large vein in Piece 1A. Pieces 1D–3C: brown to red brown clay minerals and Fe-oxides, some pseudomorphing primary minerals. Alteration fronts in Pieces 1F, 3A–3C, showing the above described alteration processes.

(iii) Vesicles: Almost non-vesicular.

(iv) Veins: Rare; except Pieces 1A and 1B. Piece 1A: 1–3 mm thick vein filled with green-blue clay minerals (smectite, some celadonite [XRD]) no calcite, no Fe-oxides. Piece 1B: Vein <1 mm thick, some filling as Piece 1A.

Section 4: BASALT (massive flow)

Macroscopic description

(i) Rock type: Fine- to medium-grained basalt with a slight coarsening of grain size from top to bottom of the section. Aphyric with rare microphenocrysts of feldspar and clinopyroxene. Gray with brown patches next to veins. Mineralogy: clinopyroxene, plagioclase and oxides. No igneous contact within section.

(ii) Alteration: Slight to moderate alteration in Pieces 1–4A. Pieces 4B–4G are almost fresh basalt, with alteration only in vicinity of veins and alteration fronts of a few cm. Pieces 1–4A show normal oxidative alteration with light brown alteration minerals and some Fe-oxides replacing pyroxene pseudomorphically.

(iii) Vesicles: Non-vesicular.

(iv) Veins: Common within section. Piece 1: green smectite filling, no celadonite (XRD), no calcite, possibly some zeolite (1–2 mm thick). All other veins are <1 mm thick with green alteration minerals and adjacent alteration halos.

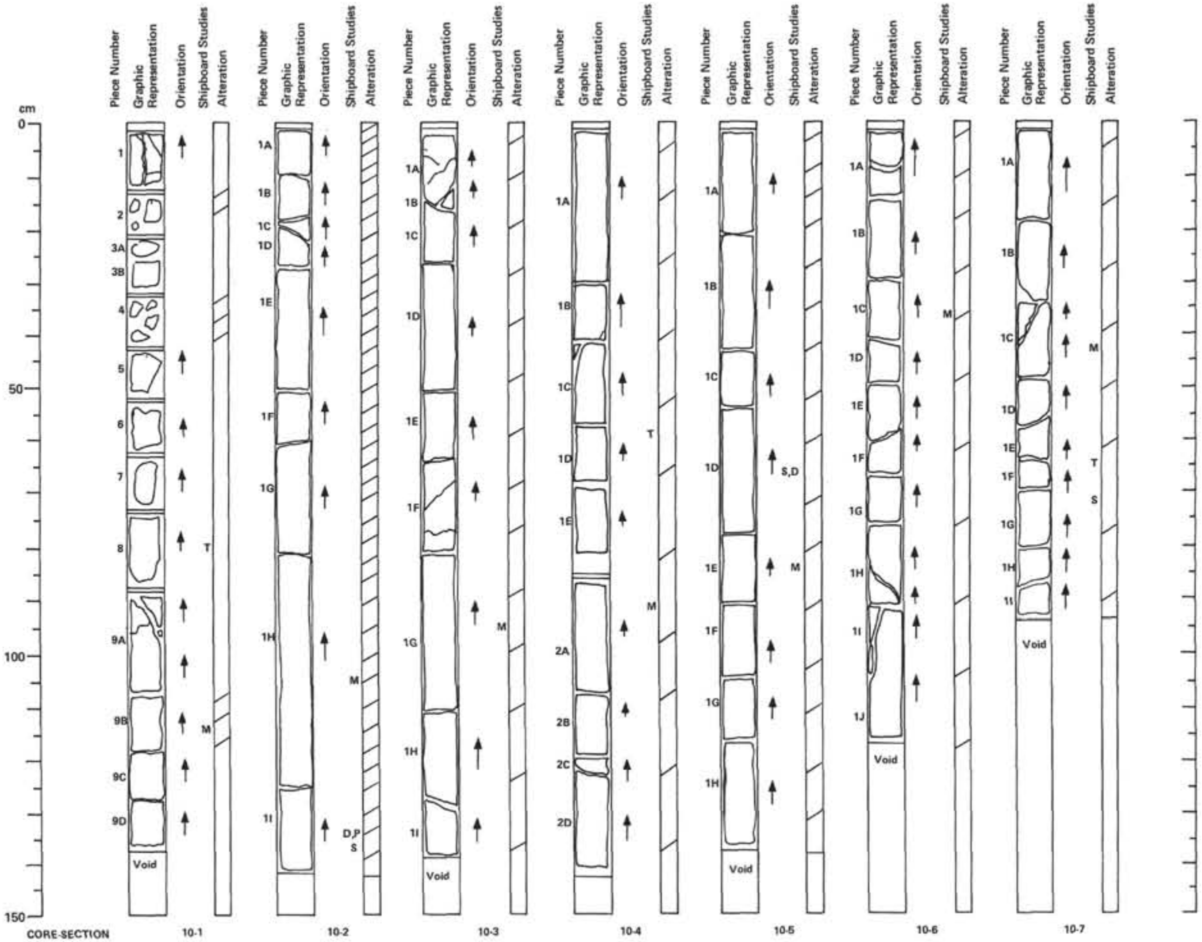

92-597C-10 Depth: 118.5–127.5 m

Section 1: BASALT (massive flow)

Macroscopic description

(i) Rock type: Fine- to medium-grained basalt, with slight increase of grain size from top to bottom. Trace microphenocrysts (1–2 mm across) of plagioclase and pyroxene. Gray with brown patches within section. Mineralogy: clinopyroxene, plagioclase (+ oxides). No igneous contact down section.

(ii) Alteration: Fresh to slightly altered basalt. Pieces 1–6: light brown alteration minerals, no complete alteration of primary minerals. Pieces 7–9D: fresh (almost) with some weak alteration fronts near veins. Piece 9B contains light green alteration minerals.

(iii) Vesicles: Non-vesicular.

(iv) Veins: Common in Pieces 1–4 with dark green smectite vein filling, no calcite. Piece 3B shows vein filling on its top side.

Section 2: BASALT (massive flow)

Macroscopic description

(i) Rock type: Fine- to medium-grained basalt. Aphyric with traces of microphenocrysts (~2 mm across) of feldspar and pyroxene and oxides(?). Gray with dark gray and brown patches within section. Mineralogy: clinopyroxene, plagioclase (+ oxides). No igneous contact down section.

(ii) Alteration: Moderately altered with pseudomorphic replacement of plagioclase and pyroxene by usually light green alteration minerals (smectite?) and sometimes zeolite (40–50% of matrix and phenocrysts are affected). Some traces of pyrite occur. Alteration fronts are common with a zone of light brown to red brown clays and Fe-oxides, esp. near veins.

(iii) Vesicles: Almost non-vesicular.

(iv) Veins: Rare; core may be broken at veins with oxidative alteration halos next to them and some traces of calcite.

Section 3: Basalt (massive flow)

Macroscopic description

(i) Rock type: Same as Core 10, Section 2; no igneous contact within section.

(ii) Alteration: Slight to moderate alteration with variation down section; same as Core 10, Section 2. No pyrite; oxidative alteration only in Pieces 1A, 1B, 1C, and 1F.

(iii) Vesicles: Almost non-vesicular. Three vesicles in Piece 1A filled with brown Fe-oxides or clay.

(iv) Veins: Trace; only Pieces 1A, 1B, and 1C with green alteration minerals as filling and little calcite.

Section 4: BASALT (massive flow)

Macroscopic description

(i) Rock type: Same as Core 10, Sections 2 and 3; no igneous contact down section.

(ii) Alteration: Slight to moderate alteration with slight variation down section; pseudomorphic replacement of plagioclase and pyroxene by yellow-white to light green alteration minerals. Almost the same as Core 10, Sections 2 and 3; no Fe-oxides as alteration minerals. Trace pyrite in Pieces 1A and 2B.

(iii) Vesicles: Almost non-vesicular.

(iv) Veins: No veins.

Section 5: BASALT (massive flow)

Macroscopic description

(i) Rock type: Same as Core 10, Sections 2, 3, and 4. No igneous contact within section.

(ii) Alteration: Slight to moderate alteration with slight variations down section. Almost the same as Core 10, Sections 2, 3, and 4. Oxidative alteration only in Pieces 1G and 1H with slight alteration fronts; no pyrite found

(iii) Vesicles: Almost non-vesicular.

(iv) Veins: Almost no veins.

Section 6: BASALT (massive flow)

Macroscopic description

(i) Rock type: Same as Core 10, Sections 2–5; no igneous contact down section.

(ii) Alteration: Slight to moderate alteration with variations down section. Pseudomorphic replacement of plagioclase and pyroxene usually by light green alteration minerals (smectite?); 30–40% of matrix and phenocrysts are affected. Alteration fronts are common with patchy brown to red-brown clays and Fe-oxides, esp. near rims. Sometimes the alteration minerals are light brown-yellow in color.

(iii) Vesicles: Almost non-vesicular.

(iv) Veins: Core usually broken at veins; which are filled with light to dark green clay minerals (e. g. chlorite). Near veins there are oxidative alteration zones (sometimes a few cm). Veins may be ~1 mm thick.

Section 7: BASALT (massive flow)

Macroscopic description

(i) Rock type: Same as Core 10, Sections 2–6; no igneous contact down section.

(ii) Alteration: Nearly the same as Core 10, Section 6, with possibly fewer brown patches down section.

(iii) Vesicles: No vesicles.

(iv) Veins: Same as Core 10, Section 6.

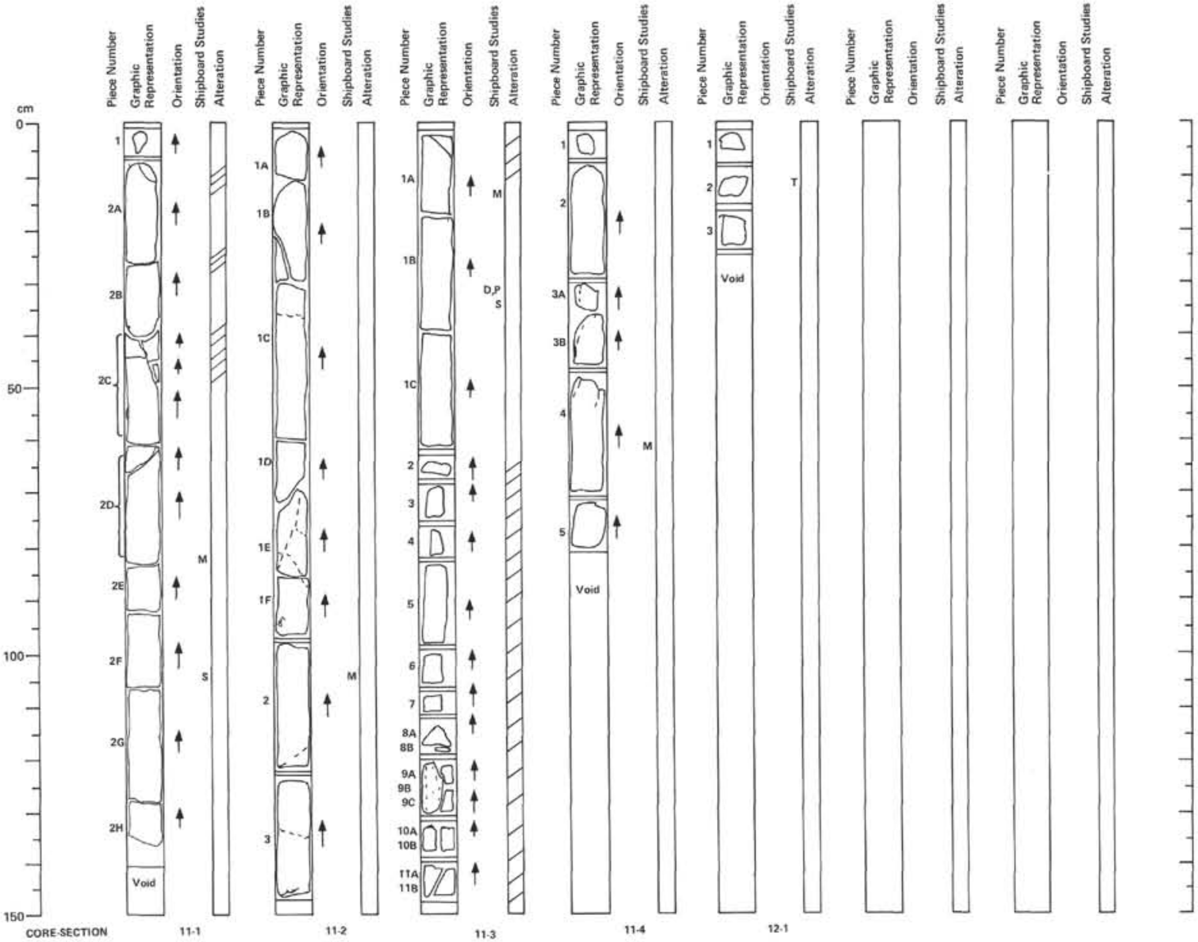

92-597C-11 Depth: 127.5–136.5 m

Section 1:

Macroscopic description

(i) Rock type: Basalt, medium-grained. Aphyric but occasional glomerocrysts of feldspar. Ophitic texture – rock is dotted with large clinopyroxenes enclosing feldspar. Clinopyroxene and feldspar only major minerals. Uniform gray color; no igneous contacts.

(ii) Alteration: Weak alteration of pyroxene and groundmass by blue green to green clay minerals. Weak superimposed oxidative alteration to yellow brown oxide/clay in alteration zones around some veins – esp. at Piece 2A–2B boundary.

(iii) Vesicles: Almost non-vesicular.

(iv) Veins: No veins within fragments but all fragment boundaries form along veins. Main vein filling is dark green to black clay mineral ($\pm MnO_2$??). Some have additional calcite and brown Fe-oxide/clay and these also have brown oxidative zone.

Section 2:

Macroscopic description

(i) Rock type: Like Core 11, Section 2, medium-grained homogeneous basalt with an ophitic texture.

(ii) Alteration: Alteration of pyroxene and fine-grained matrix by green to blue/green clay. Oxidative alteration zones common around fractures in Piece 1: yellow brown oxide/clay the common product.

(iii) Vesicles: Almost non-vesicular.

(iv) Veins: Dark gray clay and calcite brown iron oxide/clay are the common products. All pieces rimmed by vein-filling: most veins horizontal.

Section 3:

Macroscopic description

(i) Rock type: Basalt, medium-grained, mostly plagioclase and clinopyroxene sometimes in ophitic relationship. Possibly olivine but grains completely replaced. Some plagioclase glomerocrysts. Color: gray, no igneous contacts.

(ii) Alteration: Dark green clay alteration of fine-grained material. Some yellow-brown alteration of ?olivine. Alteration weak to moderate.

(iii) Vesicles: Non-vesicular.

(iv) Veins: Quite strongly veined as indicated by small sizes of Pieces 2–11 which are all bounded by veins. Vein filling is green botryoidal clay, white calcite and yellow-brown crystals (?stained zeolite/clay).

Section 4:

Macroscopic description

(i) Rock type: Fine- to medium-grained basalt, generally aphyric containing plagioclase and clinopyroxene. No igneous contacts. Color: gray with brownish patches.

(ii) Alteration: Weak alteration of fine-grained matrix and some pyroxenes to blue-green and green clay minerals. Some zones of oxidative alteration.

(iii) Vesicles: Non-vesicular.

(iv) Veins: Sub-vertical dark green clay and calcite veins, especially at left hand margin of Pieces 3 and 4.

92-597C-12 Depth: 136.5–143.5 m

Section 1: BASALT

Macroscopic description

(i) Rock type: Same as Core 11, Section 4.

(ii) Alteration: Same as Core 11, Section 4.

(iii) Vesicles: Non-vesicular.

(iv) Veins: No veins.

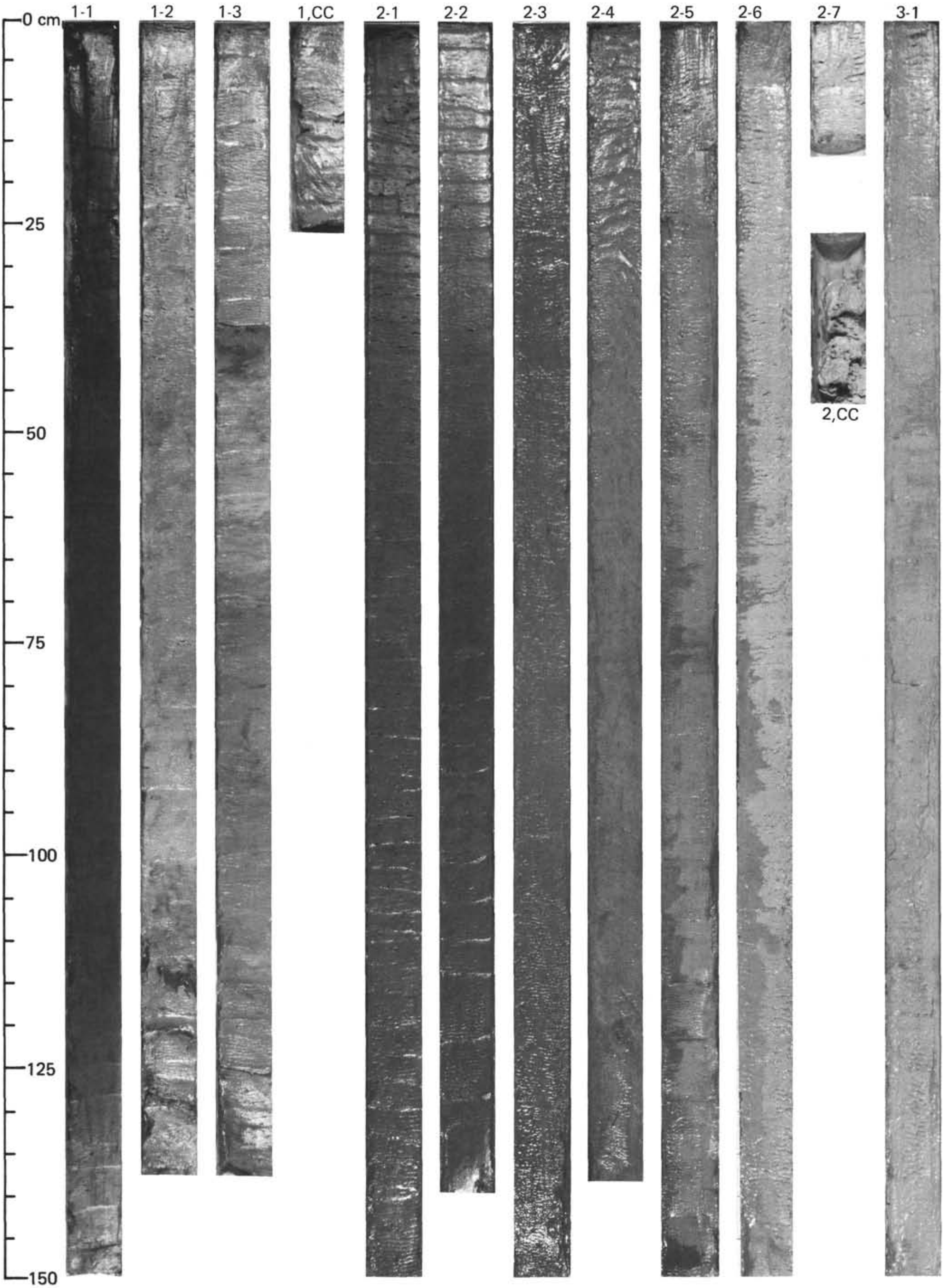
0 cm
25
50
75
100
125
150
1-1
1-2
1-3
1,CC
2-1
2-2
2-3
2-4
2-5
2-6
2-7
2,CC
3-1

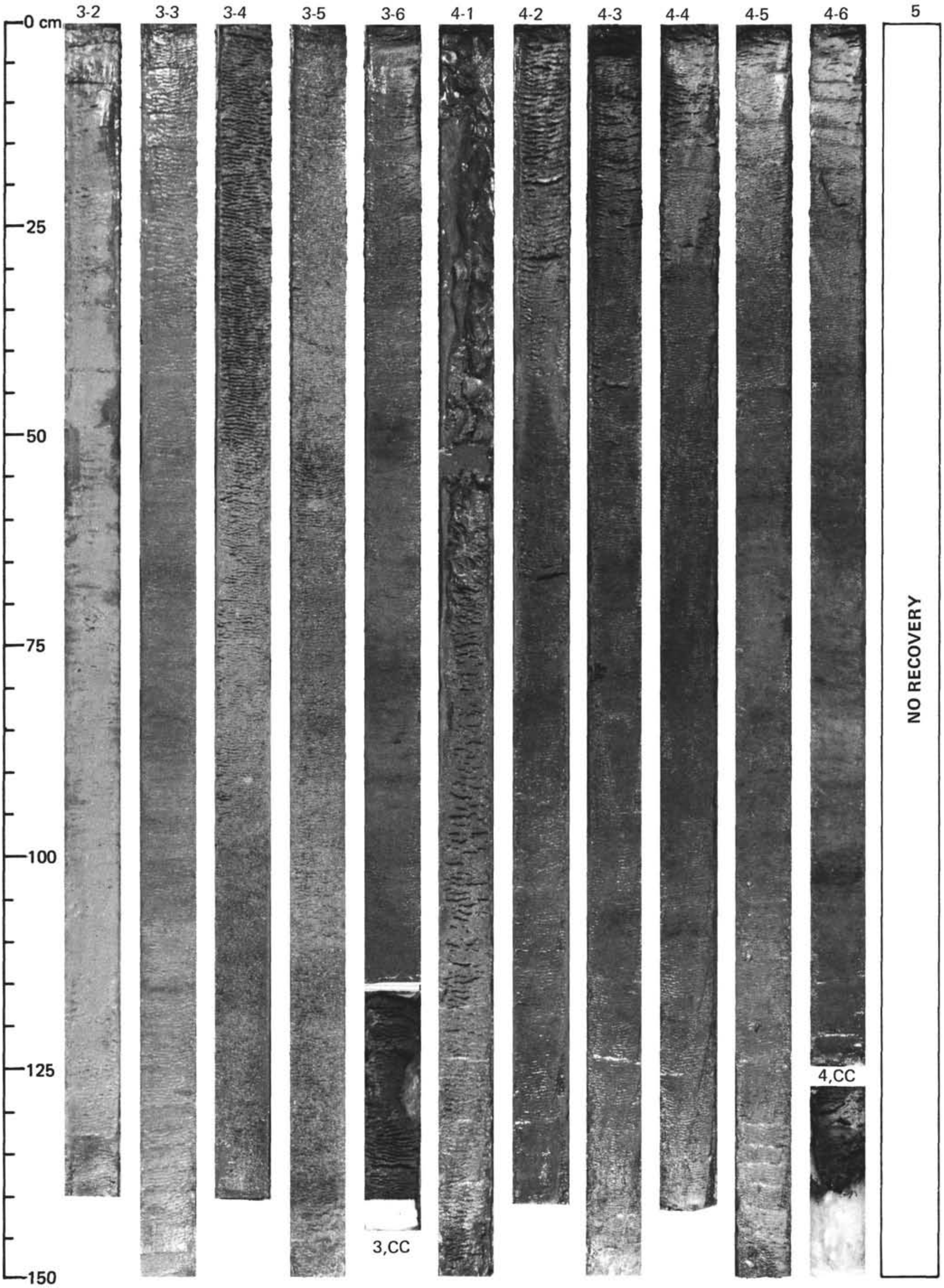
0 cm
25
50
75
100
125
150
3-2
3-3
3-4
3-5
3-6
3,CC
4-1
4-2
4-3
4-4
4-5
4-6
4,CC
5
NO RECOVERY

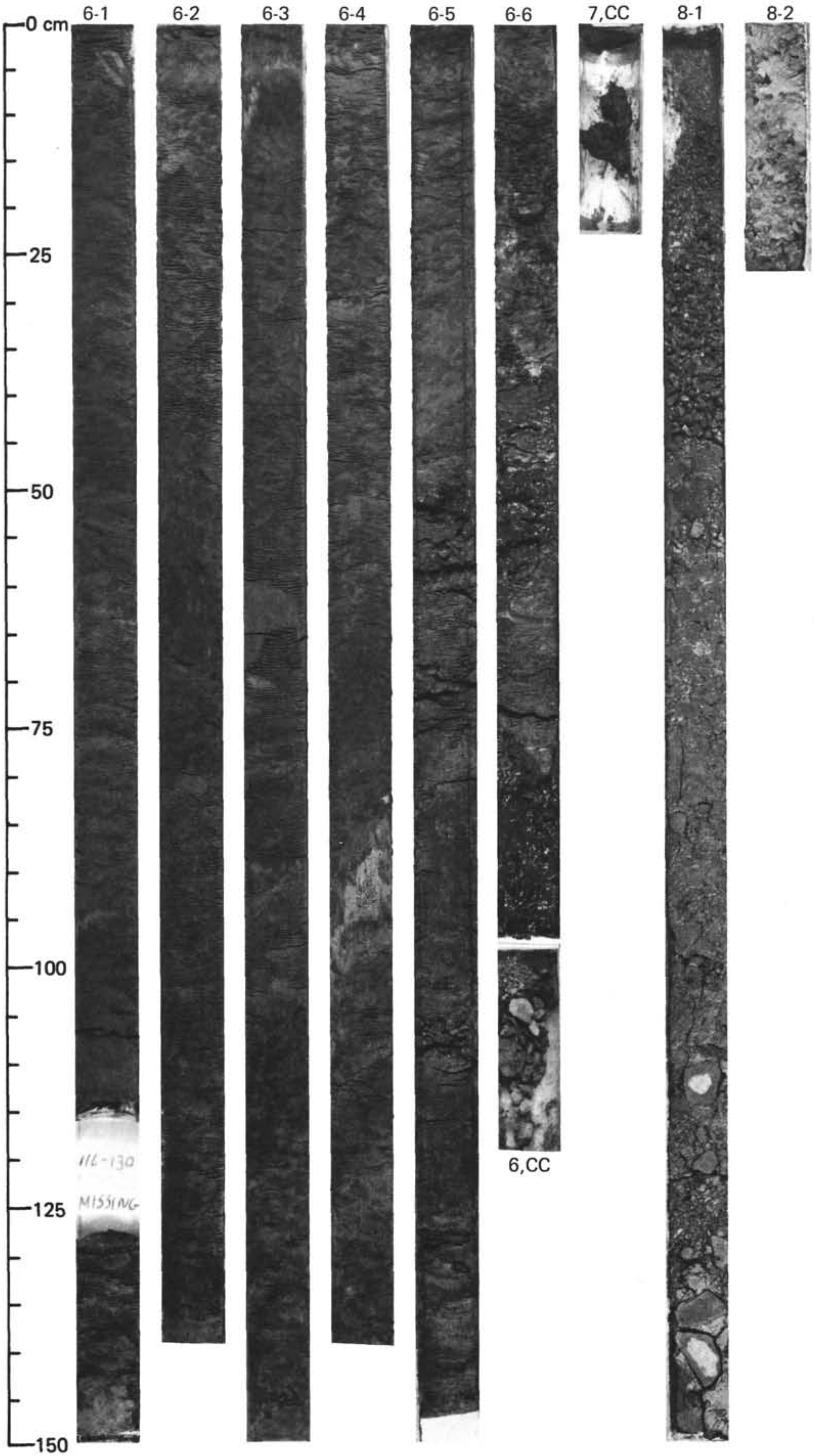
0 cm
25
50
75
100
125
150
6-1
6-2
6-3
6-4
6-5
6-6
7,CC
8-1
8-2
6,CC
116-130
MISSING

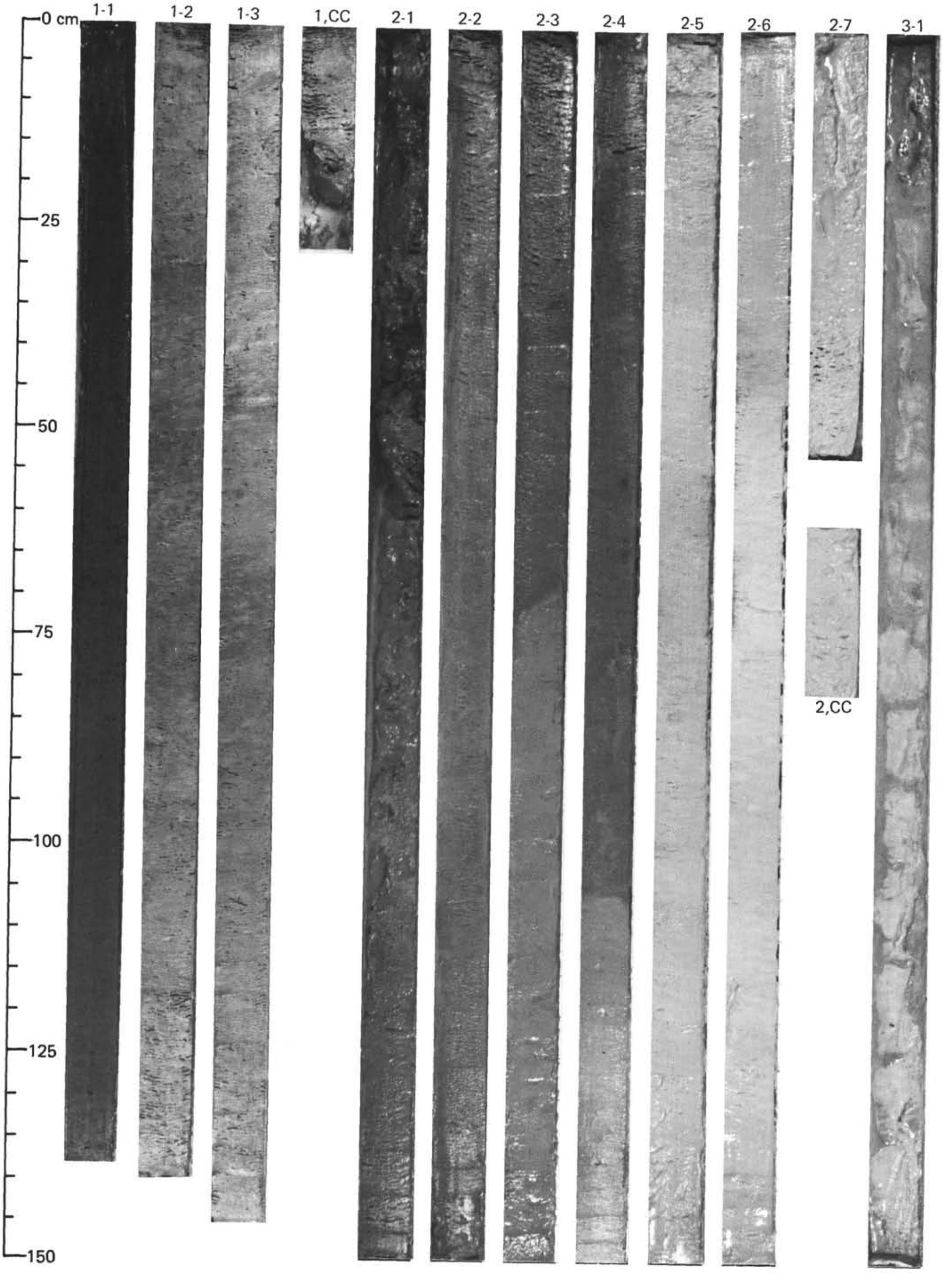
0 cm
25
50
75
100
125
150
1-1
1-2
1-3
1,CC
2-1
2-2
2-3
2-4
2-5
2-6
2-7
2,CC
3-1

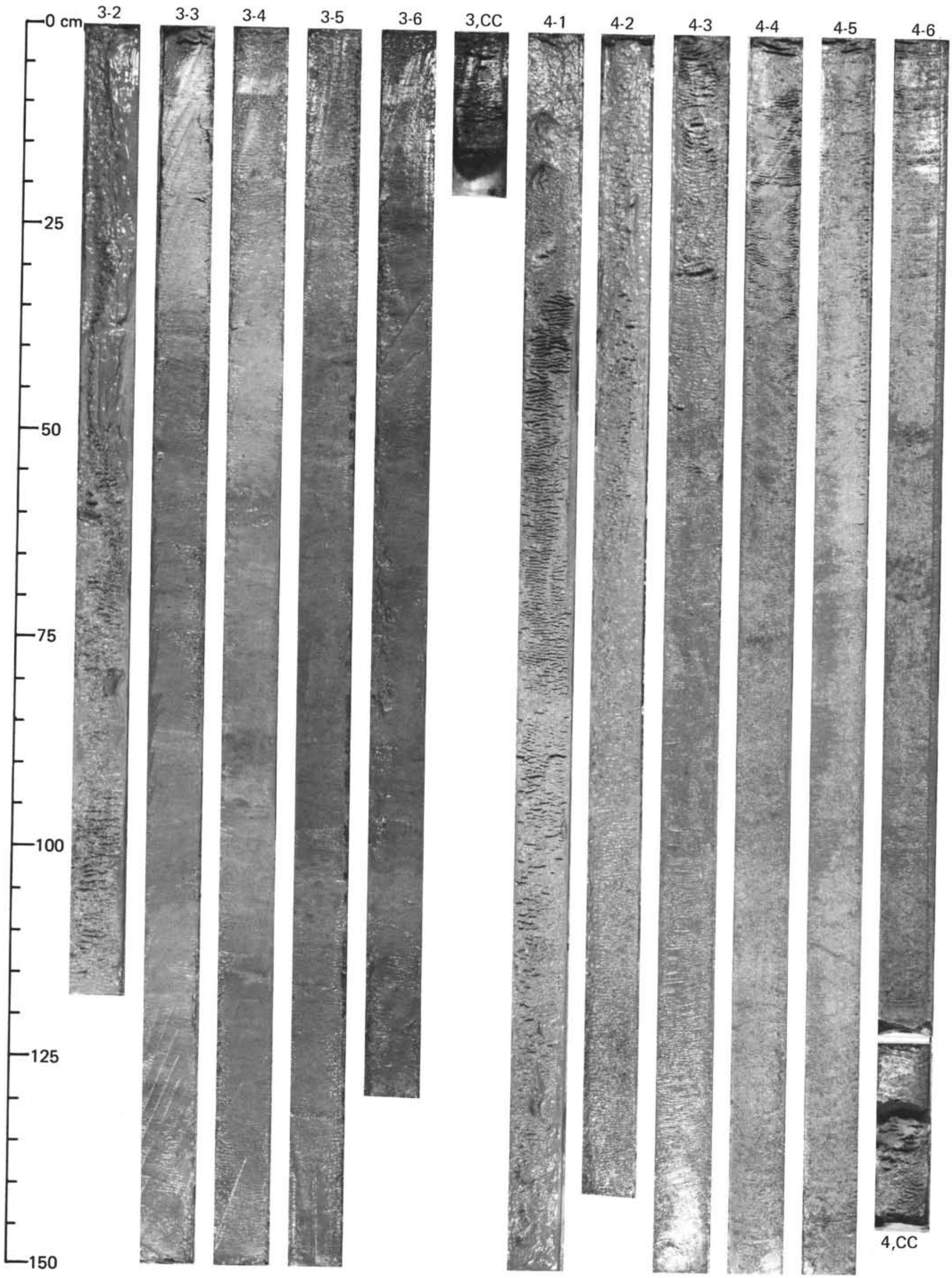
0 cm
25
50
75
100
125
150
3-2
3-3
3-4
3-5
3-6
3,CC
4-1
4-2
4-3
4-4
4-5
4-6
4,CC

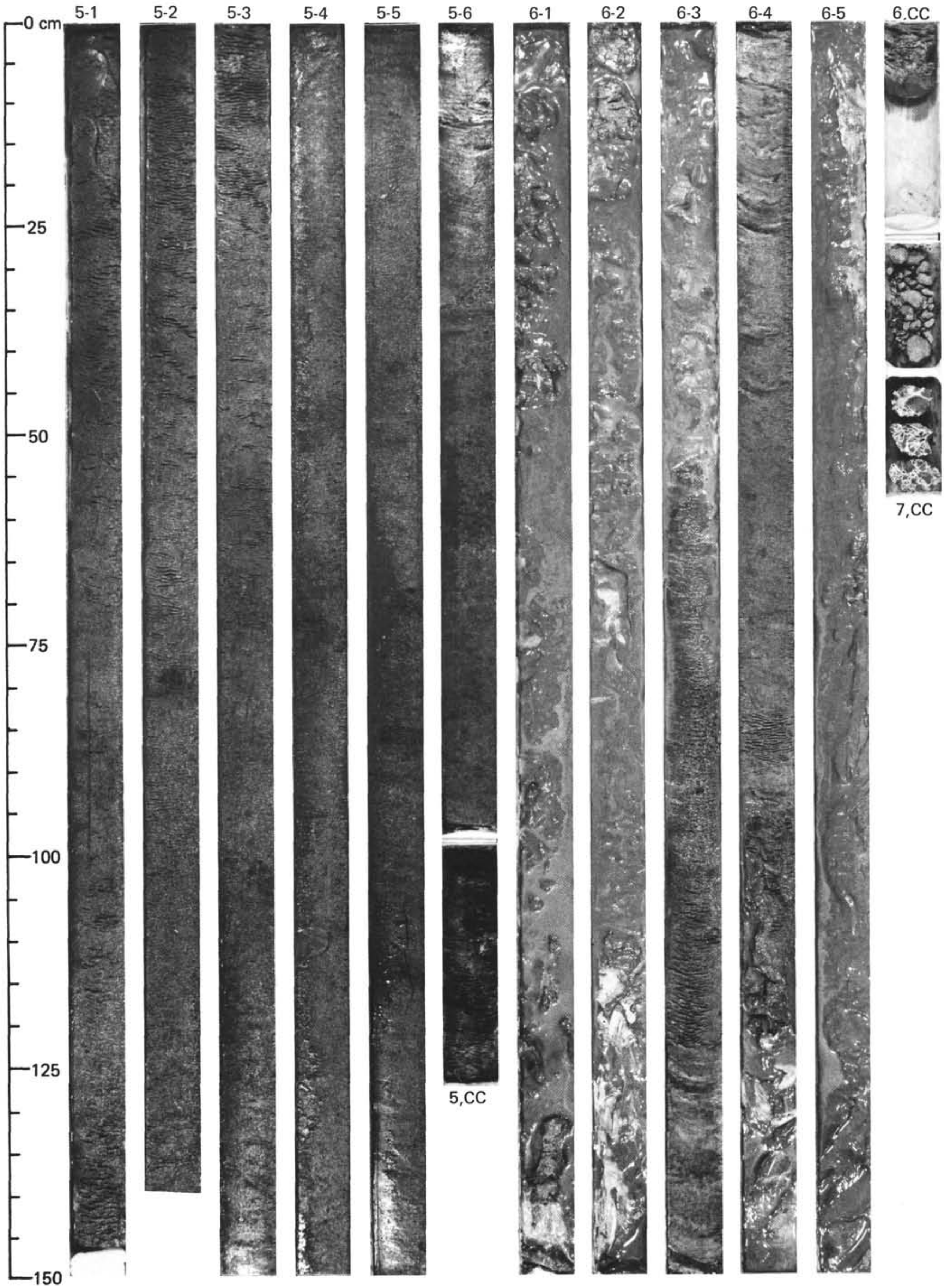
0 cm
25
50
75
100
125
150
5-1
5-2
5-3
5-4
5-5
5-6
5,CC
6-1
6-2
6-3
6-4
6-5
6,CC
7,CC

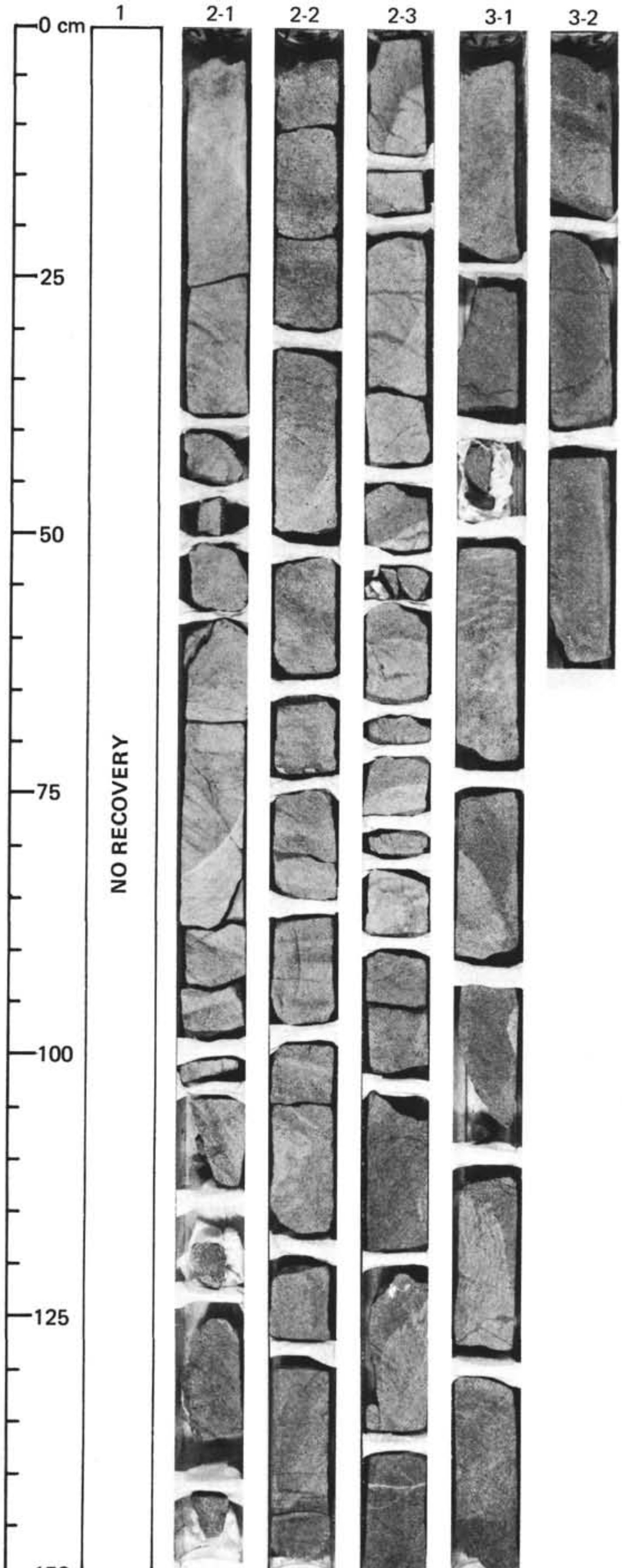
0 cm
25
50
75
100
125
150
1
2-1
2-2
2-3
3-1
3-2
NO RECOVERY

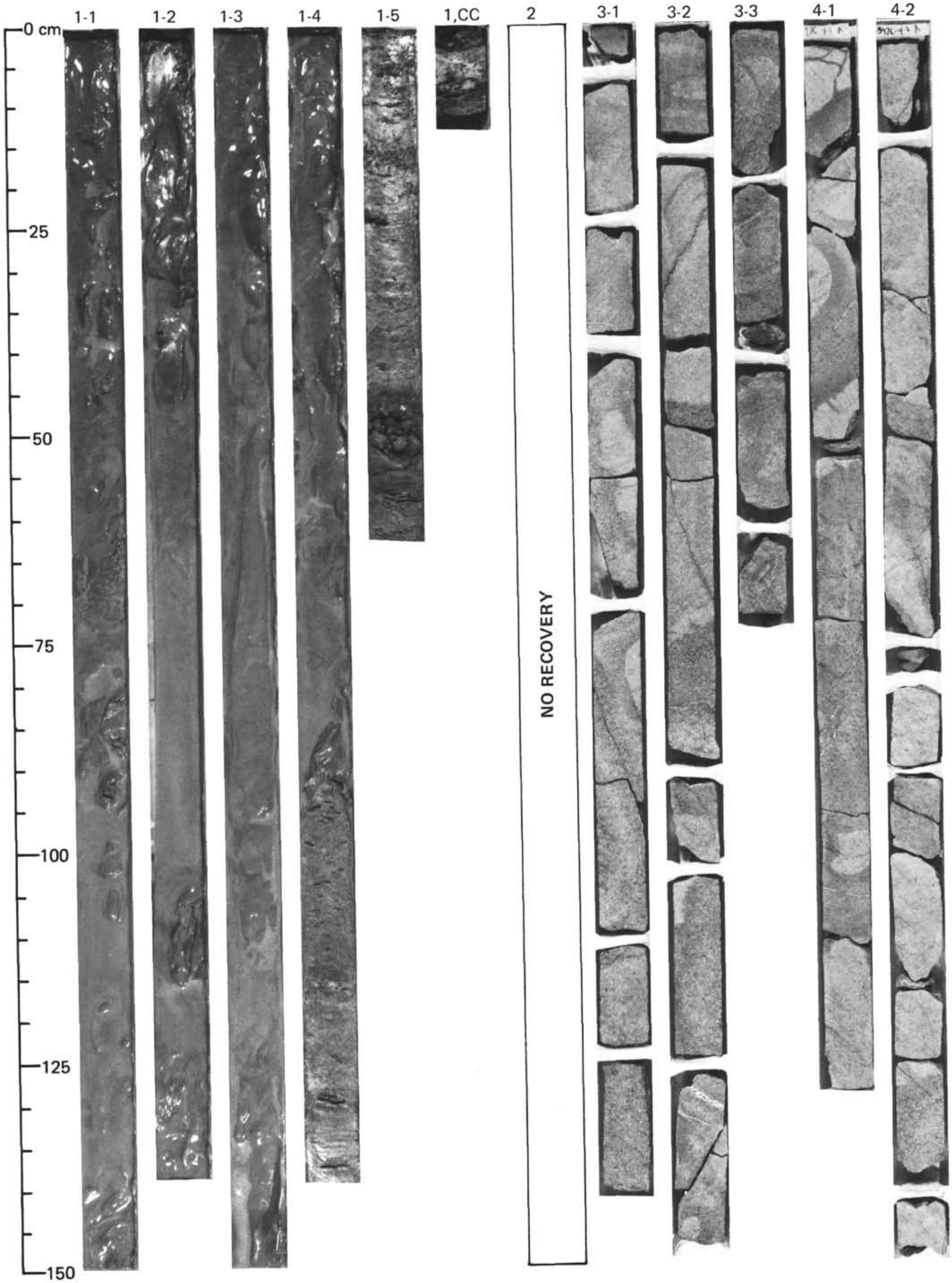
1-1
1-2
1-3
1-4
1-5
1,CC
2
3-1
3-2
3-3
4-1
4-2
0 cm
25
50
75
100
125
150
NO RECOVERY

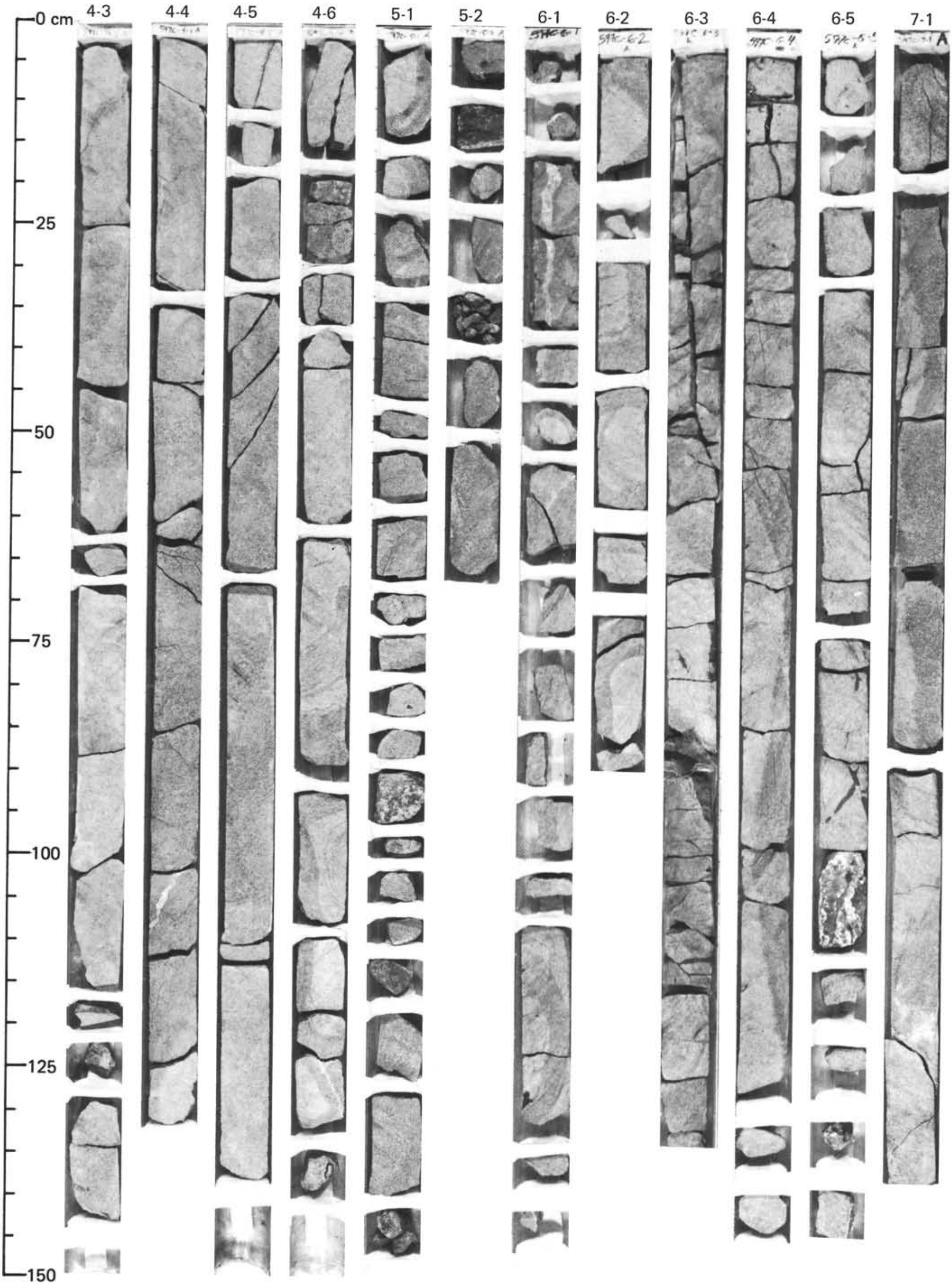
0 cm
25
50
75
100
125
150
4-3
4-4
4-5
4-6
5-1
5-2
6-1
6-2
6-3
6-4
6-5
7-1

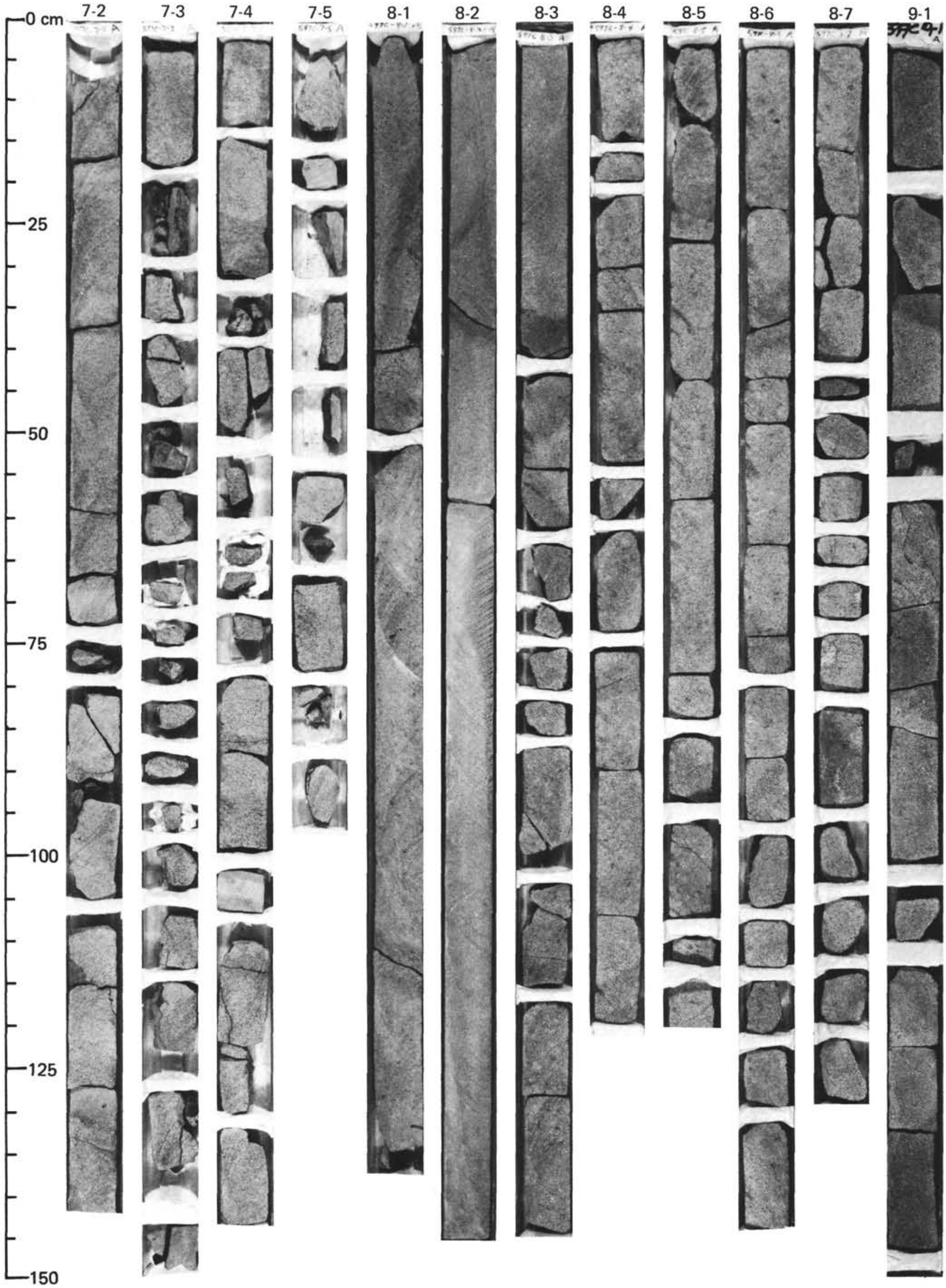
0 cm
25
50
75
100
125
150
7-2
7-3
7-4
7-5
8-1
8-2
8-3
8-4
8-5
8-6
8-7
9-1

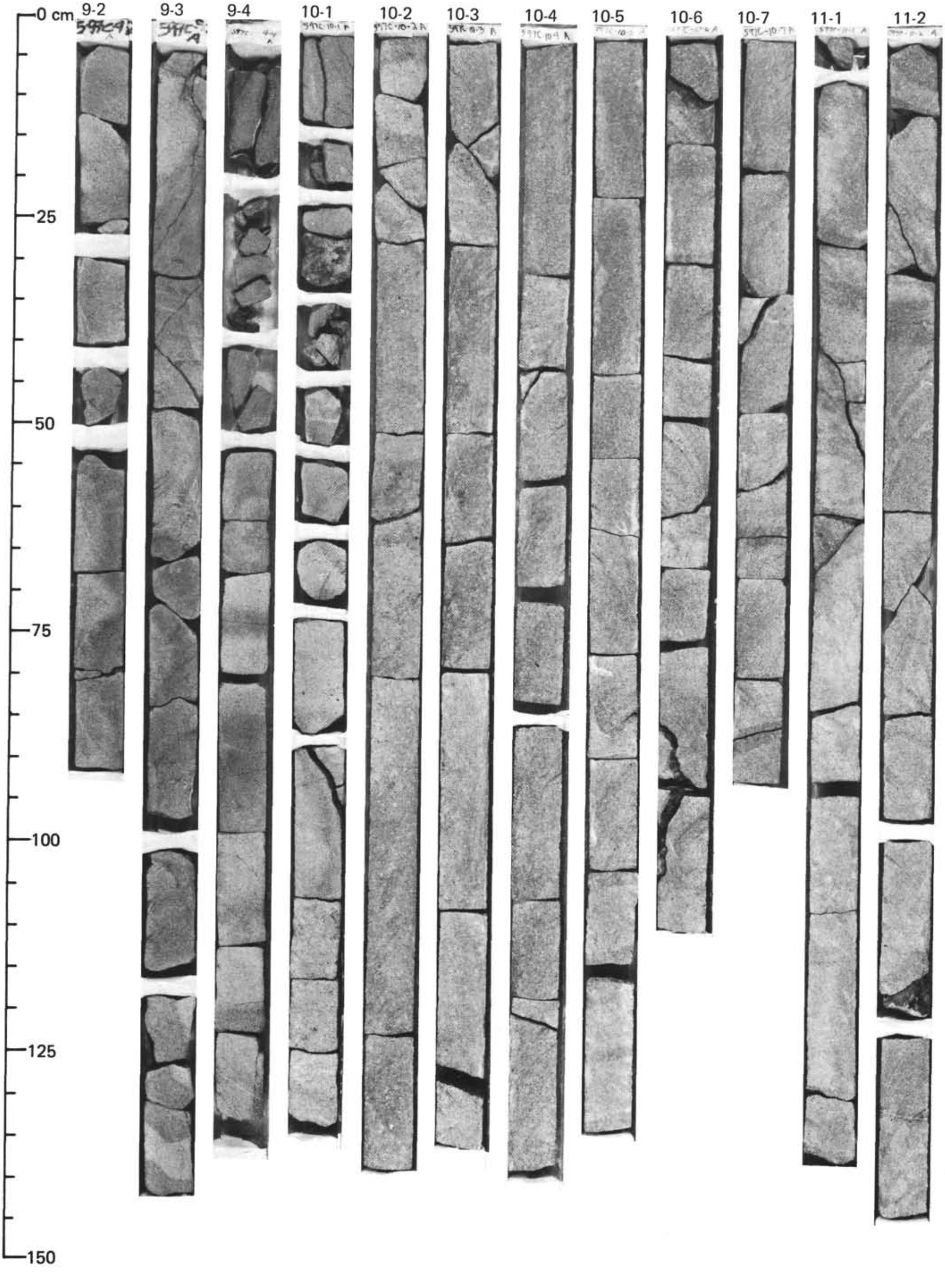
0 cm
25
50
75
100
125
150
9-2
9-3
9-4
10-1
10-2
10-3
10-4
10-5
10-6
10-7
11-1
11-2

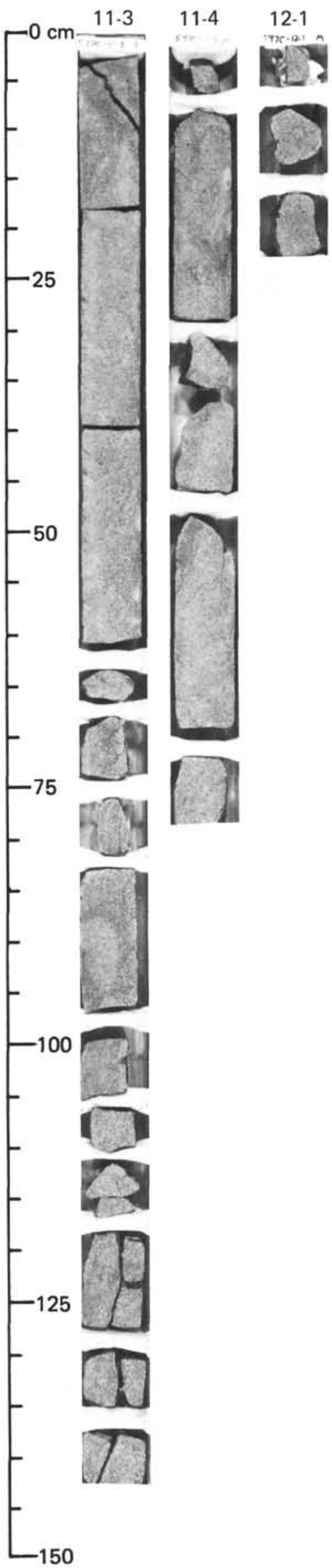
11-3
11-4
12-1
0 cm
25
50
75
100
125
150